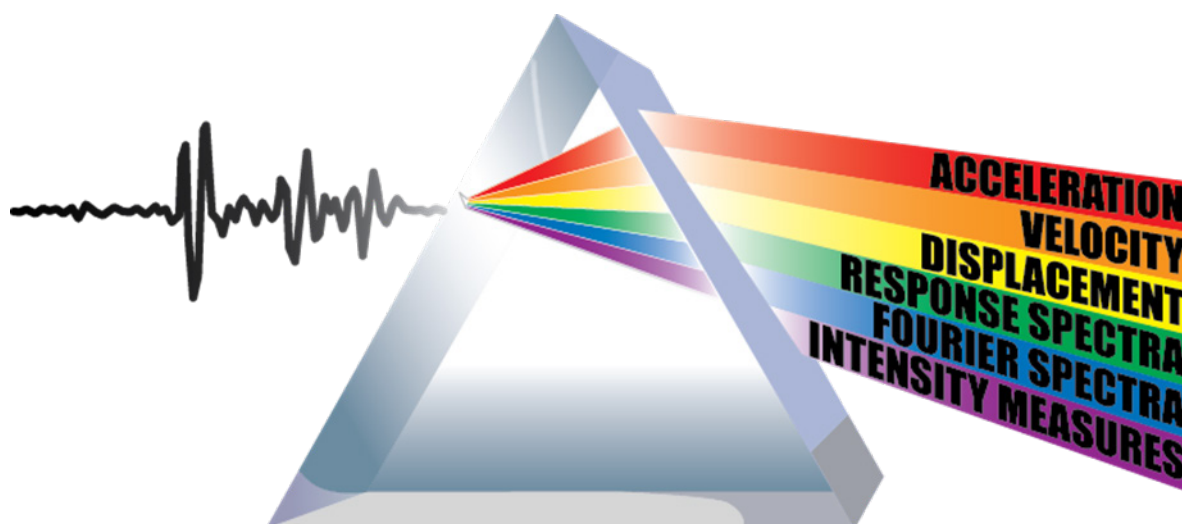




Processing and Review Interface for Strong Motion Data (PRISM) Software, Version 1.0.0—Methodology and Automated Processing

By Jeanne Jones, Erol Kalkan, and Christopher Stephens



Open-File Report 2017–1008

U.S. Department of the Interior
U.S. Geological Survey

U.S. Department of the Interior
SALLY JEWELL, Secretary

U.S. Geological Survey
Suzette M. Kimball, Director

U.S. Geological Survey, Reston, Virginia: 2017

For more information on the USGS—the Federal source for science about the Earth, its natural and living resources, natural hazards, and the environment—visit <http://www.usgs.gov/> or call 1-888-ASK-USGS (1-888-275-8747).

For an overview of USGS information products, including maps, imagery, and publications, visit <http://store.usgs.gov/>.

Any use of trade, firm, or product names is for descriptive purposes only and does not imply endorsement by the U.S. Government.

Although this information product, for the most part, is in the public domain, it also may contain copyrighted materials as noted in the text. Permission to reproduce copyrighted items must be secured from the copyright owner.

Suggested citation:

Jones, J., Kalkan, E., and Stephens, C., 2017, Processing and review interface for strong motion data (PRISM) software, version 1.0.0—Methodology and automated processing: U.S. Geological Survey Open-File Report 2017–1008, 81 p., <https://doi.org/10.3133/ofr20171008>.

ISSN 2331-1258 (online)

Acknowledgments

The retrieval, processing, and dissemination of seismic data involve a large number of individuals with a range of scientific and technological skills. We thank our colleagues at the U.S. Geological Survey, and in particular David Boore for providing his Fortran codes, the technicians of the National Strong-Motion Project (NSMP) network who install and maintain the strong motion instrumentation, and those involved in collecting and vetting data and providing easy access to the recordings. We also wish to thank the NSMP Working Group members for initiation of the Processing and Review Interface for Strong Motion data (PRISM) project. Special thanks are extended to Jamie Steidl, Robert Darragh, and Brad Aagaard for their reviews, and for providing their constructive comments and suggestions. Finally, we would like to thank Sarah Nagorsen for editing.

Contents

Abstract.....	1
Introduction	1
Input/Output Files.....	2
Input Files	2
Output Files.....	3
Automated Processing Workflow.....	3
V1 (Volume 1) Processing	3
V2 (Volume 2) Processing	3
Step 1—Event Onset Detection.....	6
Step 2—Remove Pre-Event Mean from Acceleration	6
Step 3—Integrate to Velocity.....	6
Step 4—Compute Best Fit Trend in Velocity.....	6
Step 5—Remove Best Fit Trend from Acceleration and Integrate to Velocity.....	7
Step 6—Quality Check (QC) for Velocity.....	7
Step 7—Tapering and Padding	7
Step 8—Bandpass Filtering	11
Step 9—Adaptive Baseline Correction (ABC)	13
Step 10—Computation of Velocity and Displacement.....	17
Step 11—Quality Check for Final Velocity and Displacement.....	17
V3 (Volume 3) Processing	18
Calculation of Response Spectra	19
Calculation of Fourier Amplitude Spectra	19
Calculation of Earthquake-Engineering Intensity Measures	19
Arias Intensity	19
Bracketed Duration.....	19
Duration Interval.....	20
Response Spectrum Intensity.....	20
Root Mean Square (RMS) Acceleration.....	20
Cumulative Absolute Velocity.....	20
Configuration File Parameters.....	21
Processing Agency	21
Data Units for Uncorrected Acceleration.....	21
Event Detection Method	21
Event Onset Buffer Amount	21
Quality Check (QC) Parameters	21
Bandpass Filter Parameters.....	21
Adaptive Baseline Correction.....	22
Strong-Motion Threshold	22
Differentiation Order.....	22
Output Array Format	22
DeleteInputV0.....	22
DebugToLog	23
WriteBaselineFunction.....	23
Example V2 and V3 Products.....	24

Run-Time Performance Assessment.....	55
Systematic Comparisons among PRISM, BAP, and CSMIP Processing.....	56
Running PRISM.....	56
Output Directory Structure.....	57
Concluding Remarks.....	58
Data and Resources.....	59
References Cited.....	59
Appendix 1. Frequency-Domain Zero-Padding Resampling.....	62
References Cited.....	65
Appendix 2. Event-Onset Detection.....	66
P _{PHASEPICKER}	66
Akaike Information Criterion (AIC) Picker.....	69
References Cited.....	72
Appendix 3. PRISM Configuration XML File.....	73
Appendix 4. Logging and Parametric Data.....	76
PrismLog.....	76
TroubleLog.....	76
DebugLog.....	77
ParameterLog.....	78
aphtable.....	78

Figures

1.	Flow chart showing volume 1 (V1) data processing to derive raw acceleration time series from volume 0 (V0).....	4
2.	Flow chart showing volume 2 (V2) data processing adopted for uncorrected acceleration time series (V1) to produce corrected acceleration, velocity, and displacement.....	5
3.	Graph showing total length of zeros (T_{pad}) added to the record as a function of acausal (two-pass) Butterworth filter order (n) and low-cut corner frequency (f_c).....	8
4.	Graphs showing effects of half-cosine taper lengths (0.5, 1, 2, 5, 10, and 15 seconds) on displacement time series computed for the NC.CPI station record from the 2014 $M6.0$ South Napa earthquake.....	9
5.	Graph showing effects of half-cosine taper length on 5-percent damped displacement response spectra of east-west (HNE) component of NC.CPI station record from the 2014 $M6.0$ South Napa earthquake.....	10
6.	Frequency response $H(w)$ of trapezoid integration; Nyquist frequency is at half of the sampling frequency (modified from Hamming, 1989).....	11
7.	Graphs showing, as a function of frequency, a low-cut Butterworth filter with a low-cut corner f_{lc} of 0.1 hertz (Hz), and a high-cut Butterworth filter with a high-cut corner f_{hc} of 40 Hz.....	12
8.	Flow chart showing adaptive baseline correction (ABC) adopted in the Processing and Review Interface for Strong Motion data (PRISM) software for correcting velocity time series for which initial baseline correction is not satisfactory for removing implausible trends.....	14
9.	Graphs showing acceleration and velocities after steps 2 through 5 of the Processing and Review Interface for Strong Motion data (PRISM) software.....	16
10.	Graphs showing velocities before and after adaptive baseline correction (ABC).....	17

11.	Flow chart showing volume 3 (V3) data processing using corrected acceleration time series to generate elastic response spectra for pseudo-acceleration, velocity, and displacement at different damping values, and Fourier amplitude spectrum	18
12.	Graphs showing a final suite of acceleration, velocity, and displacement time series (V2 products) for channel HNE at station MLI recorded from the 2014 <i>M4.4</i> South Dos Palos earthquake in California	25
13.	Graphs showing a final suite of acceleration, velocity, and displacement time series (V2 products) for channel HNN at station MLI recorded from the 2014 <i>M4.4</i> South Dos Palos earthquake in California	26
14.	Graphs showing a final suite of acceleration, velocity, and displacement time series (V2 products) for channel HNZ at station MLI recorded from the 2014 <i>M4.4</i> South Dos Palos earthquake in California	27
15.	Graphs showing a final suite of pseudo-spectral acceleration, pseudo-spectral velocity, and spectral displacement spectra computed at different damping levels (0, 2, 5, 10, and 20 percent of critical) for three channels of MLI record with 100 samples-per-second from the 2014 <i>M4.4</i> South Dos Palos earthquake in California.....	28
16.	Graphs showing Fourier amplitude spectrum (V3 products) for three channels of MLI record with 100 samples-per-second from the 2014 <i>M4.4</i> South Dos Palos earthquake in California	29
17.	Graphs showing a final suite of acceleration, velocity, and displacement time series (V2 products) for channel HNE at station SAO recorded with 100 samples-per-second from the 2014 <i>M4.4</i> Greenfield earthquake in California	30
18.	Graphs showing a final suite of acceleration, velocity, and displacement time series (V2 products) for channel HNN at station SAO recorded with 100 samples-per-second from the 2014 <i>M4.4</i> Greenfield earthquake in California	31
19.	Graphs showing a final suite of acceleration, velocity, and displacement time series (V2 products) for channel HNZ at station SAO recorded with 100 samples-per-second from the 2014 <i>M4.4</i> Greenfield earthquake in California	32
20.	Graphs showing a final suite of pseudo-spectral acceleration, pseudo-spectral velocity, and spectral displacement spectra computed at different damping levels (0, 2, 5, 10, and 20 percent of critical) for three channels of SAO record with 100 samples-per-second from the 2014 <i>M4.4</i> Greenfield earthquake in California	33
21.	Graphs showing Fourier amplitude spectrum (V3 products) for three channels of SAO record with 100 samples-per-second from the 2014 <i>M4.4</i> Greenfield earthquake in California.....	34
22.	Graphs showing a final suite of acceleration, velocity, and displacement time series (V2 products) for channel HNE at station C002 recorded with 200 samples-per-second from the 2014 <i>M6.0</i> South Napa earthquake in California.....	35
23.	Graphs showing a final suite of acceleration, velocity, and displacement time series (V2 products) for channel HNN at station C002 recorded with 200 samples-per-second from the 2014 <i>M6.0</i> South Napa earthquake in California.....	36
24.	Graphs showing a final suite of acceleration, velocity, and displacement time series (V2 products) for channel HNZ at station C002 recorded with 200 samples-per-second from the 2014 <i>M6.0</i> South Napa earthquake in California.....	37
25.	Graphs showing a final suite of pseudo-spectral acceleration, pseudo-spectral velocity, and spectral displacement spectra computed at different damping levels (0, 2, 5, 10, and 20 percent of critical) for three channels of C002 record with 200 samples-per-second from the 2014 <i>M6.0</i> South Napa earthquake in California.....	38

26.	Graphs showing Fourier amplitude spectrum (V3 products) for three channels of C002 record with 200 samples-per-second from the 2014 <i>M</i> 6.0 South Napa earthquake in California.....	39
27.	Graphs showing a final suite of acceleration, velocity, and displacement time series (V2 products) for channel HNE at station G006 recorded with 200 samples-per-second from the 2014 <i>M</i> 6.0 South Napa earthquake in California.....	40
28.	Graphs showing a final suite of acceleration, velocity, and displacement time series (V2 products) for channel HNN at station G006 recorded with 200 samples-per-second from the 2014 <i>M</i> 6.0 South Napa earthquake in California.....	41
29.	Graphs showing a final suite of acceleration, velocity, and displacement time series (V2 products) for channel HNZ at station G006 recorded with 200 samples-per-second from the 2014 <i>M</i> 6.0 South Napa earthquake in California.....	42
30.	Graphs showing a final suite of pseudo-spectral acceleration, pseudo-spectral velocity, and spectral displacement spectra computed at different damping levels (0, 2, 5, 10, and 20 percent of critical) for three channels of G006 record with 200 samples-per-second from the 2014 <i>M</i> 6.0 South Napa earthquake in California.....	43
31.	Graphs showing Fourier amplitude spectrum (V3 products) for three channels of G006 record with 200 samples-per-second from the 2014 <i>M</i> 6.0 South Napa earthquake in California.....	44
32.	Graphs showing a final suite of acceleration, velocity, and displacement time series (V2 products) for channel HNE at station NMI recorded with 100 samples-per-second from the 2014 <i>M</i> 6.0 South Napa earthquake in California.....	45
33.	Graphs showing a final suite of acceleration, velocity, and displacement time series (V2 products) for channel HNN at station NMI recorded with 100 samples-per-second from the 2014 <i>M</i> 6.0 South Napa earthquake in California.....	46
34.	Graphs showing a final suite of acceleration, velocity, and displacement time series (V2 products) for channel HNZ at station NMI recorded with 100 samples-per-second from the 2014 <i>M</i> 6.0 South Napa earthquake in California.....	47
35.	Graphs showing a final suite of pseudo-spectral acceleration, pseudo-spectral velocity, and spectral displacement spectra computed at different damping levels (0, 2, 5, 10, and 20 percent of critical) for three channels of NMI record with 100 samples-per-second from the 2014 <i>M</i> 6.0 South Napa earthquake in California.....	48
36.	Graphs showing Fourier amplitude spectrum (V3 products) for three channels of NMI record with 100 samples-per-second from the 2014 <i>M</i> 6.0 South Napa earthquake in California.....	49
37.	Graphs showing a final suite of acceleration, velocity, and displacement time series (V2 products) for channel HNE at station N019B recorded with 200 samples-per-second from the 2014 <i>M</i> 6.0 South Napa earthquake in California.....	50
38.	Graphs showing a final suite of acceleration, velocity, and displacement time series (V2 products) for channel HNZ at station N019B recorded with 200 samples-per-second from the 2014 <i>M</i> 6.0 South Napa earthquake in California.....	51
39.	Graphs showing a final suite of acceleration, velocity, and displacement time series (V2 products) for channel HNZ at station N019B recorded with 200 samples-per-second from the 2014 <i>M</i> 6.0 South Napa earthquake in California.....	52
40.	Graphs showing a final suite of pseudo-spectral acceleration, pseudo-spectral velocity, and spectral displacement spectra computed at different damping levels (0, 2, 5, 10, and 20 percent of critical) for three channels of N019B record with 200 samples-per-second from the 2014 <i>M</i> 6.0 South Napa earthquake in California.....	53
41.	Graphs showing Fourier amplitude spectrum (V3 products) for three channels of N019B record with 200 samples-per-second from the 2014 <i>M</i> 6.0 South Napa earthquake in California.....	58

1-1.	Graphs showing spectrograms.....	63
1-2.	Graphs showing analytical and resampled chirp signals.....	64
2-1.	Illustration showing idealized fixed-base single-degree-of-freedom oscillator with viscous damping used for <i>P</i> -wave phase picking.....	66
2-2.	Graphs showing raw acceleration record of AZ-BZN station with 100 samples-per-second from 03/29/2014 <i>M</i> 5.1 La Habra earthquake in southern California used to demonstrate the energy metrics for idealized single-degree-of-freedom (SDF) oscillator as fixed-base with a short period and high damping ratio ($T_n = 0.01$ s, $\zeta = 0.6$).....	67
2-3.	Graphs showing <i>P</i> -phase detection results for three-component acceleration records obtained from a <i>M</i> 6.1 earthquake on 05/05/2014 in Thailand with 100 samples-per-second.....	68
2-4.	Graphs showing HN1 component of acceleration record obtained from a <i>M</i> 6.1 earthquake on 05/05/2014 in Thailand with 100 samples-per-second, and its corresponding Akaike information criterion (AIC) values.....	70
2-5.	Graphs showing HN2 component of acceleration record from a <i>M</i> 6.1 earthquake on 05/05/2014 in Thailand with 100 samples-per-second, and its corresponding Akaike information criterion (AIC) values.....	71
2-6.	Graph showing seismic noise data and its Akaike information criterion (AIC) values.....	72

Tables

1.	Magnitude dependent bandpass filter corner frequencies.....	13
2.	Configuration file parameters and defaults.....	23
3.	Runtime statistics for three recent earthquake event.....	55
4-1.	Example of ParameterLog comma-separated value (CSV) file for the 2014 moment magnitude 6.0 South Napa earthquake ground-motion processing.....	79
4-2.	Example of an apktable comma-separated value (CSV) file for the 2014 moment magnitude 6.0 South Napa earthquake ground-motion processing.....	81

Abbreviations

ABC	adaptive baseline correction
AIC	Akaike information criterion
ANSS	Advanced National Seismic System
API	application programming interface
AQMS	Advanced National Seismic System Quake Monitoring System
BAP	Basic Strong-Motion Accelerogram Processing software
CAV	cumulative absolute velocity
CAV _{Total}	total cumulative absolute velocity
COSMOS	Consortium of Organizations for Strong-Motion Observation Systems
CSV	comma-separated value
DC	direct current
FAS	Fourier amplitude spectrum
FFT	fast Fourier transform
GUI	graphical user interface
id	identifier
IM	intensity measure
<i>M</i>	moment magnitude
ML	local magnitude
NSMP	National Strong-Motion Project
PGA	peak ground acceleration
PGD	peak ground displacement
PGV	peak ground velocity
PRISM	Processing and Review Interface for Strong Motion data
PSV	pseudo-velocity response spectrum
PWD	<i>P</i> -wave phase onset time detector (also abbreviated as <i>P_{PHASEPICKER}</i>)
QC	quality check
RMS	root mean square
S _a	spectral acceleration at a particular period
SDF	single-degree of freedom
<i>S_I</i>	response spectrum intensity
SNR	signal-to-noise ratio
sps	samples-per-second
SRSS	square root of the sum of the squares
V0	COSMOS volume 0
V1	COSMOS volume 1
V2	COSMOS volume 2
V3	COSMOS volume 3

Notation

a_{rms}	root mean square of acceleration
c	damping of single-degree-of-freedom oscillator
d	sample delay
df	inverse of the record duration in seconds
E_{ζ}	damping energy
f	frequency
f_{hc}	high-cut corner frequency
f_{lc}	low-cut corner frequency
f_n	resonance frequency of undamped single-degree-of-freedom oscillator
g	gravitational acceleration = 9.80665 meters per second squared (m/s ²)
i	sample index
I_A	Arias intensity
k	stiffness of single-degree-of-freedom oscillator
m	mass of single-degree-of-freedom oscillator

m_b	body-wave magnitude
m_X	mean of signal x
m_Y	mean of signal y
n	Butterworth filter order
n_p	polynomial order
N	number of data points in the input time series
N_{taper}	number of data points in full cosine taper
N_1	number of one-second intervals in the record
$P_{\text{PHASEPICKER}}$	P -wave phase onset time detector (also abbreviated as PWD)
$P_{xx}(f)$	power spectral density of signal x
$P_{xy}(f)$	cross power spectral density of signals x and y
R_{xx}	normalized cross-correlation sequence
$RMSD$	root mean square deviation
\overline{RMSD}	square root of the sum of the squares of root mean square-deviation
$\theta_{xy}(f)$	relative phase between signals x and y
T	spectral period
$T_{\text{bracketed}}$	bracketed duration
T_d	duration of ground motion
T_D	resonance period of damped single-degree-of-freedom oscillator
T_{interval}	duration interval
T_n	resonance period of undamped single-degree-of-freedom oscillator
T_{pad}	total length of zeros in padding
T_{taper}	half-cosine taper length in seconds
T_1	first moment that the absolute value of acceleration is greater than 5 percent g
T_2	last moment that the absolute value of acceleration is greater than 5 percent g
t	time instant
t_p	event onset
t_1	ending time of first polynomial in adaptive baseline correction
t_2	beginning time of second polynomial in adaptive baseline correction
Y	filter response
X_n	difference between the velocity time series and the baseline fit
u	relative displacement of the mass of the single-degree-of-freedom oscillator with respect to base
\dot{u}	relative velocity of the mass of the single-degree-of-freedom oscillator with respect to base
\ddot{u}_g	ground-motion acceleration
\dot{u}_g	ground-motion velocity
ζ	damping ratio (fraction of critical damping)
wt	weight function
τ_0	time delay
ω	cyclic frequency, in radians
ω_D	cyclic frequency of damped single-degree-of-freedom oscillator
Δt	sampling interval of time series in seconds
Δt_{ABC}	sampling interval as number of samples in adaptive baseline correction

Processing and Review Interface for Strong Motion Data (PRISM) Software, Version 1.0.0—Methodology and Automated Processing

By Jeanne Jones, Erol Kalkan, and Christopher Stephens

Abstract

A continually increasing number of high-quality digital strong-motion records from stations of the National Strong-Motion Project (NSMP) of the U.S. Geological Survey (USGS), as well as data from regional seismic networks within the United States, call for automated processing of strong-motion records with human review limited to selected significant or flagged records. The NSMP has developed the Processing and Review Interface for Strong Motion data (PRISM) software to meet this need. In combination with the Advanced National Seismic System Quake Monitoring System (AQMS), PRISM automates the processing of strong-motion records. When used without AQMS, PRISM provides batch-processing capabilities. The PRISM version 1.0.0 is platform independent (coded in Java), open source, and does not depend on any closed-source or proprietary software. The software consists of two major components: a record processing engine and a review tool that has a graphical user interface (GUI) to manually review, edit, and process records. To facilitate use by non-NSMP earthquake engineers and scientists, PRISM (both its processing engine and review tool) is easy to install and run as a stand-alone system on common operating systems such as Linux, OS X, and Windows. PRISM was designed to be flexible and extensible in order to accommodate new processing techniques. This report provides a thorough description and examples of the record processing features supported by PRISM. All the computing features of PRISM have been thoroughly tested.

Introduction

PRISM (Processing and Review Interface for Strong Motion data) originally was conceived as a modern graphical user interface (GUI) to replace the outdated software program BAP (Basic Strong-Motion Accelerogram Processing Software) (Converse and Brady, 1992) developed and used by the U.S. Geological Survey (USGS) National Strong-Motion Project (NSMP) to process earthquake strong-motion records. Because BAP is command-line driven, it is challenging to adapt it to efficiently handle processing demands posed by the large and growing volume of digital strong-motion records acquired by the NSMP network, as well as records of engineering interest from other Advanced National Seismic System (ANSS) regional seismic networks.

The PRISM version 1.0.0 consists of two major components: a record processing engine and a review tool that has a GUI to manually review, edit, and process records. For PRISM, we follow a three-sequence identifier (a.b.c) as a versioning scheme: increment “a” if there are major changes in the software; increment “b” if there are minor changes, such as a new module or an enhancement; and increment “c” if there are bug fixes in the code.

This report documents the record processing engine component of PRISM that was developed to process many records with little or no human intervention. The review tool component of PRISM will be presented in a companion report.

PRISM was designed to be versatile and extensible in order to accommodate new processing techniques and multiple forms of input. Key design features of PRISM include (1) batch processing without the need for human intervention; (2) modularity to allow easy inclusion of new or alternative algorithms in any of the processing steps; (3) tracking of key parameters used in each of the processing steps, which are embedded in the metadata of the data products to ensure the ability to replicate the processed record from the original input; and (4) a GUI for manually reviewing and processing records. To facilitate use by non-NSMP earthquake engineers and scientists, PRISM (including its processing engine and review tool) is easy to install and run as stand-alone software on common operating systems; such as Linux, Mac OS X, and Windows.

Record processing in PRISM implements each step according to a well-defined application programming interface (API) to allow incorporation of alternative implementations of each step. The main features of PRISM batch processing include the following:

- Platform-independent, modular, extensible, open-source software
- Customizable processing parameters with a configuration file
- P-phase time and maximum amplitude detection
- Time-domain mean-removal, integration, and differentiation
- Acausal bandpass filtering
- Baseline correction computed in the velocity domain, and its derivative applied as a baseline correction to the acceleration waveform
- Generation of products that include compatible acceleration, velocity and displacement time series, response spectra, Fourier amplitude spectra, and standard earthquake-engineering intensity measures. Compatible data products means that released acceleration can be used to calculate velocity, displacement, and spectra, which match those released with the acceleration
- Log files for quality control and reproducibility
- Use of Consortium of Organizations for Strong-Motion Observation Systems (COSMOS) V0 input format with metadata in COSMOS headers (Consortium of Organizations for Strong-Motion Observation Systems, 2001)
- Products in COSMOS data format (V1, V2, and V3)

The processing steps in the automated workflow are clearly defined and use a conservative set of default parameters—specified in a configuration file—to generate V1, V2, and V3 data products. NSMP has determined default parameters that permit processing of about 95 percent of records without human interaction. The processing includes quality assurance steps to flag records that require further review by analysts and manual tuning of processing parameters.

Input/Output Files

Input Files

Input to PRISM currently is limited to data files in standard COSMOS V0 format (Consortium of Organizations for Strong-Motion Observation Systems, 2001), so all retrieved acceleration time series need to be converted to this format. COSMOS V0 files contain original acceleration time series data in digital counts. Instrument response parameters are not required in the COSMOS V0 file headers, but it is recommended that all associated station and event metadata be included.

Output Files

Products are COSMOS V1, V2, and V3 files containing the following:

- Unfiltered acceleration time series in physical units with mean removed (V1)
- Baseline-corrected and filtered acceleration, velocity, and displacement time series (V2)
- Response spectra, Fourier amplitude spectrum, and common earthquake-engineering intensity measures (V3)

Automated Processing Workflow

When PRISM is started, the software looks in a user-specified input directory for acceleration time series in V0 format. The software automatically processes the waveforms on a channel-by-channel basis using an established set of steps. These steps, which are hard-wired to the computer code, are explained under V1, V2, and V3 processing. During the processing flow, logging functions record information such as product files generated, warnings issued for invalid metadata, and key parameter values identified for diagnostics. Critical processing information, such as event onset time and baseline correction steps, is recorded in the comment section of the product files for reproducibility.

V1 (Volume 1) Processing

Data in digital counts (V0) are converted to physical units, and the mean of the entire raw acceleration trace is removed. Figure 1 illustrates the workflow to generate the uncorrected acceleration. A full instrument response correction is not applied, because the cutoff frequency of the low-pass filter applied in V2 processing (explained later) is lower than that of the natural frequency of an accelerometer (>50 hertz [Hz]). Instead, a simple scaling factor is used (Graizer, 2012).

V2 (Volume 2) Processing

Corrected acceleration, velocity, and displacement time series are obtained by applying prescribed baseline correction methods and filtering to remove low- and high-frequency noise.

The first step is to check the sampling rate of the acceleration time series. If the V1 acceleration has low time resolution (less than about 200 samples-per-second [sps]), then the time series is interpolated to 200 sps by resampling in the frequency domain (as described in appendix 1) prior to V2 processing in order to reduce numerical noise (Kalkan and Stephens, 2017).

The V2 processing protocol, illustrated in figure 2, is performed in the time domain and involves the following steps:

1. Detect event onset
2. Remove pre-event mean from acceleration
3. Integrate to velocity
4. Compute best fit trend in velocity record
5. Remove derivative of best fit trend from acceleration, and integrate to velocity
6. Perform quality check of velocity record
7. Taper and pad acceleration record to condition for filtering
8. Apply acausal bandpass filter to acceleration in the time domain
9. Integrate acceleration and check for ill-behaved velocity record and apply an adaptive baseline correction as needed
10. Compute velocity and displacement from processed acceleration
11. Perform quality check on final velocity and displacement

V1 Process

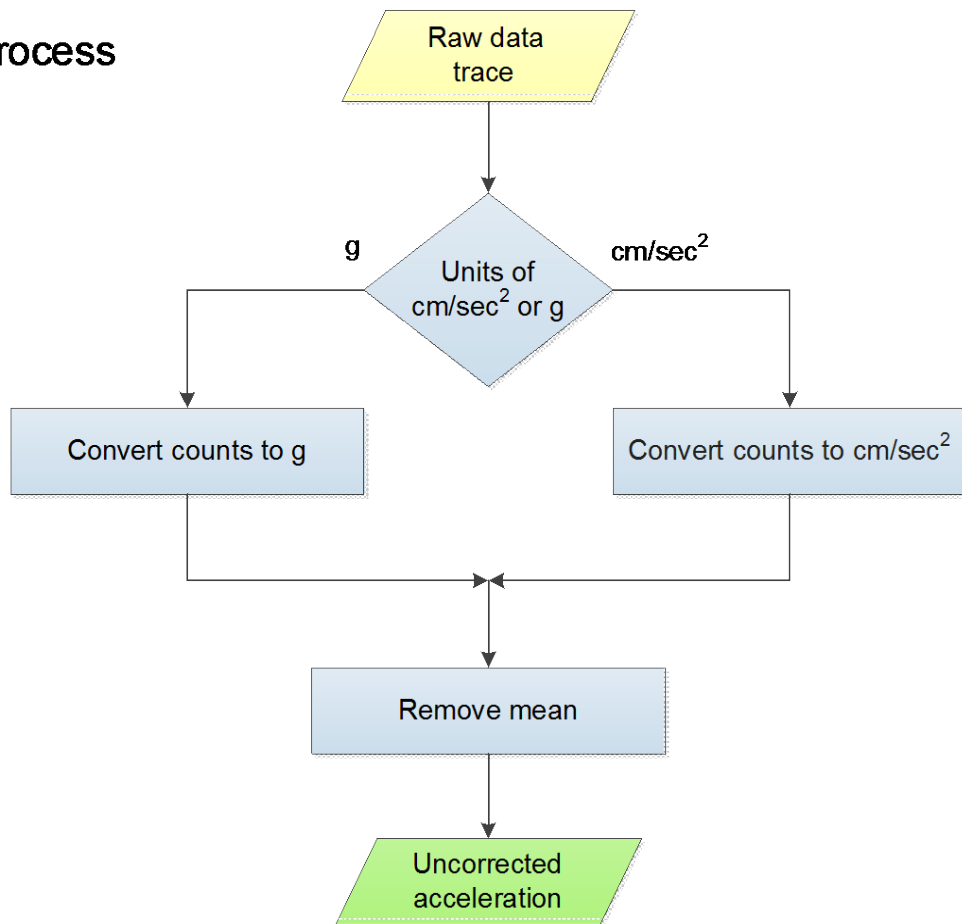


Figure 1. Flow chart showing volume 1 (V1) data processing to derive raw acceleration time series from volume 0 (V0). cm/sec², centimeters per second squared; g, gravitational acceleration.

V2 Process

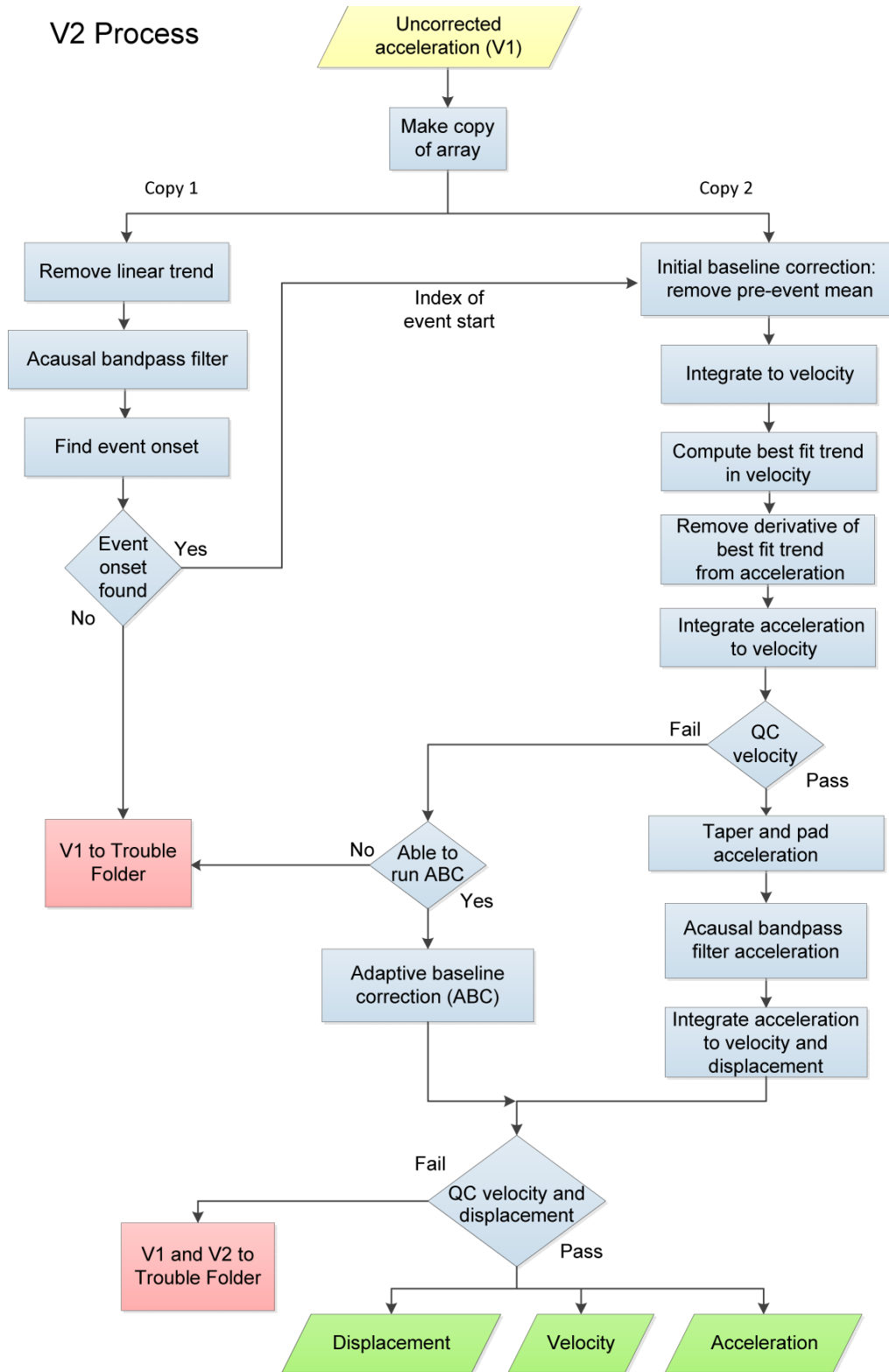


Figure 2. Flow chart showing volume 2 (V2) data processing adopted for uncorrected acceleration time series (V1) to produce corrected acceleration, velocity, and displacement.

Step 1—Event Onset Detection

The pre-event interval of the time series is useful in determining a suitable initial baseline correction and the spectral character of the background noise. PRISM has two options for computing the event onset time (that is, *P*-phase arrival time); these are the *P_{PHASE}PICKER* (Kalkan, 2016) and the Akaike information criterion (AIC) picker (Maeda, 1985). Summaries of these two pickers are presented in appendix 2.

For either of the picking methods, PRISM operates on a copy of the uncorrected acceleration (V1) to remove a linear trend from the record, applies a 4th-order acausal Butterworth bandpass filter with corner frequencies at 0.1 and 20 Hz, and then determines the index corresponding to the event onset in this filtered array. This event onset index is then used in the following steps of the V2 processing, and the filtered array is discarded.

Step 2—Remove Pre-Event Mean from Acceleration

Prior to integration to velocity, the mean of the pre-event interval is subtracted from the entire uncorrected acceleration time series. This interval is defined as beginning of the record to the event onset, minus a buffer interval. The buffer interval allows for uncertainty in the onset time. The buffer interval is set in the configuration file, and its default value in the configuration file is zero seconds.

Step 3—Integrate to Velocity

The trapezoidal rule is used to integrate from acceleration to velocity and subsequently integrate from velocity to displacement. In each integration step, the unknown initial value introduces a linear trend in the result that, on a physical basis, is expected to have a slope near zero. The slope of the trend is equal to the unknown initial value. Thus, after the initial integration, the slope of the pre-event interval is used as an estimate of the initial value and a correction is made to the integrated time series.

Step 4—Compute Best Fit Trend in Velocity

Low-frequency noise of both natural and instrumental origin is present in nearly all strong- and weak-motion records (Trifunac, 1971; Graizer, 1979; Boore and others, 2002). This noise becomes readily apparent in the form of long-period wandering or monotonic drift from zero in velocity and displacement time series obtained from single- and double-integration, respectively, of acceleration (integration effectively being a low-pass filter). The process of integration itself introduces additional low-frequency noise. The variety and complexity of the noise sources preclude designing a simple correction scheme (Graizer, 2010).

Physically, the mean of the velocity time series should be near zero at the start and end of the record. In order to choose an appropriate baseline correction to achieve a zero mean of the velocity record, PRISM first calculates the root mean square deviation (*RMSD*) for two functions: a simple linear regression and a second-order polynomial regression. *RMSD* is a statistical measure of the scatter of data about the mean of a collection of data samples, and it is computed as

$$RMSD = \sqrt{\frac{1}{n} \sum_{n=1}^N [X_n(t)]^2} \quad (1)$$

where X_n is the difference between the velocity and the fit, and N is number of data points. The function with the smallest *RMSD* is selected as the baseline correction.

Step 5—Remove Best Fit Trend from Acceleration and Integrate to Velocity

The derivative of the best fit trend computed in the velocity domain is subtracted from the acceleration time series. After trend removal, the acceleration record is integrated to velocity and reviewed for quality.

Step 6—Quality Check (QC) for Velocity

On the basis of physical plausibility, the velocity prior to the earthquake onset and after the interval of strong motion is expected to oscillate around zero. To satisfy this criterion, the following quality control steps are applied to the velocity record:

Step 6a: Determine a suitable window length for intervals at the beginning and end of the velocity time series for the quality check (QC) as

$$\text{window length} = \max\left(\text{length of pre-event interval}, \frac{1}{f_{lc}}\right) \quad (2)$$

where f_{lc} is low-cut corner frequency (explained below). For the leading velocity interval, find the mean from the start of the time series to the last zero crossing before the end of the initial window; for the final trailing velocity interval, find the mean from the first zero crossing after the start of the interval to the end of the time series.

Step 6b: Compare these two means against QC thresholds specified in the configuration file. QC passes if both leading and trailing means are less than or equal to the thresholds. Default threshold values, which can be overwritten in the configuration file, are as follows:

Leading velocity threshold = 0.01 centimeter per second (cm/s)

Trailing velocity threshold = 0.01 cm/s

Step 7—Tapering and Padding

PRISM performs filtering in the time domain. Time-domain filtering assumes that the time series is zero-valued outside the data interval. To accommodate filter transients from bidirectional acausal filtering, PRISM temporarily extends the time series with zero padding at the leading and trailing edges. According to Converse and Brady (1992), the total length of the zero padding in seconds (T_{pad}) required can be determined from

$$T_{pad} = \frac{1.5n}{f_{lc}} \quad (3)$$

where n is the order of the Butterworth filter. In a typical case where $n = 4$ and $f_{lc} = 0.1$ Hz, T_{pad} should be 60 seconds. Thus, the time series is extended symmetrically at both ends with zero padding, each of duration $T_{pad}/2$. In figure 3, T_{pad} is presented as a function of n for the three values of f_{lc} (0.1, 0.3, and 0.5 Hz) currently used in PRISM for time-domain filtering (see table 1).

To avoid introduction of spurious low-frequency noise from any discontinuity between the signal and the padding (that is, a jump in the value or a change in the gradient), cosine tapers are applied to the ends of the data intervals so that there are smooth transitions to zero where they abut the zero paddings. An alternative to using cosine tapering would be to apply a rectangular weighting function with end points set to the first zero crossing inward from each end of the time series (for example, Converse and Brady, 1992), provided that this does not result in the loss of a significant part of the record, as can occur if the beginning or end of the record is completely above or below zero (for example, Boore and Bommer, 2005). Currently this alternative approach is not an option in PRISM.

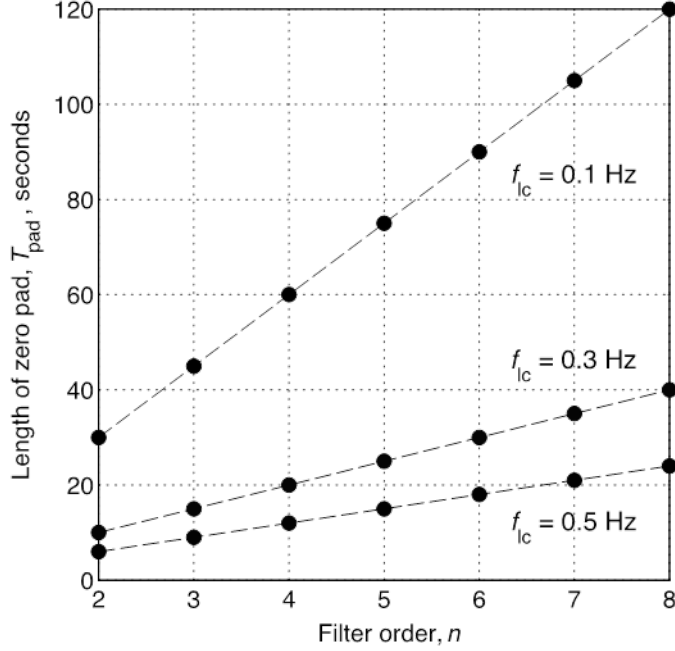


Figure 3. Graph showing total length of zeros (T_{pad}) added to the record as a function of acausal (two-pass) Butterworth filter order (n) and low-cut corner frequency (f_{lc}). In time-domain filtering, half of T_{pad} is added to the front and half is added to the back of the time series. Thus, the original record after padding is longer in duration by T_{pad} . These pads are necessary whether the filtering is performed in the time or frequency domain (figure modified from figure 3 in Boore, 2005).

The width of the full cosine taper, N_{taper} (in samples), is taken as the number of samples from the beginning of the record to the last zero crossing before the event onset. The weights, wt , as a function of sample index, i , are computed as

$$wt(i) = \frac{1}{2} \left[1 - \cos \left(\pi \frac{i}{N_{taper}/2} \right) \right], \quad i = 0, \frac{N_{taper}}{2}-1 \quad (4a)$$

and

$$wt(i) = \frac{1}{2} \left[1 + \cos \left(\pi \frac{i - \left(N - \frac{N_{taper}}{2} \right) + 1}{N_{taper}/2} \right) \right], \quad i = N - \frac{N_{taper}}{2}, N - 1 \quad (4b)$$

where N is the total number of data samples in the time series. Note that $N_{taper}/2$ is the taper length applied at each end symmetrically.

In order to demonstrate the overall effect of taper length, the record obtained from station NP.CPI during the 2014 moment magnitude $M6.0$ South Napa earthquake was processed by using six taper lengths—0.5, 1, 2.5, 5, 10, and 15 seconds (s). Figures 4 and 5 present the resultant displacement time series and 5-percent damped displacement response spectra, respectively. For this particular record, the event onset time (30.6 s) is longer than the taper length, so that even a 15-s taper only affects the filter transients in the beginning. A visual comparison of the different plots clearly shows that the effects of the taper length on the beginning of the record are negligible. Only the 10- and 15-s tapers slightly reduce the displacement amplitude within the final 10 and 15 s. Nonetheless, the displacement spectra

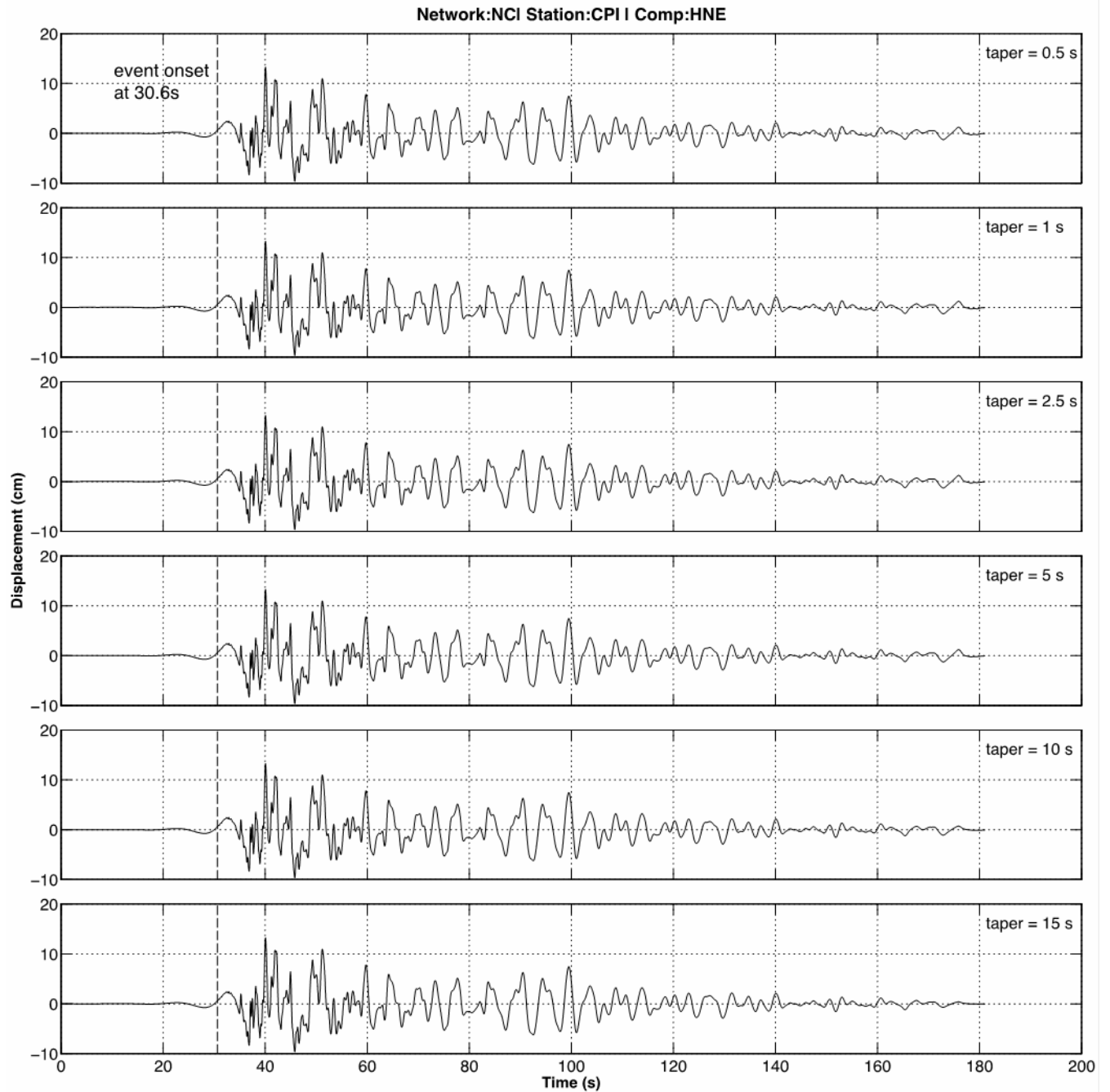


Figure 4. Graphs showing effects of half-cosine taper lengths (0.5, 1, 2, 5, 10, and 15 seconds [s]) on displacement time series computed for the NC.CPI station record from the 2014 $M6.0$ South Napa earthquake [$f_{lc} = 0.1$ Hz and $f_{hc} = 40$ Hz]. Dashed vertical lines show the event onset picked automatically using $P_{PHASEPICKER}$ on the acceleration time series. cm, centimeters.

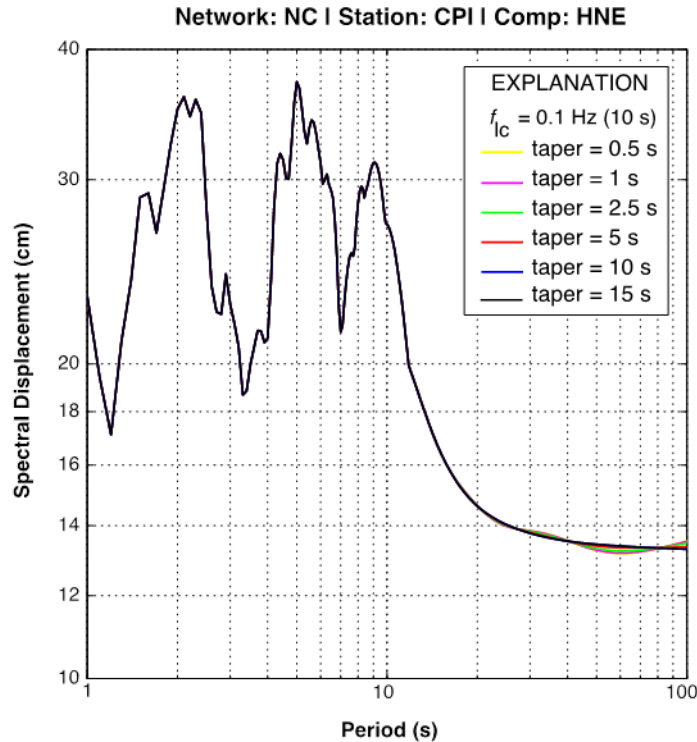


Figure 5. Graph showing effects of half-cosine taper length on 5-percent damped displacement response spectra of east-west (HNE) component of NC.CPI station record from the 2014 *M*_{6.0} South Napa earthquake. cm, centimeters; s, seconds.

show that the peak displacement response values are not affected by taper lengths ranging from 0 to 15 s for periods shorter than about 30 s.

In PRISM processing engine, the window length of the cosine taper is set to be 3 s at the end of the signal. For the beginning, the taper length typically is one half of the duration of the pre-event.

Note that in order to maintain compatibility, the padded sections of the filtered velocity are retained when deriving acceleration, displacement, and response spectra. For computing the Fourier amplitude spectra, the zero-pads are extended so that the total number of data points is a power of 2. All time-series pads are removed after final processing for dissemination of the V2 products. The reasons for this practice are to reduce file size (the padded segments of the data—filter transients—can be long and have small amplitudes in the acceleration time series), and to avoid the misinterpretation that the transient motions before and after the recorded data are representing actual motion. Note that acausal filtering also introduces apparent “pre-event” motions in the retained time series. Removing the pads after filtering can result in incompatibilities and biases in quantities derived from pad-stripped accelerations (Boore and others, 2012). One way of overcoming this incompatibility is to provide the initial values of the processed time series in the V2 and V3 file headers so that if a user needs to obtain velocity by integrating directly the acceleration time series in V2 file, the initial value stored in the header should be added to the integration as a constant. Similarly, in computing the displacement, the initial value for displacement also needs to be considered. The PRISM processing engine also offers an option in the configuration file to write out time series with filter transients.

Step 8—Bandpass Filtering

It was found during the development stage that when bandpass filters are applied in velocity rather than in acceleration, the resultant amplitudes of higher frequencies are systematically low. This is because integration acts as a low-pass filter (fig. 6). PRISM version 1.0.0 applies bandpass filters in acceleration component-by-component to avoid this distortion in the frequency content of the signals.

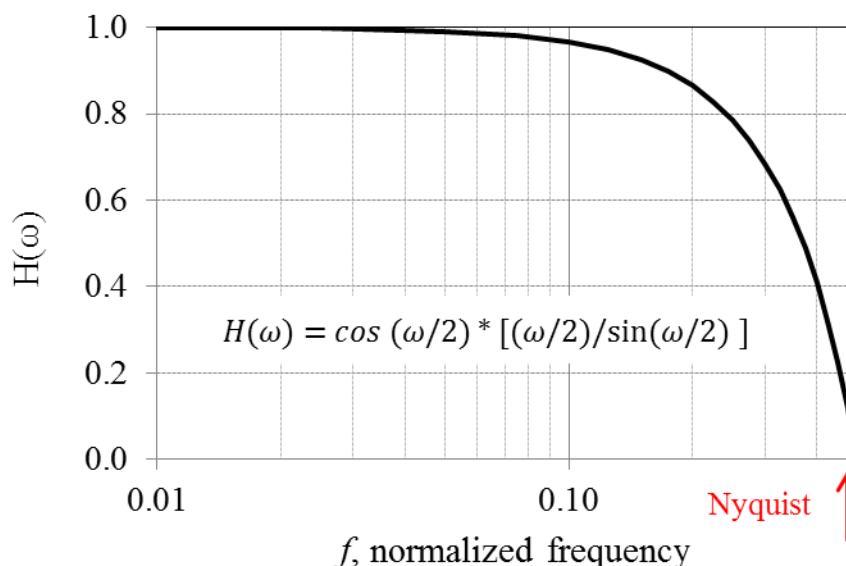


Figure 6. Frequency response $H(\omega)$ of trapezoid integration; Nyquist frequency is at half of the sampling frequency (modified from Hamming, 1989).

In order to remove high- and low-frequency noise, the acceleration record is bandpass filtered by applying a causal Butterworth filter in two passes, one pass in the forward direction and one pass in the reverse direction. This is called acausal filtering, which is preferred over causal filtering to avoid phase distortion in the signal (Boore and Akkar, 2003; Bazzurro and others, 2005); causal filtering is not an option in PRISM. The acausal filter is applied in the time domain by convolution of its transform with the time history. Following Kanasewich (1975), the response of a low-cut acausal Butterworth filter is defined as

$$Y = \frac{(f/f_{lc})^{2n}}{1+(f/f_{lc})^{2n}} \quad (5)$$

and high-cut acausal Butterworth filter is defined as

$$Y = 1 - \frac{(f/f_{hc})^{2n}}{1+(f/f_{hc})^{2n}} \quad (6)$$

where Y is filter response (0 through 1), f is frequency, and n is filter order. Selecting n is a compromise between effectively removing unwanted low-frequency noise and avoiding excessive ringing caused by using too high of an order. In PRISM, the default value for n is 4, which can be overwritten in the configuration file.

In strong-motion data processing, and at least for ground-motion reference sites, it is desirable to use the broadest frequency bandwidth with a high signal-to-noise ratio (SNR) (sources of low-frequency noise are discussed in step 9). When the SNR is sufficiently high—at least twice as high as the

background—a simple low-cut filter can usually eliminate the part of the signal contaminated by long-period noise (Trifunac, 1971). The transition bands of a Butterworth filter at typical low- and high-frequency corners and for a range of filter orders are shown in figure 7. Methods for selecting an appropriate low-cut filter corner are generally subjective, but often are based on approaches such as the following: a comparison between the Fourier amplitude spectrum or pseudo-velocity response spectrum of the record with that of a model of the noise, obtained from pre-event time window (Trifunac, 1977; Shakal and Ragsdale, 1984); a comparison of the behavior of the Fourier amplitude spectrum at long periods to that expected from theoretical models (at long periods the Fourier amplitude spectrum is expected to decay in proportion to $1/f^2$; Brune, 1970, 1971); or the physical plausibility of the velocity and displacement time series obtained by integration, which requires a subjective manual review. For example, Pacific Earthquake Engineering Research Center standard practice makes use of all three approaches as described in Darragh and others (2004), Chiou and others, (2008), Ancheta and others (2013), and Goulet and others (2014). Another common approach is the use of response spectrum for selecting the low-cut corner frequency (Shakal and others, 2004).

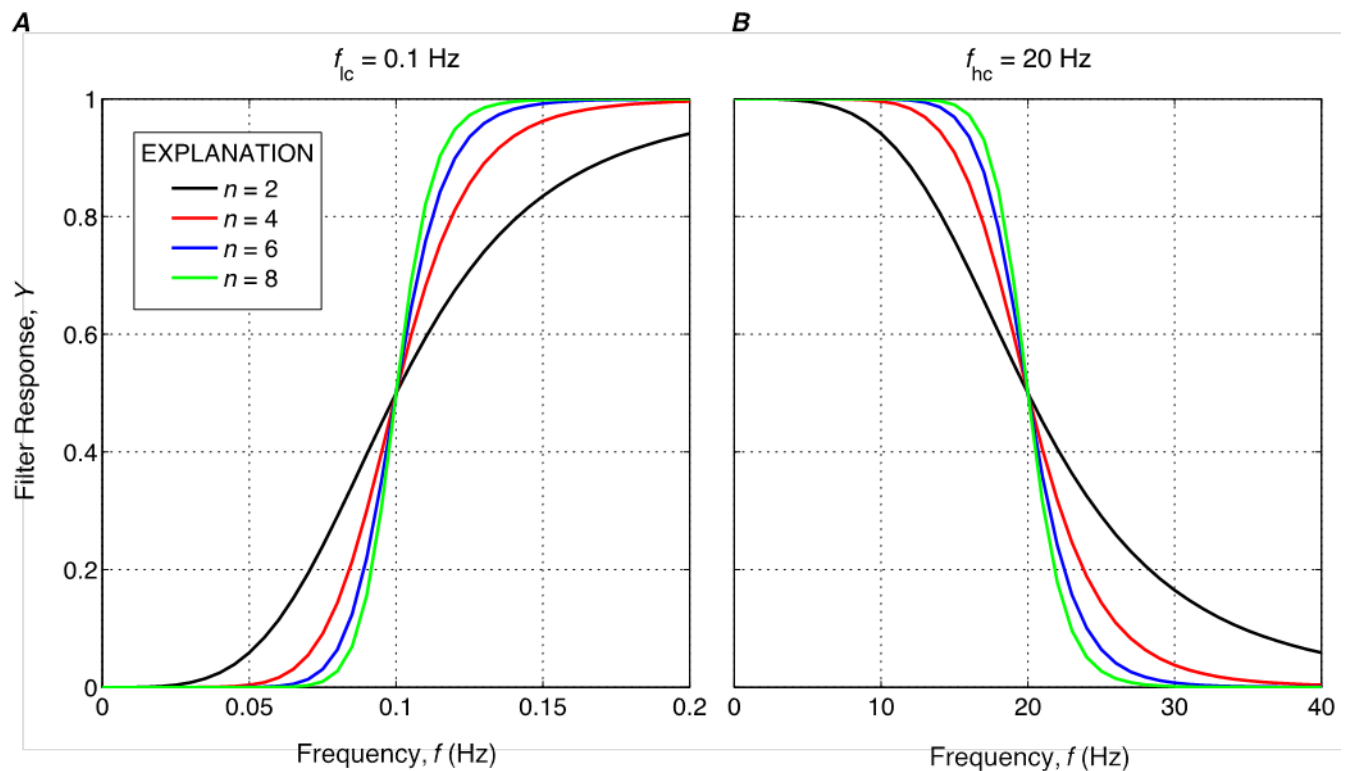


Figure 7. Graphs showing, as a function of frequency, a low-cut Butterworth filter with a low-cut corner f_{lc} of 0.1 hertz (Hz) (A), and a high-cut Butterworth filter with a high-cut corner f_{hc} of 40 Hz (B). The curves are color coded according to different filter orders (n): the higher the order, the more abrupt the cutoff.

A high-cut filter is applied to remove high-frequency noise in the record, which commonly occurs in urban areas with high levels of background noise, or may result from contamination from 60 Hz alternating current (AC) power. In modern data loggers, the upper frequency limit on the usable range of high frequencies in the record is typically controlled by the anti-alias filter at 80 percent of the Nyquist frequency, which is at half of the sampling frequency.

When PRISM is run in batch mode, the high- and low-cut filter corner frequencies are pre-selected on the basis of the local magnitude (ML) of the earthquake. The filter cutoff frequencies, presented in table 1, are adapted and modified from Massa and others (2010). It should be noted that the value of f_{hc} for $ML \geq 5.5$ is valid for records with a sampling rate of at least 100 sps. The limits on sampling rates are also presented in table 1. If relative noise levels are high, it is important that f_{lc} values are chosen individually considering the noise level—based on where the amplitude of Fourier spectrum of the signal approaches to that of noise floor. This only can be done by resetting values in the configuration file or by using the PRISM review tool.

Table 1. Magnitude dependent bandpass filter corner frequencies. Hz, hertz; sps, samples-per-second.

Earthquake local magnitude (ML)	Low-cut corner frequency, f_{lc} (Hz)	High-cut corner frequency, f_{hc} (Hz)	Nyquist frequency (Hz)	Minimum sampling rate (sps)
$ML \geq 5.5$	0.1	40	50	100
$3.5 \leq ML < 5.5$	0.3	35	45	90
$ML < 3.5$	0.5	25	30	60

In order to determine the low- and high-pass corner frequencies, an alternative approach to table 1 would be to use the Fourier amplitude spectrum of the unfiltered acceleration record. The high-frequency corner can be identified as the flattening or increase resulting from noise, and low-frequency corner can be identified as the departure from $1/f^2$. This approach requires testing for automation, and it has not been implemented to PRISM yet.

Step 9—Adaptive Baseline Correction (ABC)

Ground-motion recordings may have physically implausible trends resulting from instrumental noise, such as spikes or step-like offsets in the baseline, or they may be contaminated by rotational or gravitational effects (for example, Graizer, 2005; Boroschek and Legrand, 2006; Kalkan and Graizer, 2007a,b). The variety and complexity of these noise signals in the record may require complex baseline schemes, such as multisegment fitting with linear or low-order polynomials, to effectively remove them from the velocity time series (Graizer, 1979; Iwan and others, 1985; Boore, 2001; Boore and others, 2002; Kalkan and Kunnath, 2006). A series of progressively higher order polynomials to fit to the velocity trace was first proposed by Graizer (1979). Iwan and others (1985) proposed a more complex baseline algorithm in which a baseline correction is determined separately within each of three segments defined by end points at times t_1 and t_2 . This baseline correction method can be applied to any record, with the advantage that the trailing and leading velocities will oscillate around zero (a physical constraint), but the method requires selection of the appropriate times t_1 and t_2 . Without a physical reason for choosing these times—for instance, based on a knowledge of a specific instrument—the choices of t_1 and t_2 remain subjective (Boore, 2001). A common simplification is to assume that t_1 is equal to t_2 . Although this seems to be a sufficient correction for many records (Boore and Bommer, 2005), it may be inadequate for records with more complex baseline irregularities that require different functional forms to be applied over several intervals.

PRISM incorporates an adaptive baseline correction (ABC) scheme to address cases where the initial baseline correction (described in step 4) is not satisfactory. The ABC scheme, illustrated in figure 8, is modified from the method of Iwan and others (1985). In this scheme, a series of piecewise linear or higher order polynomials are fit to the velocity time series obtained in step 3 to remove or to minimize the long-period noise or drift in the signal. Specifically, the first step is to independently fit polynomials

Adaptive Baseline Correction

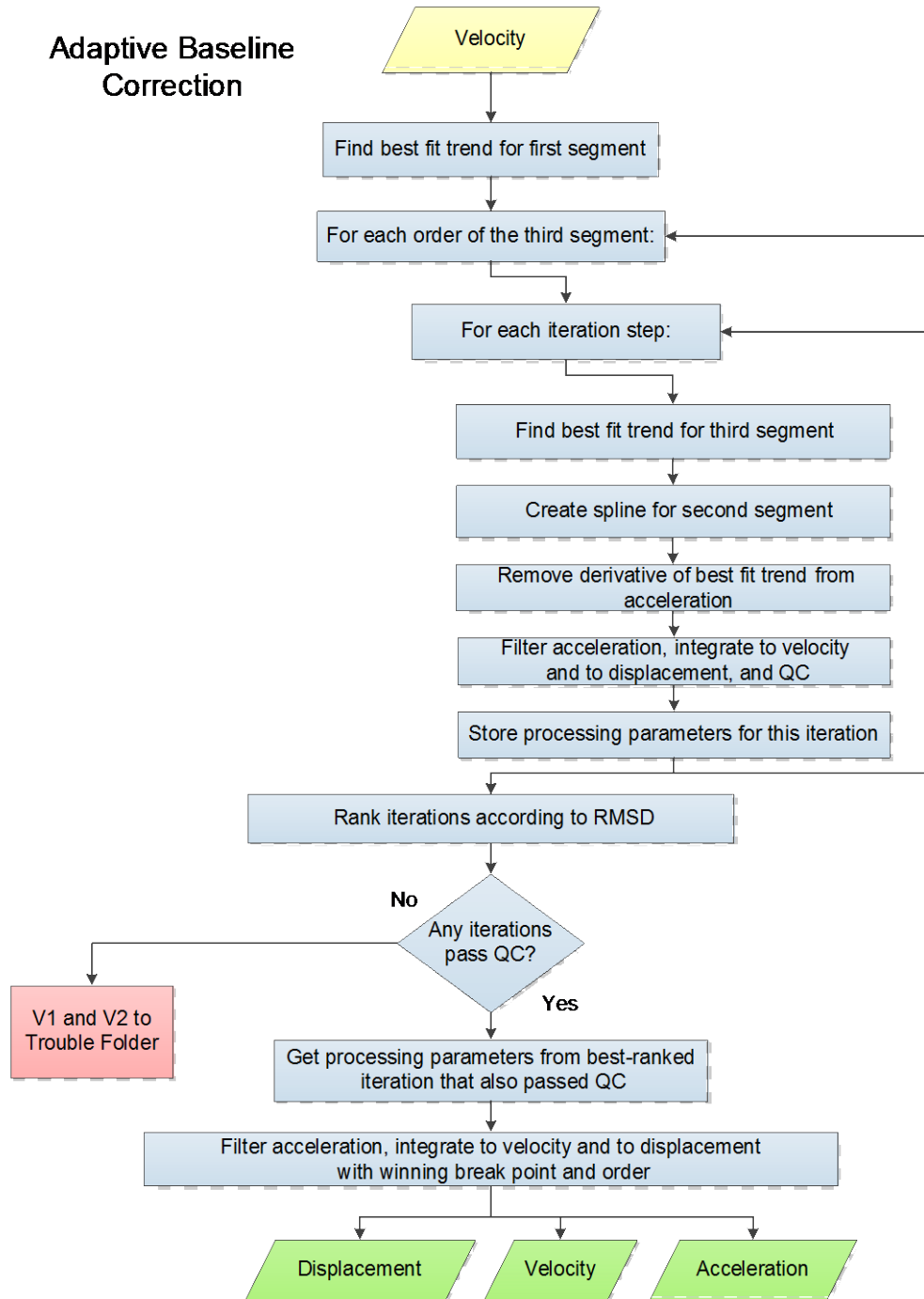


Figure 8. Flow chart showing adaptive baseline correction (ABC) adopted in the Processing and Review Interface for Strong Motion data (PRISM) software for correcting velocity time series for which initial baseline correction is not satisfactory for removing implausible trends.

to the leading (0 to t_1) and trailing (t_2 to end) sections of the velocity time series, outside the interval of strongest motions. These two polynomials, computed with a least-square method, are connected by a cubic spline between t_1 and t_2 (Wang, 1996).

In ABC, the time t_1 is set equal to t_p (the event onset time). The ABC fitting routine then uses a heuristic-based iterative method to determine optimal values for the time t_2 and the order of polynomials (n_p), such that the following requirements are satisfied:

1. A goodness of fit parameter should be minimized.
2. Boundary conditions should be met within specified tolerances. The boundary conditions are that the leading and trailing velocities and the trailing displacements should all oscillate around zero reference.

This method generates a sequence of approximate solutions by incrementing t_2 by the configurable parameter Δt_{ABC} , and by varying n_p over a range specified in the configuration file (currently 1 [linear] to 2 [quadratic] for the first polynomial and 1 [linear] thru 3 [cubic] for the second polynomial). Smaller Δt_{ABC} values yield more accurate results at the expense of increasing the processing time. t_2 gets closer to t_p as much as $1/f_{lc}$ to avoid introducing an artifact. By trial and error, it was determined that a value of Δt_{ABC} corresponding to 200 samples produces reasonably robust fits while maintaining acceptable processing times. The method is called “convergent” if the corresponding sequence minimizes the square root of the sum of the squares (SRSS) of root mean square deviation ($RMSD$), and the boundary conditions (described previously) are met within the specified tolerances (described in step 11 and given in the configuration file). For the entire velocity record, the \overline{RMSD} is computed by taking SRSS of $RMSD$ values of the three individual segments—first polynomial, spline, and second polynomial— as

$$\overline{RMSD} = \sqrt{\sum_{n=1}^3 (RMSD_n)^2} \quad (7)$$

After the ABC, any residual low-frequency noise is removed by bandpass filtering, as described in step 8.

In order to demonstrate how ABC works, figure 9A shows a sample record—the north-south component of acceleration recorded at the USGS Northern California (NC) seismic station JBR from the 2014 $M6.0$ South Napa earthquake—after removal of the pre-event mean (step 2). Figure 9B shows the integration to velocity (step 3) where there is a clearly identifiable, time-varying offset in the baseline beginning at about 100 s. The initial baseline correction (step 4) is applied to correct for the type of baseline shift shown in figure 9B, and the adjusted velocity is plotted in figure 9C. Although the initial baseline correction removed the apparent trend in the later part of the record (approximately 100 to 180 s), it distorted the beginning part (0 to 33 s). This record failed the QC in step 6 because the average leading velocity is higher than the tolerance value (0.01 cm/s), and the record was flagged automatically for further processing by ABC.

As shown in figure 10A, the ABC procedure is applied to identify sections of the velocity after step 3 (marked in the figure as “Pre ABC”) that appear to have different baseline offsets identified by t_p (33.3 s) and t_2 (43.3 s), and then fitting two quadratic polynomials connected by a spline to these intervals. Although polynomial orders of 1 and 3 were also tried, quadratic polynomials within each interval resulted in the best fit for this particular record. The red curve, obtained adaptively, is then differentiated and subtracted from the acceleration trace. The velocity time series is obtained by integrating the best trend removed acceleration time series. In the end, the ABC procedure was able to remove the long-period distortions of the baseline visible in uppermost plot as shown in figure 10B.

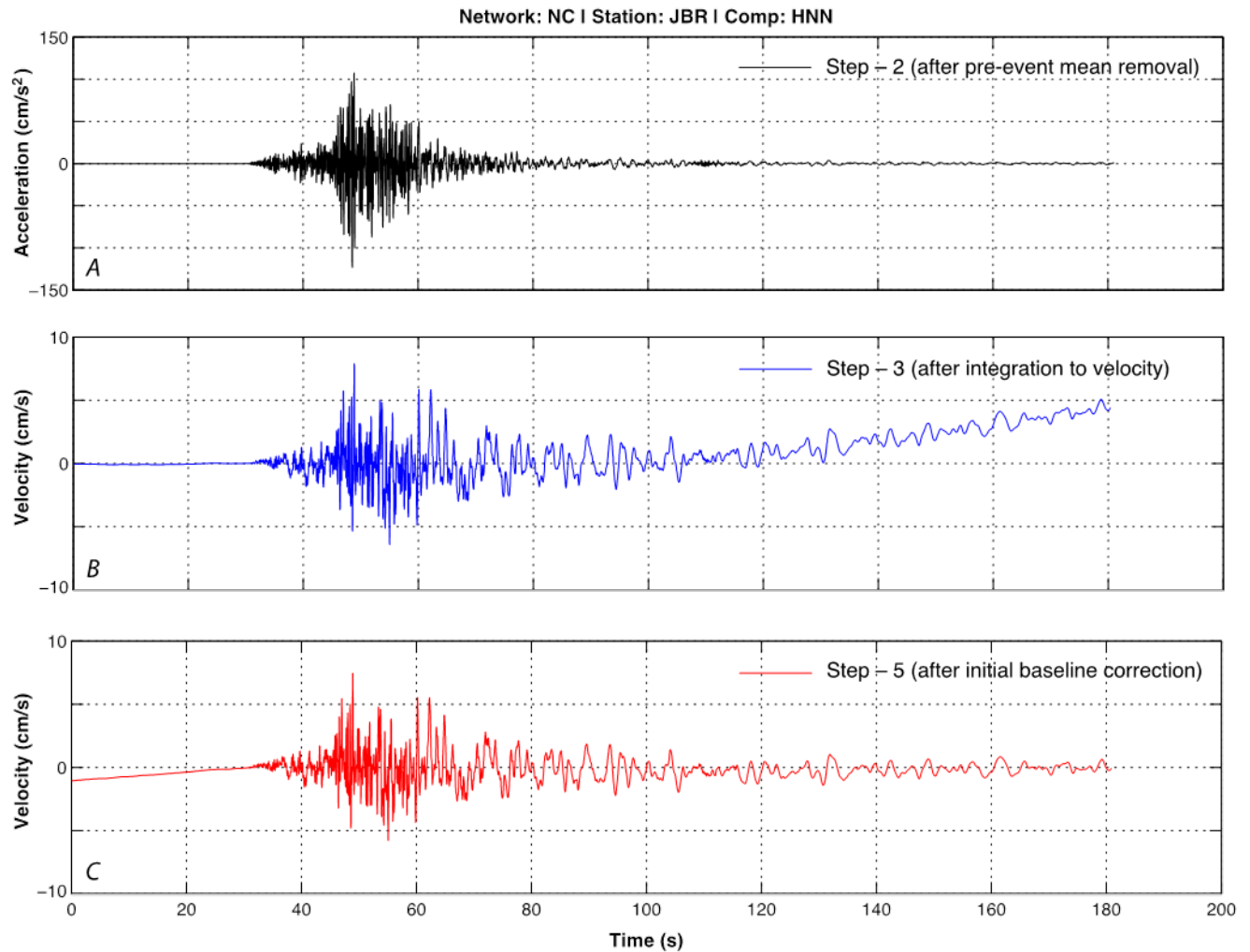


Figure 9. Graphs showing acceleration and velocities after steps 2 through 5 of the Processing and Review Interface for Strong Motion data (PRISM) software. *A*, North-south component acceleration recorded at station JBR from the 2014 *M*6.0 South Napa earthquake, after removal of the pre-event mean from the whole record (step 2, black line). *B*, Velocity from integration of the acceleration (step 3, blue line). *C*, Velocity after initial baseline correction (step 5, red line). Although the initial baseline correction removed the apparent trend in later part of the signal (~100 to 180 seconds [s]), it distorted the beginning part (0 to 33 s). This record was flagged for further processing using adaptive baseline correction. cm/s, centimeters per second; cm/s², centimeters per second squared.

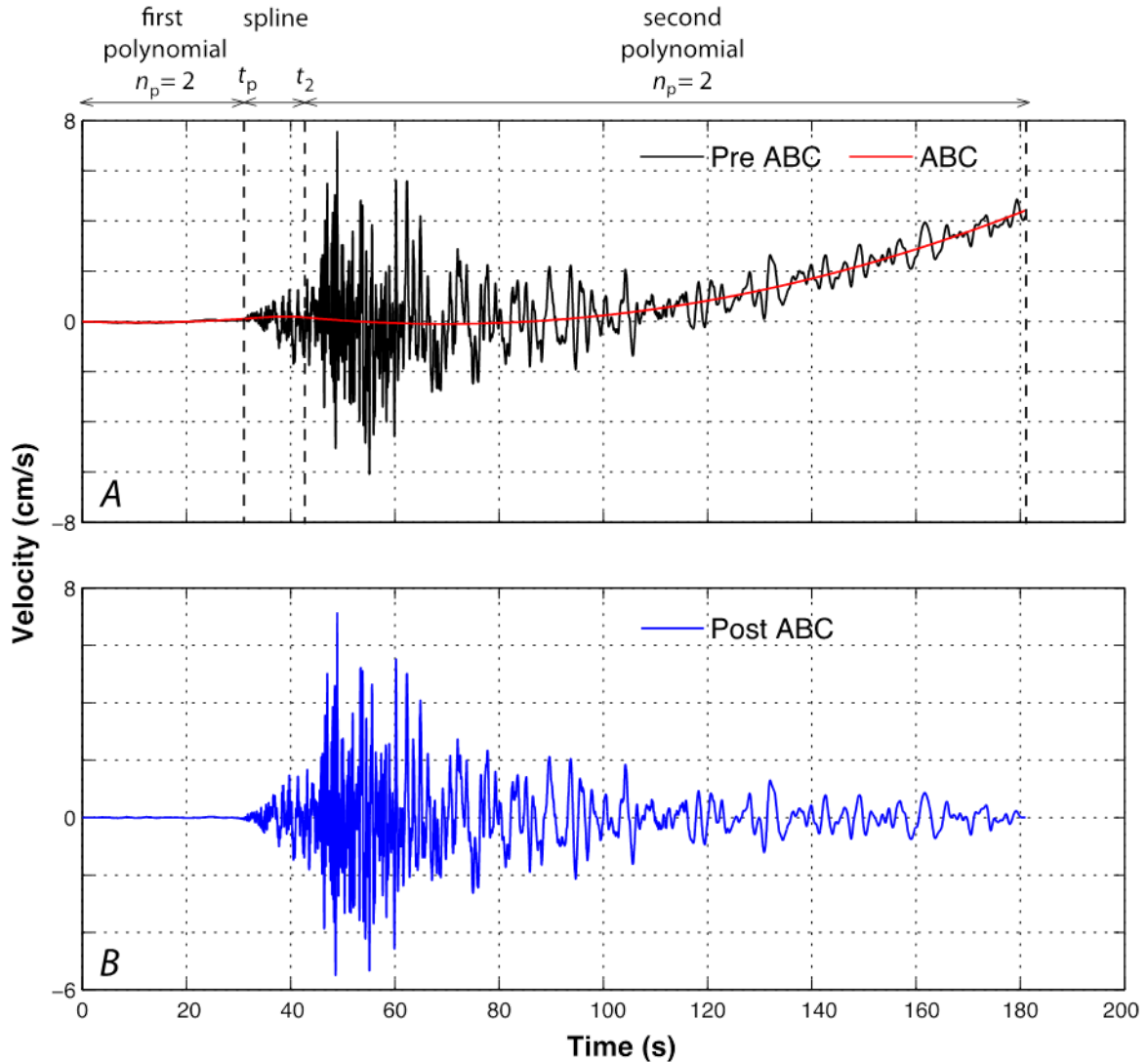


Figure 10. Graphs showing velocities before and after adaptive baseline correction (ABC). A, Uncorrected velocity (black line) and adaptive baseline fit (red line). The baseline fit consists of a quadratic ($n_p = 2$) polynomial fit to the velocity from 0 to event onset (t_p) at 33.3 seconds (s), a quadratic polynomial fit from $t_2 = 43.3$ s to the end of the record, and a spline connecting these two polynomials between t_p and t_2 . B, Velocity with the adaptive baseline correction (blue line), which does not show visible long-period distortions. The sampling rate is 200 samples-per-second. cm/s, centimeters per second.

Step 10—Computation of Velocity and Displacement

Velocity and displacement are obtained by using the trapezoid rule for numerical integration of the corrected acceleration time series.

Step 11—Quality Check for Final Velocity and Displacement

Using the same procedure described in step 6, PRISM finds the means of the leading and trailing velocity windows and the trailing displacement window, and compares these to threshold values

specified in the configuration file. QC passes if all three means are less than or equal to the specified thresholds values. Default threshold values are as follows:

- Leading velocity threshold = 0.01 cm/s
- Trailing velocity threshold = 0.01 cm/s
- Trailing displacement threshold = 0.01 cm

This final QC assures physical plausibility of the velocity and displacement time series, such that both quantities oscillate around zero prior to earthquake onset and after the interval of strong motion.

It should be noted that strong-ground motions recorded close to a fault rupture (generally within about 20 kilometers [km]) may contain static offsets in displacement as a result of the faulting mechanism. Because of filtering, the automated processing does not retain such offsets; alternative methods could be implemented in PRISM to recover such offsets.

V3 (Volume 3) Processing

V3 processing involves computation of response spectra, Fourier amplitude spectra (FAS), and earthquake-engineering intensity measures (IMs). The V3 processing, illustrated in figure 11, is performed in either the time or frequency domain as appropriate.

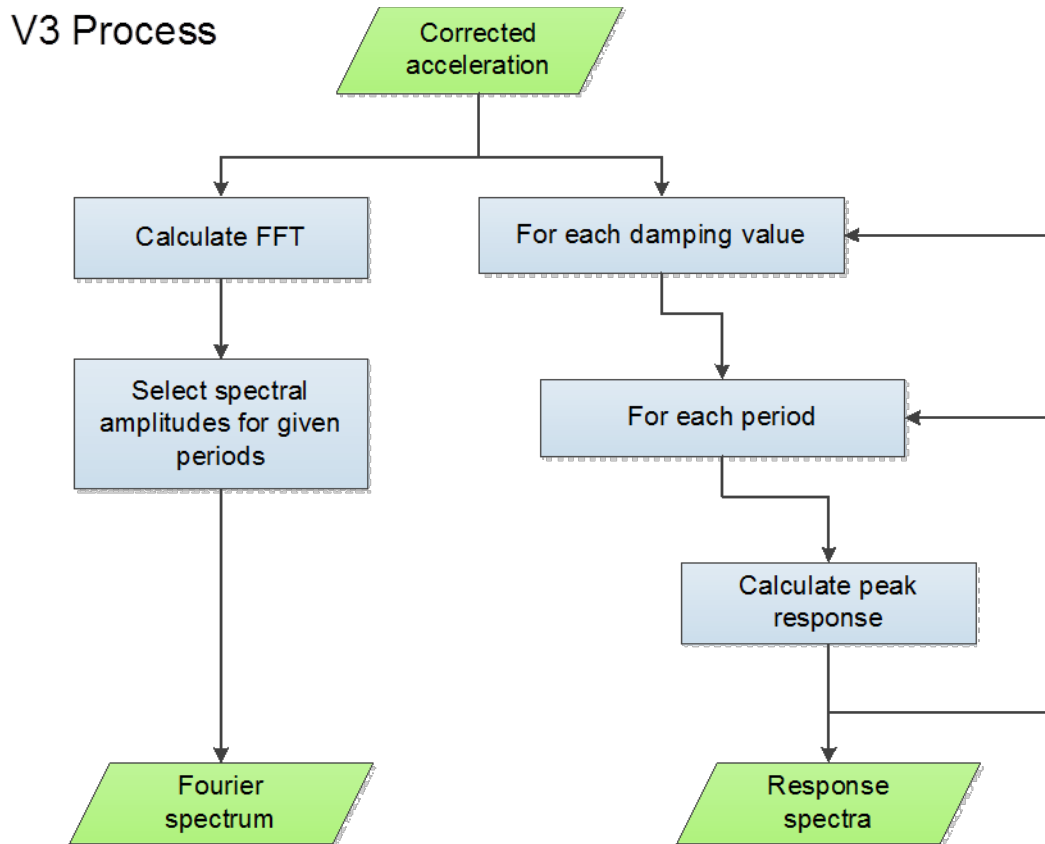


Figure 11. Flow chart showing volume 3 (V3) data processing using corrected acceleration time series to generate elastic response spectra for pseudo-acceleration, velocity, and displacement at different damping values, and Fourier amplitude spectrum.

Calculation of Response Spectra

Elastic response spectra for pseudo-acceleration, velocity, and displacement are computed following the numerical method of Nigam and Jennings (1969), which is based on the exact solution of the second-order ordinary differential equation of motion describing the peak response of a single-degree-of-freedom (SDF) oscillator subjected to base acceleration. The spectra are computed for 0, 2, 5, 10, and 20 percent of critical damping over a wide range of periods (0.04 to 15 s). The lower and upper bounds on spectral periods are independent of the filter corners.

Calculation of Fourier Amplitude Spectra

The Fourier amplitude spectrum (FAS) is computed by applying a fast Fourier transform (FFT) to the acceleration time series derived from the corrected velocity in step 9. The FFT requires that the number of samples in the input time series be an integral power of 2. Also, a weighting function is applied to minimize spectral leakage (caused by sudden jump between zero-padding and the signal). Tapering and zero-padding were applied in the filtering step, so PRISM ensures that the number of data points is a power of 2 by extending the time series with additional zero-padding as needed.

Standard COSMOS format requires computation of Fourier amplitudes at certain frequencies (0.066 to 25 Hz); these frequencies correspond to spectral periods (0.04 to 15 s) used for computation of response spectra. Low sampling at high frequencies results in smooth FAS.

Calculation of Earthquake-Engineering Intensity Measures

PRISM calculates various earthquake-engineering IMs related to the duration and amplitude of the seismic signal to include in header of COSMOS V3 files. The IMs computed include the following:

Arias Intensity

The Arias intensity (I_A) is defined as a constant multiplied by the integral of the square of the acceleration time series over the entire duration of the record (Arias, 1970). It has units of velocity and is expressed in meters per second (m/s) as

$$I_A = \frac{\pi}{2g} \int_0^{\infty} \ddot{u}_g(t)^2 dt \quad (8)$$

Where $\ddot{u}_g(t)$ is the acceleration of ground motion, and g is gravitational acceleration ($1 g = 9.80665 \text{ m/s}^2$).

Bracketed Duration

The bracketed duration ($T_{\text{bracketed}}$) (Bolt, 1969) is defined as the time between the first and last exceedance of a threshold acceleration value, usually 5 percent g (Kramer, 1996). It is computed as

$$T_{\text{bracketed}} = T_2 - T_1 \quad (9)$$

where T_1 is the first moment that the absolute value of acceleration is greater than 5 percent g , and T_2 is the last moment that the absolute value of acceleration is greater than 5 percent g . The unit of $T_{\text{bracketed}}$ is second.

Duration Interval

The duration interval (T_{interval}) is based on the time interval between the points at which 5 and 95 percent of the total energy (Trifunac and Brady, 1975), and it is defined as

$$T_{\text{interval}} = t(I_{Ai} = 0.95 \times I_A) - t(I_{Ai} = 0.05 \times I_A) \quad (10)$$

where I_A is the Arias intensity of the whole ground-motion time series, I_{Ai} is the Arias intensity on the i^{th} moment of ground motion, and $t(I_{Ai} = 0.95 \times I_A)$ is the moment that the I_{Ai} equals 95 percent of I_A . The unit of T_{interval} is in seconds.

Response Spectrum Intensity

Because most regular buildings (low- and midrise) typically have a fundamental vibration period (T_n) between 0.1 and 2.5 s, the response spectrum ordinates within this period range should indicate the potential response of these structures. Based on this premise, the response spectrum intensity (SI), as defined in Housner (1959), corresponds to the area under the pseudo-velocity response spectrum (PSV) between spectral period (T) 0.1 and 2.5 s for a particular damping ratio (ζ). In computing SI , the ordinates of PSV are taken as centimeters per second as

$$SI(SI(\zeta)) = \int_{0.1}^{2.5} PSV(\zeta, T) dT \quad (11)$$

Root Mean Square (RMS) Acceleration

A single intensity measure that includes amplitude effects and strong-ground motion duration is the root mean square acceleration (a_{rms}), defined as

$$a_{rms} = \sqrt{\frac{1}{T_d} \int_{t_1}^{t_2} \ddot{u}_g(t)^2 dt} \quad (12)$$

where T_d is the duration of the strong motion; $t_1 = t(I_{Ai} = 0.05 \times I_A)$, $t_2 = t(I_{Ai} = 0.09 \times I_A)$, and I_A are the Arias intensity of the whole ground-motion time history. a_{rms} is influenced most by motion duration, and it is not strongly influenced by large, high-frequency accelerations, which take place only over a short time interval. The value of a_{rms} is sensitive to the method used to define T_d . In PRISM, T_d is defined as duration interval (T_{interval}). The unit of a_{rms} is meters per second squared (m/s^2).

Cumulative Absolute Velocity

Cumulative absolute velocity (CAV) is the area under the absolute accelerogram, and it is sensitive to potentially damaging low-frequency motions but less sensitive to high-frequency motions. The total CAV (denoted as CAV_{Total}) is defined by the Electric Power Research Institute (1991) as

$$CAV_{\text{Total}} = \left[\sum_{i=1}^N \int_{t_i}^{t_{i+1}} |\ddot{u}_g(t)| dt \right] \quad (13)$$

where $\ddot{u}_g(t)$ is acceleration values in g during a one-second interval in which at least one absolute acceleration value exceeds 0.025g, and $i=1$ through N_i are the number of one-second intervals in the record. The unit of CAV_{Total} is gravitational acceleration per second (g-s); it is converted to meters per second in the V3 file.

Configuration File Parameters

PRISM uses a configuration file for controlling and customizing the processing steps. Table 2 presents default values for parameters that can be specified in the configuration file.

Processing Agency

The agency that processes a strong-motion record is identified according to table 2, Strong-Motion Network Codes, in the COSMOS Strong Motion Data Format specification (Consortium of Organizations for Strong-Motion Observation Systems, 2001). For each agency, there is a full name, an abbreviation, a COSMOS agency code, and Incorporated Research Institutions for Seismology (IRIS) network (agency) code (<http://ds.iris.edu/ds/nodes/dmc/services/network-codes/?sort=netcountry&initial=I>, last accessed January 2017). Current PRISM software utilizes the COSMOS agency abbreviation and agency code. The current version of COSMOS tables can be downloaded from <http://strongmotioncenter.org/aboutcesmd.html> (last accessed January 2017).

Data Units for Uncorrected Acceleration

The data units specified here identify the units to use for conversion from counts to uncorrected acceleration during V1 processing. The V1 product file will contain the uncorrected acceleration time series in these units. Entries are taken from table 2, Data unit code, in the COSMOS Strong Motion Data Format specification (Consortium of Organizations for Strong-Motion Observation Systems, 2001). Units of either centimeters per second or gravitational acceleration are currently supported. This does not affect units of the data time series of the V2 product files; those units are fixed at centimeters per second square for acceleration, centimeters per second for velocity, and centimeters for displacement.

Event Detection Method

There are currently two algorithms available in PRISM for event onset detection: PWD (synonymous with $P_{PHASEPICKER}$ in Kalkan, 2016), and AIC, the modified Akaike Information Criterion method (Maeda, 1985). These algorithms are explained in appendix 2.

Event Onset Buffer Amount

The pre-event time interval is set to the computed event onset time less a short time interval (event onset buffer amount) to allow for uncertainty in onset time.

Quality Check (QC) Parameters

The QC parameters define acceptable limits for initial and trailing velocities and displacements during V2 processing. If, during QC tests, the average of the initial and (or) trailing values within prescribed intervals are less than or equal to these parameters, then the record passes on to V3 processing.

Bandpass Filter Parameters

The configuration file bandpass filter parameters allow selection of the filter order (n), taper length (T_{taper}), and high-cut (f_{hc}) and low-cut (f_{lc}) filter corners for the time-domain Butterworth filter in certain cases. Filtering is performed on the uncorrected acceleration record during event onset detection (step 1 of volume 2 processing), and on the acceleration record to remove high- and low-frequency

noise before integrating to velocity and subsequently integrating to displacement (step 10). The filter order (n) in the configuration file is used to define the Butterworth filter order for both step 1 and step 7. This filter implementation expects an even-valued filter order. If an odd number is entered, it will be truncated by integer division to the next lower multiple of two. The values of f_{hc} and f_{lc} in the configuration file apply only to the filtering in step 1, and the values of these parameters used in step 8 are chosen as defined in table 1. The taper length in the configuration file defines the length of time (in seconds) at the beginning and end of the time series over which to apply the cosine taper during step 1. This is used in place of the taper length calculations defined in step 7, which rely on a known event onset value.

Adaptive Baseline Correction

The adaptive baseline correction (ABC) algorithm is similar to the method developed by Iwan and others (1985), in which three segments are defined for constructing a baseline correction function. The first segment, from the start of the velocity time series until the event onset, is fitted with a polynomial that has a range of orders defined by the FirstPolyOrder tag. The third segment, for which the start is determined by an iterative process, is fitted with a polynomial that has a range of orders defined by the ThirdPolyOrder tag. The middle segment is fitted with a cubic spline that connects smoothly the first and third segments. Table 2 shows the default values for the upper and lower limits of the first and third polynomials, which can be customized in the configuration file. As an example, if the first polynomial upper limit equals 2, then the ABC algorithm will perform first- and second-order fits for the first polynomial (first segment). Upper limits of 2 and 3 for the first and third polynomials, respectively, are found to be sufficient for correcting most strong-motion records.

Strong-Motion Threshold

The strong-motion threshold parameter determines the percent of gravitational acceleration that the PGA of the corrected acceleration needs to meet or exceed in order to classify the record as being strong motion. If the record qualifies, then the earthquake-engineering IMs are calculated and reported in the V3 files.

Differentiation Order

The differentiation order defines the solution order for the central difference operator for differentiation.

Output Array Format

The output array format controls the number of data values written to each line in the COSMOS output file. A value of "SingleColumn" will result in one data value per line in the output file, and a value of "Packed" will pack multiple values per line to fill the 80-character line width.

DeleteInputV0

The DeleteInputV0 flag controls the deletion of files from the input folder as they are processed. If the flag is set to "Yes," then input files that are successfully processed will be deleted from the input folder. This option is for an automated processing configuration. To leave the input files in the input folder after execution is complete, set this flag to "No."

DebugToLog

The DebugToLog flag controls the amount of information that is written to the DebugLog text file and the ParameterLog comma-separated value (CSV) file during processing. If this flag is set to “Off,” then only information about records that fail to pass V2 processing QC tests will be written to the debug logs. If the flag is set to “On,” then debug information about all processed records will be written to the debug logs. This flag does not affect the contents of the PrismLog and the TroubleLog.

WriteBaselineFunction

To assist in analyzing potentially problematic records, the WriteBaselineFunction option is provided. If set to “On,” the WriteBaselineFunction will write to the output folder text files of baseline functions created during ABC. It will also write to a text file the velocity time series as it appears before baseline correction (after step 3 in V2 processing description). File names will be the V0 file name with either baseline.txt or afterIntegrationToVel.txt appended to it. If the flag is set to “On” and no baseline text files are output, then ABC was not used for processing.

Table 2. Configuration file parameters and defaults.

[AIC, Akaike information criterion; cm, centimeters; cm/s, centimeters per second; COSMOS, Consortium of Organizations for Strong-Motion Observation Systems; Hz, hertz; PWD, *P*-wave phase onset time detector (that is, $P_{PHASEPICKER}$); s, seconds; UNKN, unknown; >, greater than; <, less than]

Parameter	Options	Default
Agency full name	See COSMOS table 4	unknown
Agency abbreviation	See COSMOS table 4	UNKN
Data unit code	See COSMOS table 2	04
Data unit name	See COSMOS table 2	cm/s/s
Event detection method	PWD or AIC	PWD
Event onset buffer amount	Value ≥ 0.0	0.0 s
Initial velocity	Value ≥ 0.0	0.1 cm/s
Trailing velocity	Value ≥ 0.0	0.1 cm/s
Trailing displacement	Value ≥ 0.0	0.1 cm
Bandpass filter order	$4 \leq \text{Value} \leq 16$	4
Taper length	Value ≥ 0	2 s
Onset pick low cutoff	Value < high cutoff	0.1 Hz
Onset pick high cutoff	Value > low cutoff	20 Hz
First polynomial lower limit	1, 2, must be \leq upper limit	1
First polynomial upper limit	1, 2, must be \geq lower limit	2
Third polynomial lower limit	1, 3, must be \leq upper limit	1
Third polynomial upper limit	1, 3, must be \geq lower limit	3
Strong-motion threshold	$0 \leq \text{Value} \leq 100$	5 percent
Differentiation order	3, 5, 7, 9	5
Output array format	SingleColumn or Packed	SingleColumn
Delete input V0	Yes or No	No
DebugToLog	On or Off	Off
WriteBaselineFunction	On or Off	Off

The configuration file (see appendix 3) is parsed according to a schema that will check for missing elements and element values that are out of acceptable range. These errors will be reported to the standard error output stream at the start of processing, and PRISM will stop execution. If the configuration file parameters are valid, then they are written to the log file (see appendix 4) as a record of the current processing environment.

Example V2 and V3 Products

To illustrate end products following the processing procedure described previously, representative processed records (those that passed QC tests) with low and high amplitudes from three events occurred in California are selected—the *M*6.0 South Napa earthquake on August 24, 2014, the *M*4.4 South Dos Palos earthquake on September 28, 2014, and the *M*4.4 Greenfield earthquake on January 20, 2015. Figures 12 through 41 show the final suite of acceleration, velocity, and displacement time histories (V2 products) together with the pseudo-spectral acceleration, pseudo-spectral velocity and displacement response spectra, and Fourier amplitude spectra (V3 products) corresponding to the three channels of each record from these events. The records shown in figures 12 through 31 were processed without a need for ABC. For the records shown in figures 32 through 41, at least one or more channels required processing with ABC; all of these records passed the QC tests. In these figures, we also show uncorrected acceleration (V1) for comparison with the corrected acceleration.

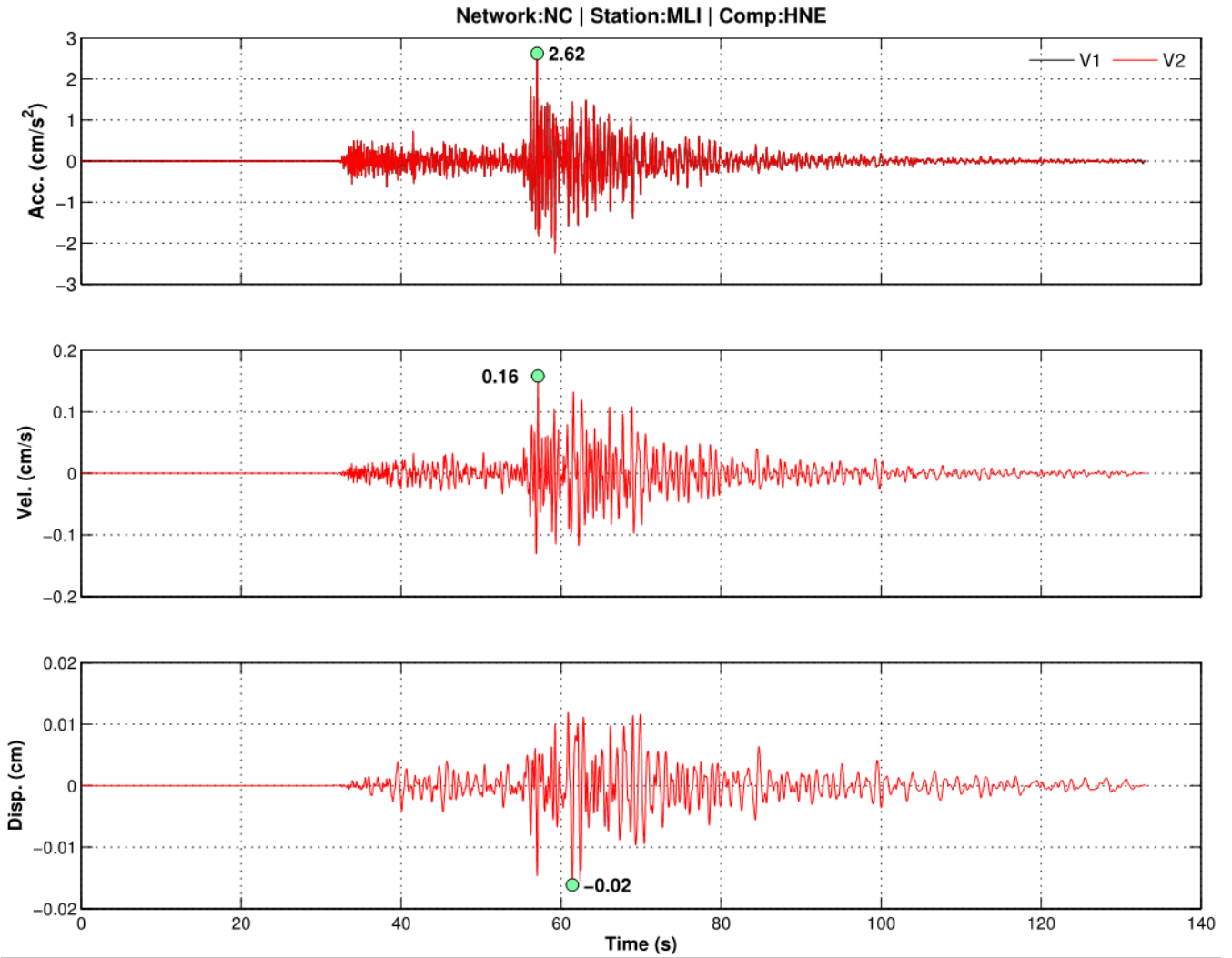


Figure 12. Graphs showing a final suite of acceleration (acc.), velocity (vel.), and displacement (disp.) time series (V2 products, red lines) for channel HNE at station MLI recorded from the 2014 *M*4.4 South Dos Palos earthquake in California. Note that this channel of the record was processed without a need for adaptive baseline correction. Acceleration time series after V1 processing (black line) is also shown in the upper graph for comparison. Green dots indicate peak values of V2 products. cm, centimeters; cm/s, centimeters per second; cm/s², centimeters per second squared; s, seconds.

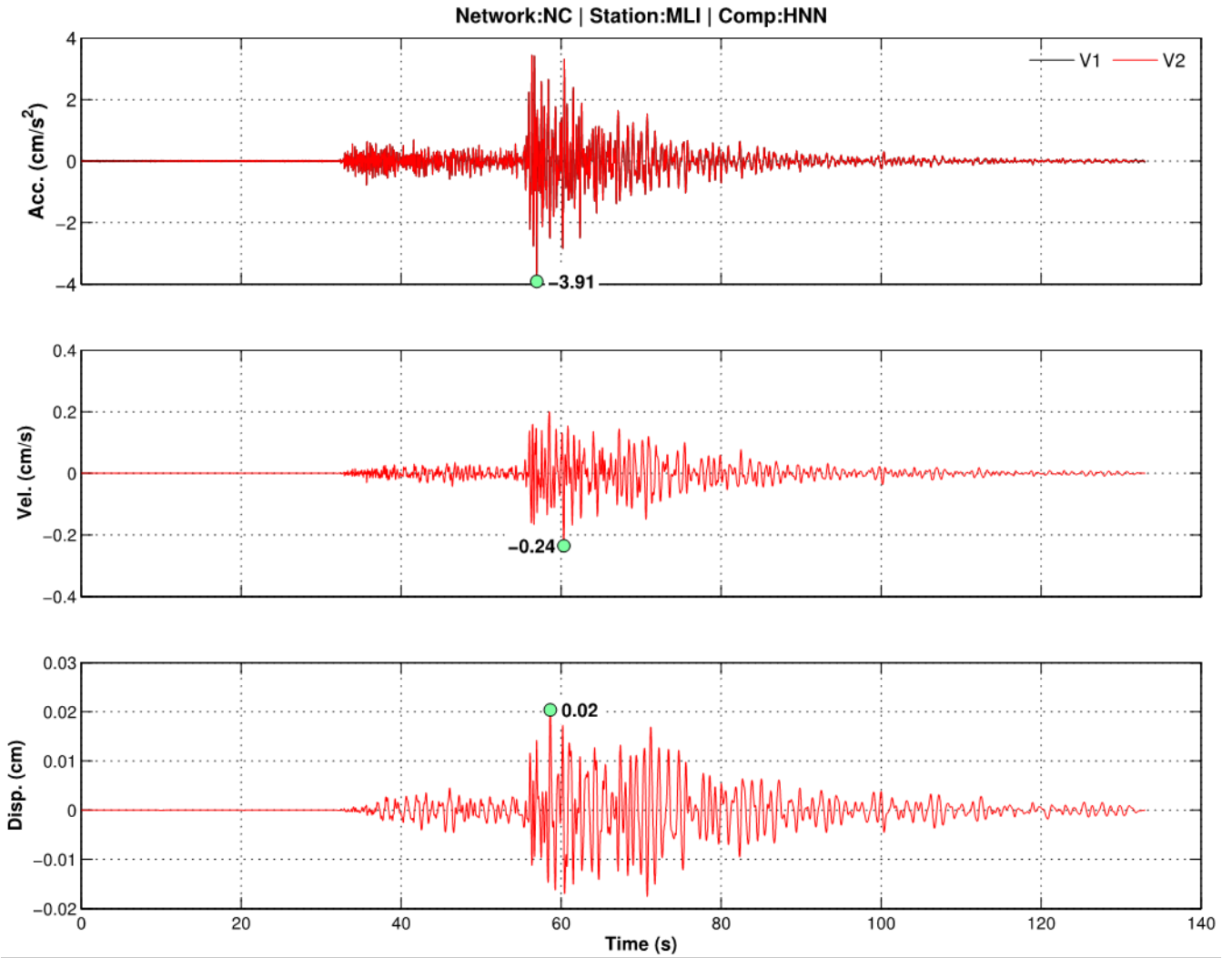


Figure 13. Graphs showing a final suite of acceleration (acc.), velocity (vel.), and displacement (disp.) time series (V2 products, red lines) for channel HNN at station MLI recorded from the 2014 *M*4.4 South Dos Palos earthquake in California. Note that this channel of the record was processed without a need for adaptive baseline correction. Acceleration time series after V1 processing (black line) is also shown in the upper graph for comparison. Green dots indicate peak values of V2 products. cm, centimeters; cm/s, centimeters per second; cm/s², centimeters per second squared; s, seconds.

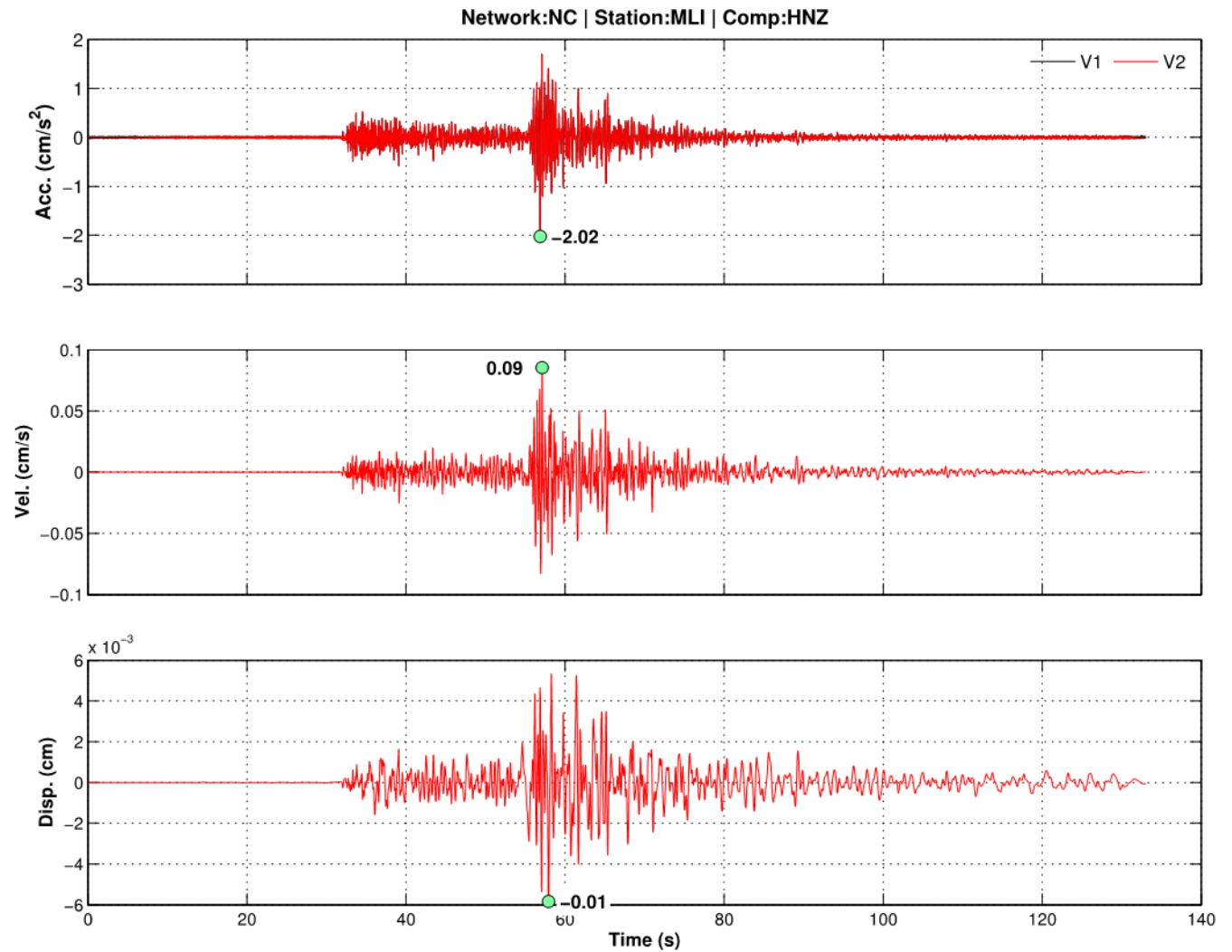


Figure 14. Graphs showing a final suite of acceleration (acc.), velocity (vel.), and displacement (disp.) time series (V2 products, red lines) for channel HNZ at station MLI recorded from the 2014 *M*4.4 South Dos Palos earthquake in California. Note that this channel of the record was processed without a need for adaptive baseline correction. Acceleration time series after V1 processing (black line) is also shown in the upper graph for comparison. Green dots indicate peak values of V2 products. cm, centimeters; cm/s, centimeters per second; cm/s², centimeters per second squared; s, seconds.

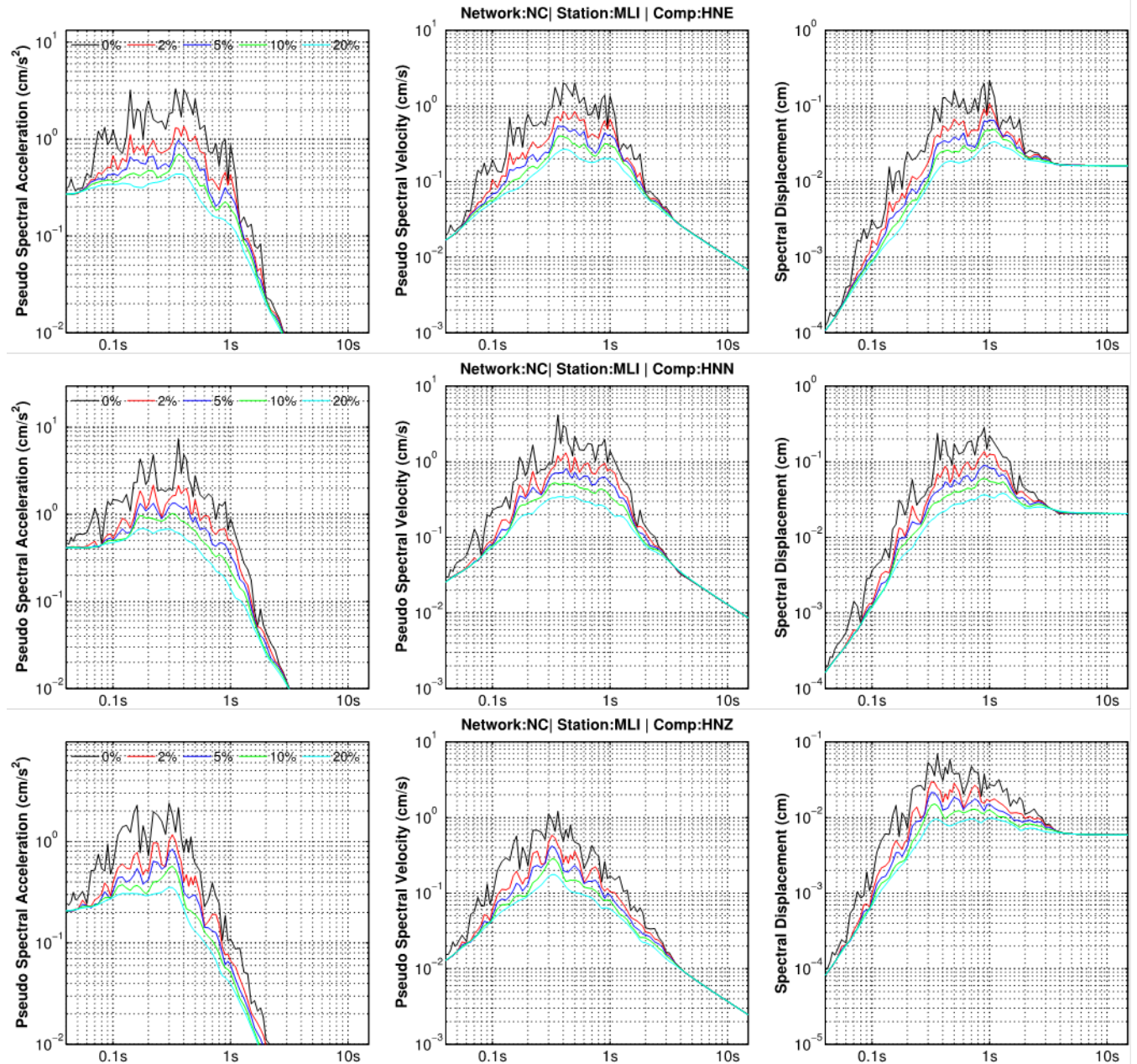


Figure 15. Graphs showing a final suite of pseudo-spectral acceleration, pseudo-spectral velocity, and spectral displacement spectra computed at different damping levels (0, 2, 5, 10, and 20 percent of critical) for three channels of MLI record with 100 samples-per-second from the 2014 *M*4.4 South Dos Palos earthquake in California. cm, centimeters; cm/s, centimeters per second; cm/s², centimeters per second squared; s, seconds.

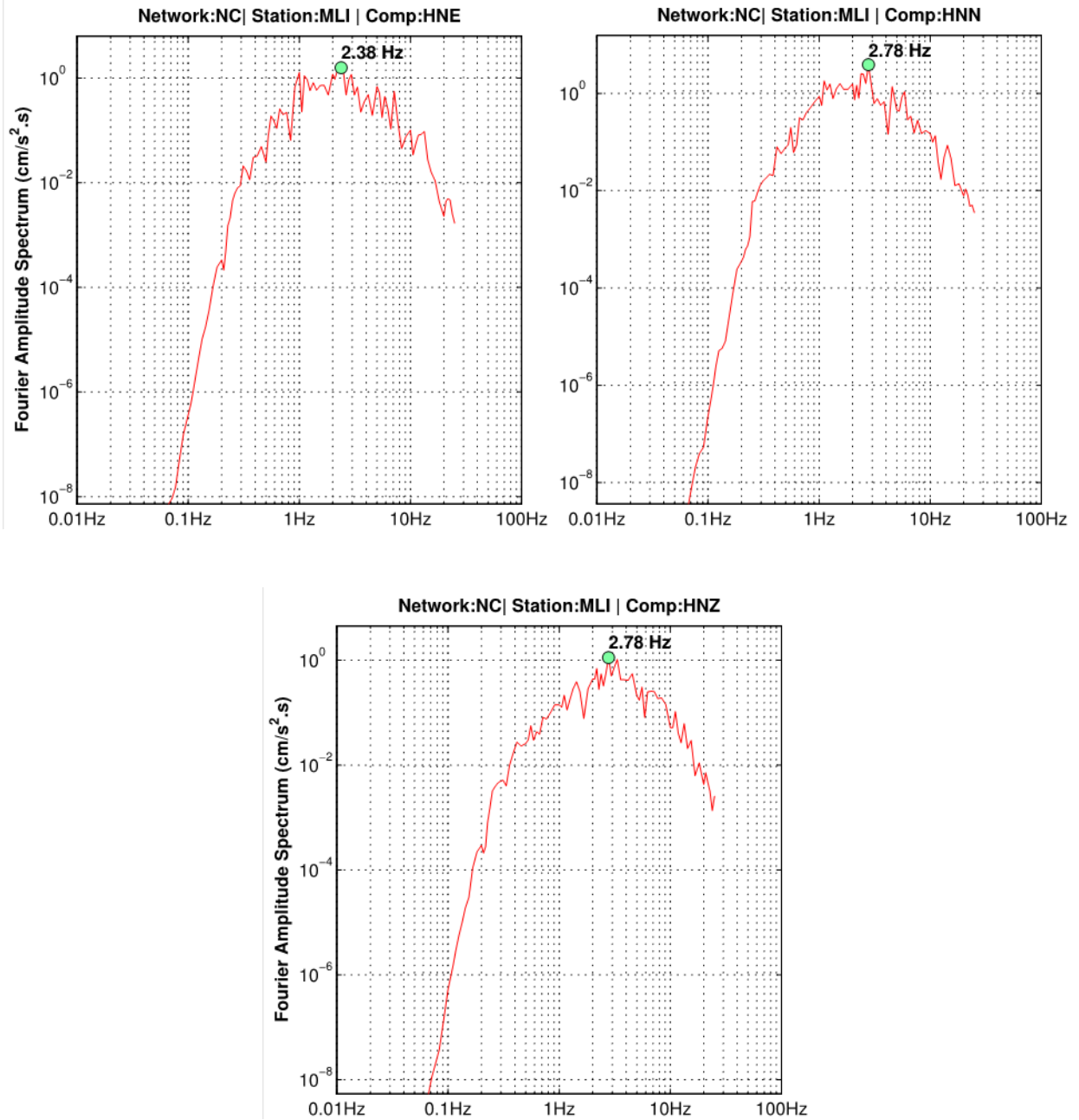


Figure 16. Graphs showing Fourier amplitude spectrum (V3 products, red lines) for three channels of MLI record with 100 samples-per-second from the 2014 *M*4.4 South Dos Palos earthquake in California. Green dots indicate predominant frequency of the signal. cm/s²·s, centimeters per second squared second; Hz, hertz.

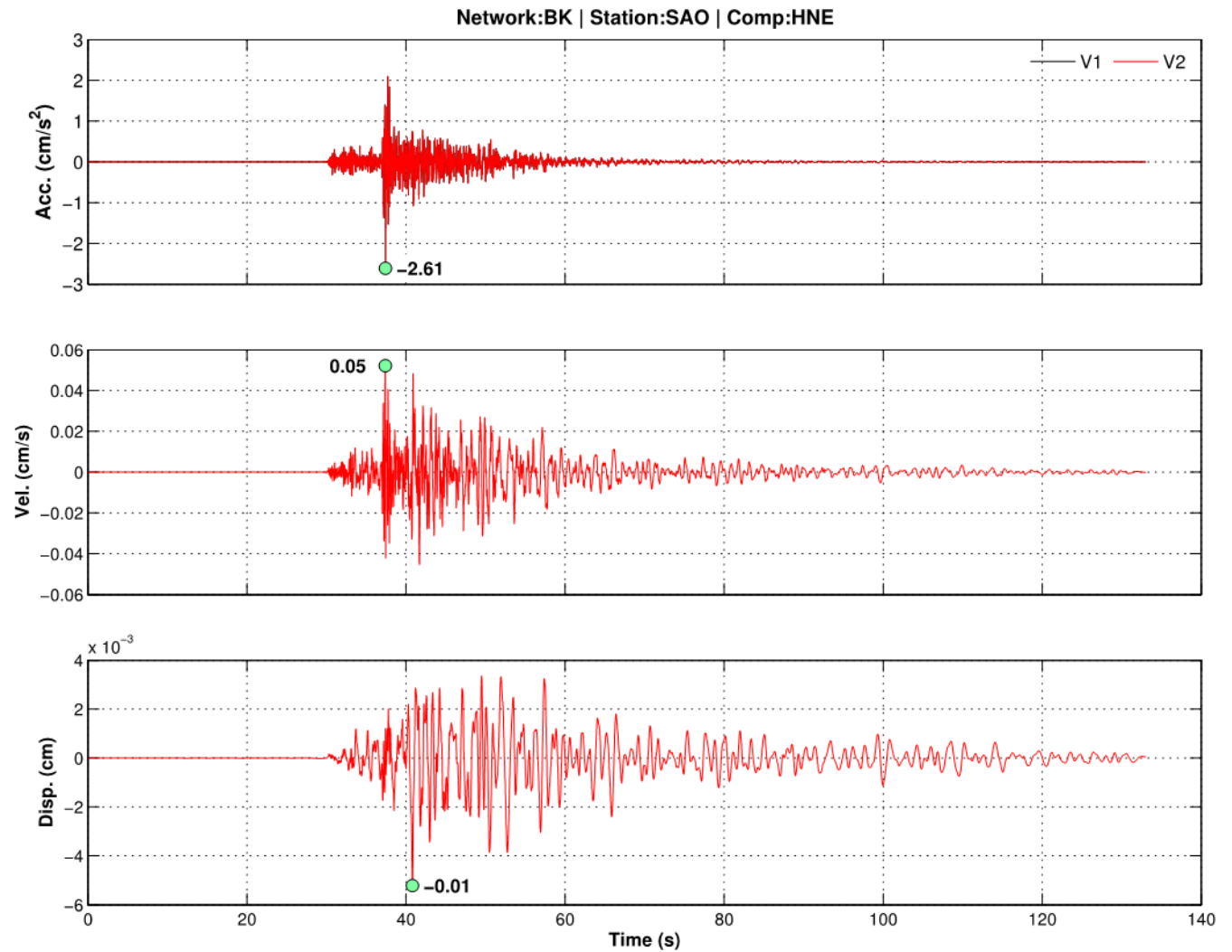


Figure 17. Graphs showing a final suite of acceleration (acc.), velocity (vel.), and displacement (disp.) time series (V2 products, red lines) for channel HNE at station SAO recorded with 100 samples-per-second from the 2014 *M*4.4 Greenfield earthquake in California. Note that this channel of the record was processed without a need for adaptive baseline correction. Acceleration time series after V1 processing (black line) is also shown in the upper graph for comparison. Green dots indicate peak values of V2 products. cm, centimeters; cm/s, centimeters per second; cm/s², centimeters per second squared; s, seconds.

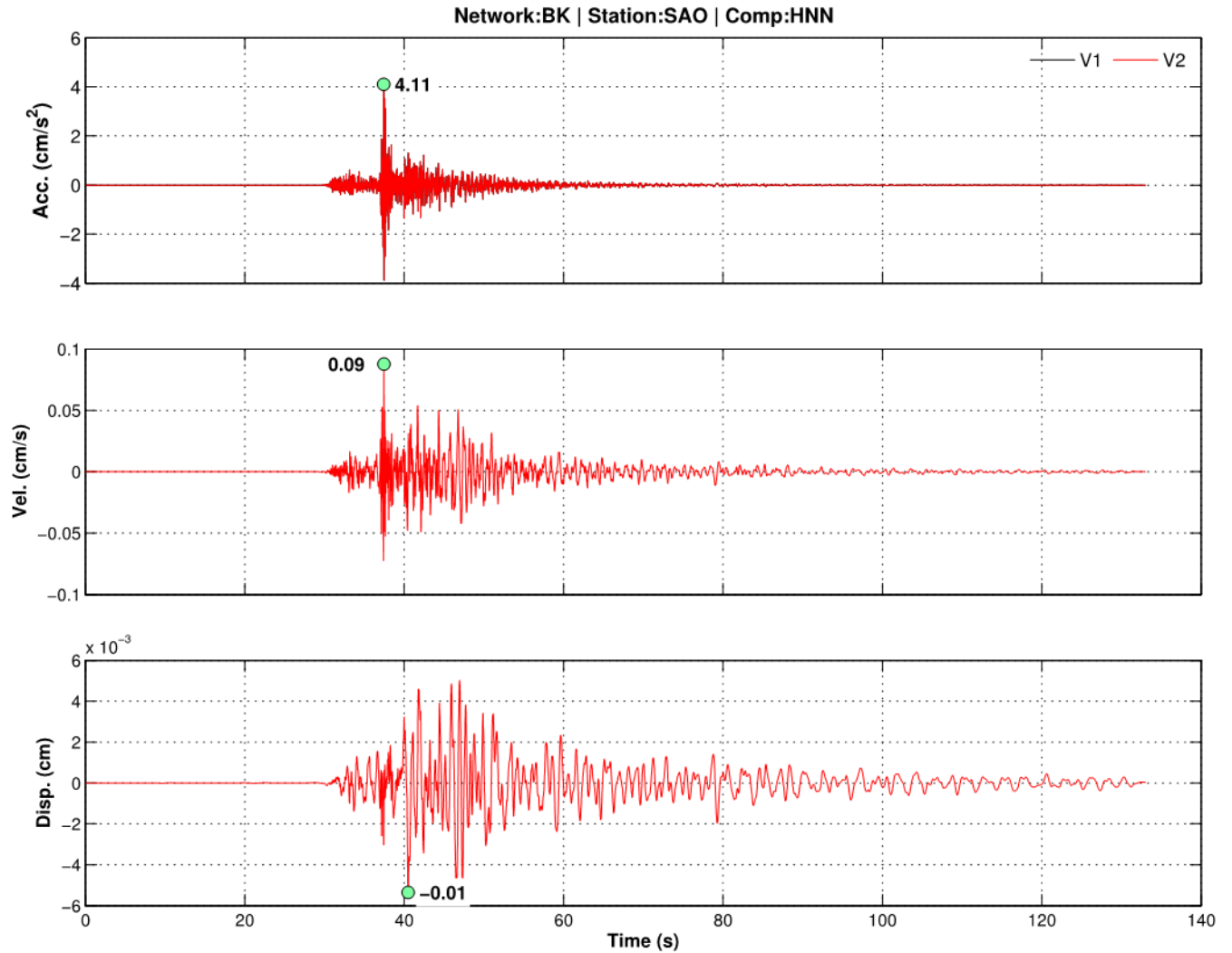


Figure 18. Graphs showing a final suite of acceleration (acc.), velocity (vel.), and displacement (disp.) time series (V2 products, red lines) for channel HNN at station SAO recorded with 100 samples-per-second from the 2014 *M*4.4 Greenfield earthquake in California. Note that this channel of the record was processed without a need for adaptive baseline correction. Acceleration time series after V1 processing (black line) is also shown in the upper graph for comparison. Green dots indicate peak values of V2 products. cm, centimeters; cm/s, centimeters per second; cm/s^2 , centimeters per second squared; s, seconds.

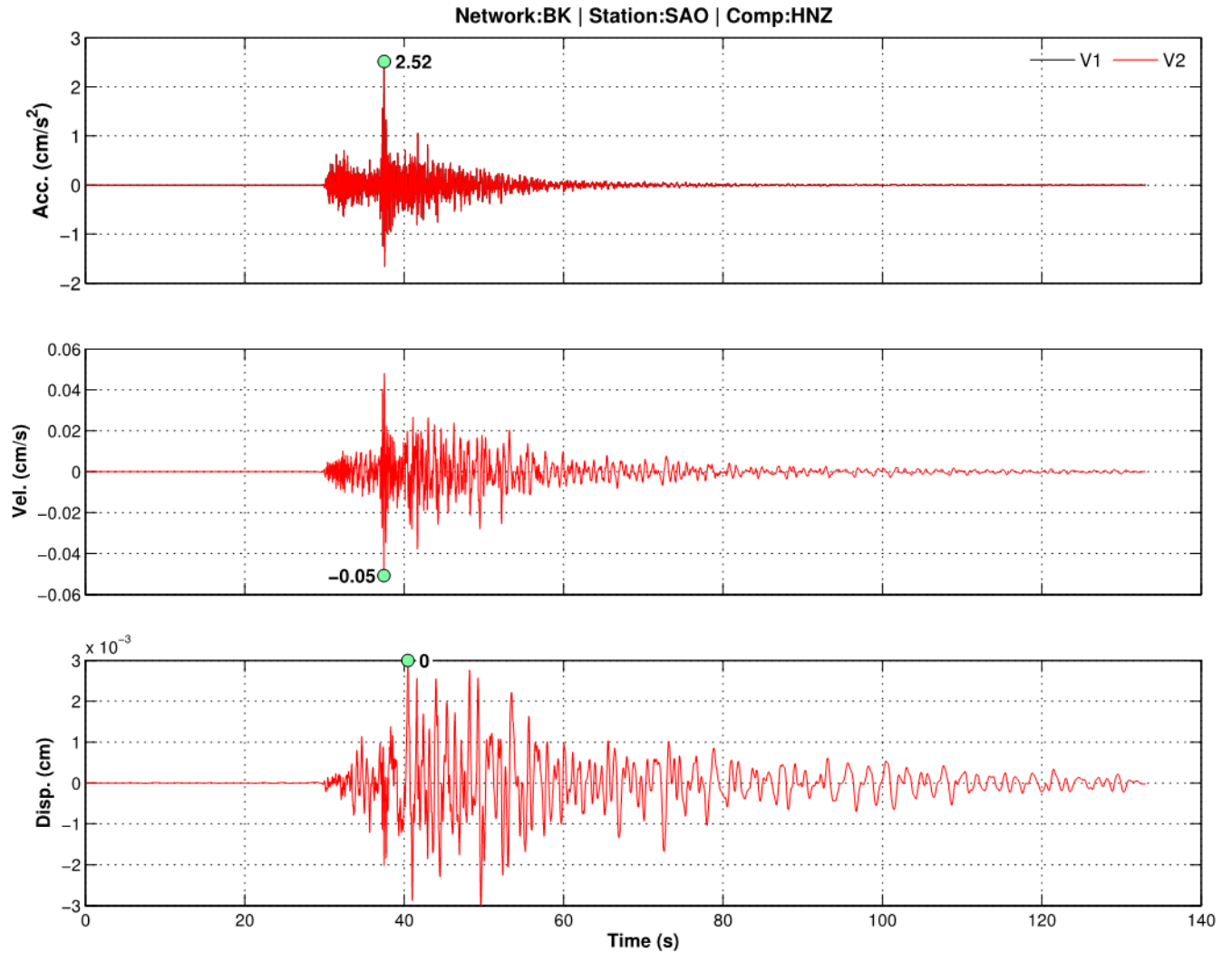


Figure 19. Graphs showing a final suite of acceleration (acc.), velocity (vel.), and displacement (disp.) time series (V2 products, red lines) for channel HNZ at station SAO recorded with 100 samples-per-second from the 2014 *M*4.4 Greenfield earthquake in California. Note that this channel of the record was processed without a need for adaptive baseline correction. Acceleration time series after V1 processing (black line) is also shown in the upper graph for comparison. Green dots indicate peak values of V2 products. cm, centimeters; cm/s, centimeters per second; cm/s², centimeters per second squared; s, seconds.

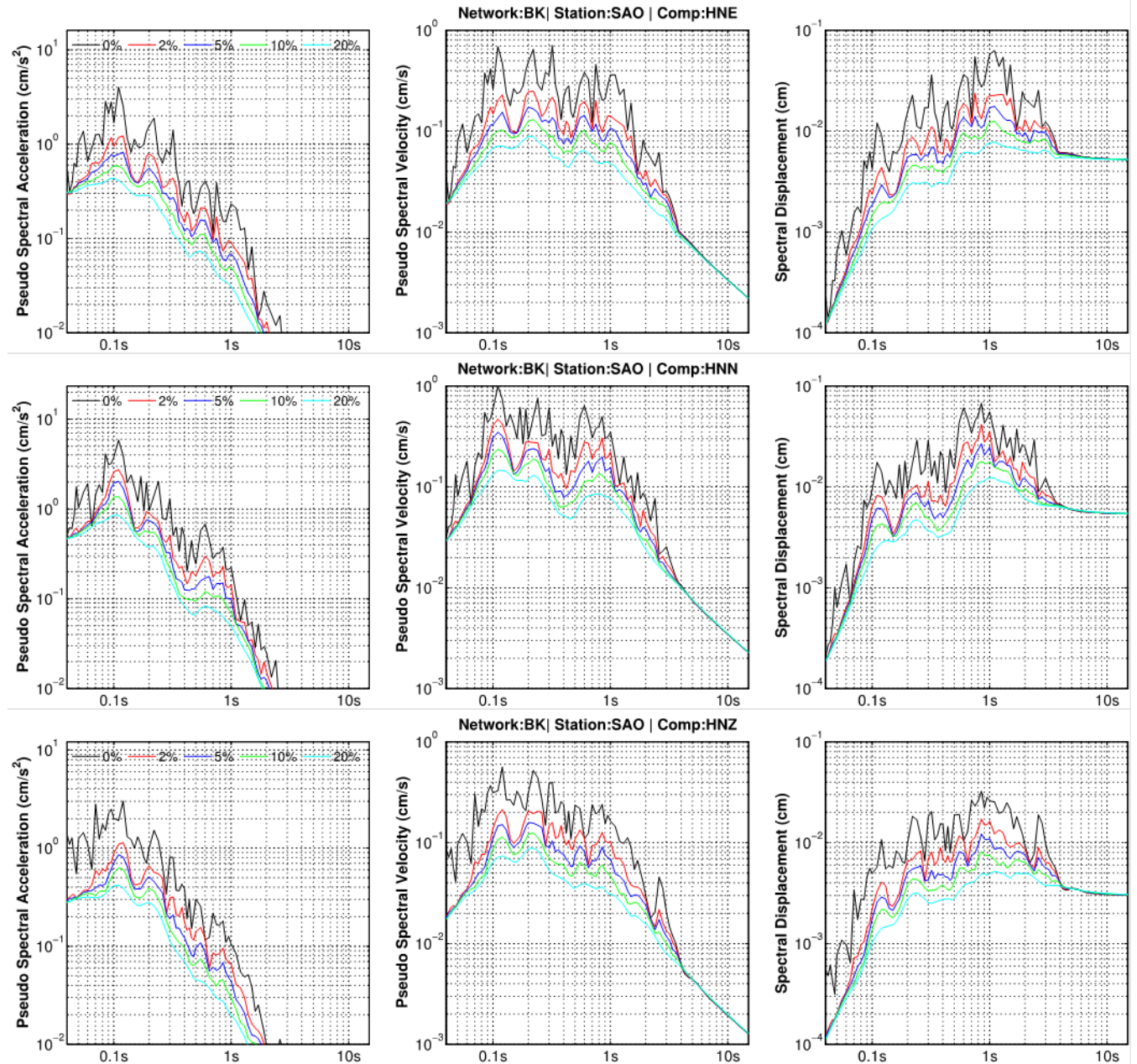


Figure 20. Graphs showing a final suite of pseudo-spectral acceleration, pseudo-spectral velocity, and spectral displacement spectra computed at different damping levels (0, 2, 5, 10, and 20 percent of critical) for three channels of SAO record with 100 samples-per-second from the 2014 *M*_{4.4} Greenfield earthquake in California. cm, centimeters; cm/s, centimeters per second; cm/s², centimeters per second squared; s, seconds.

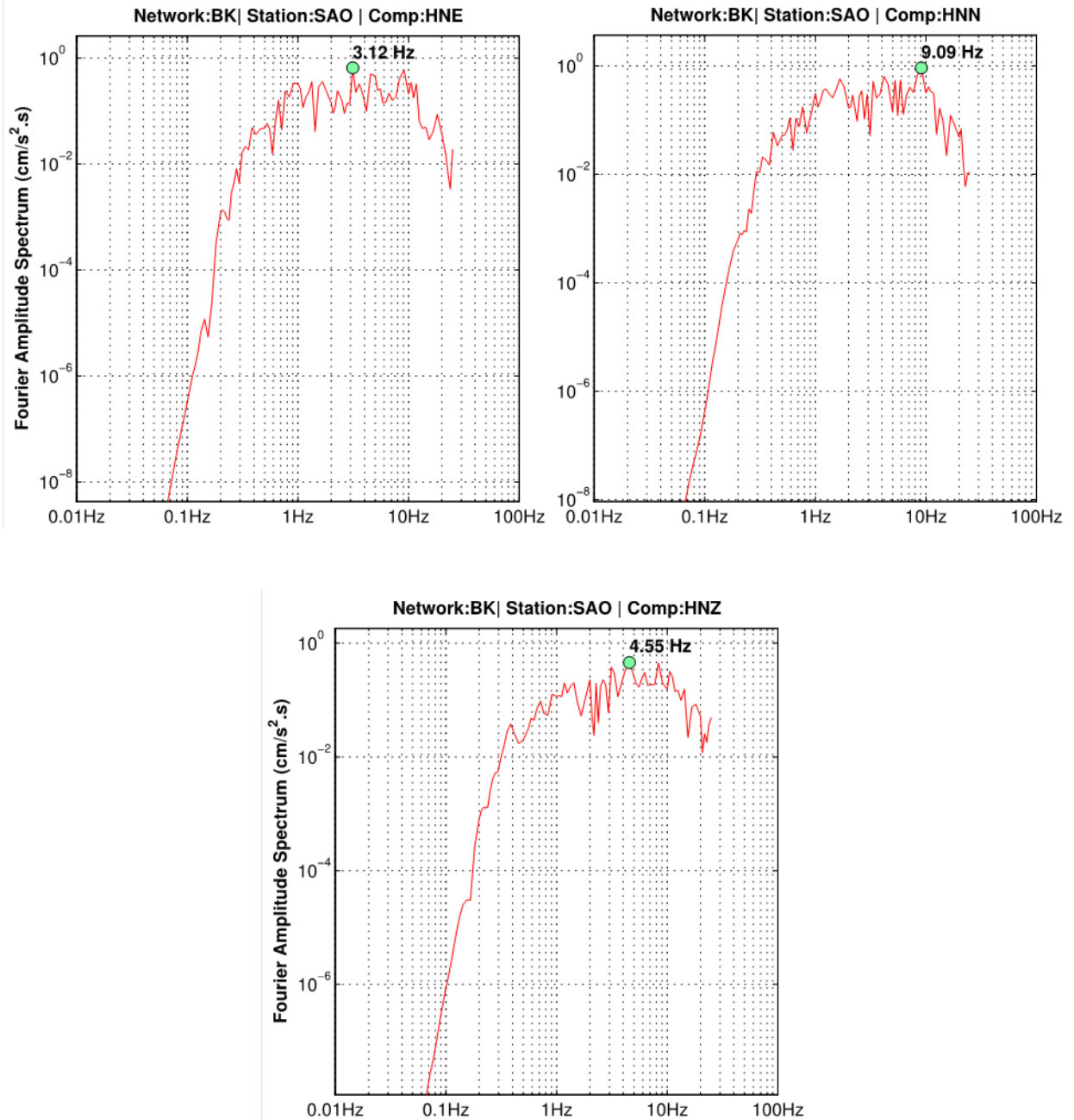


Figure 21. Graphs showing Fourier amplitude spectrum (V3 products, red lines) for three channels of SAO record with 100 samples-per-second from the 2014 *M*_{4.4} Greenfield earthquake in California. Green dot indicates predominant frequency of signal. cm/s²·s, centimeters per second squared second; Hz, hertz.

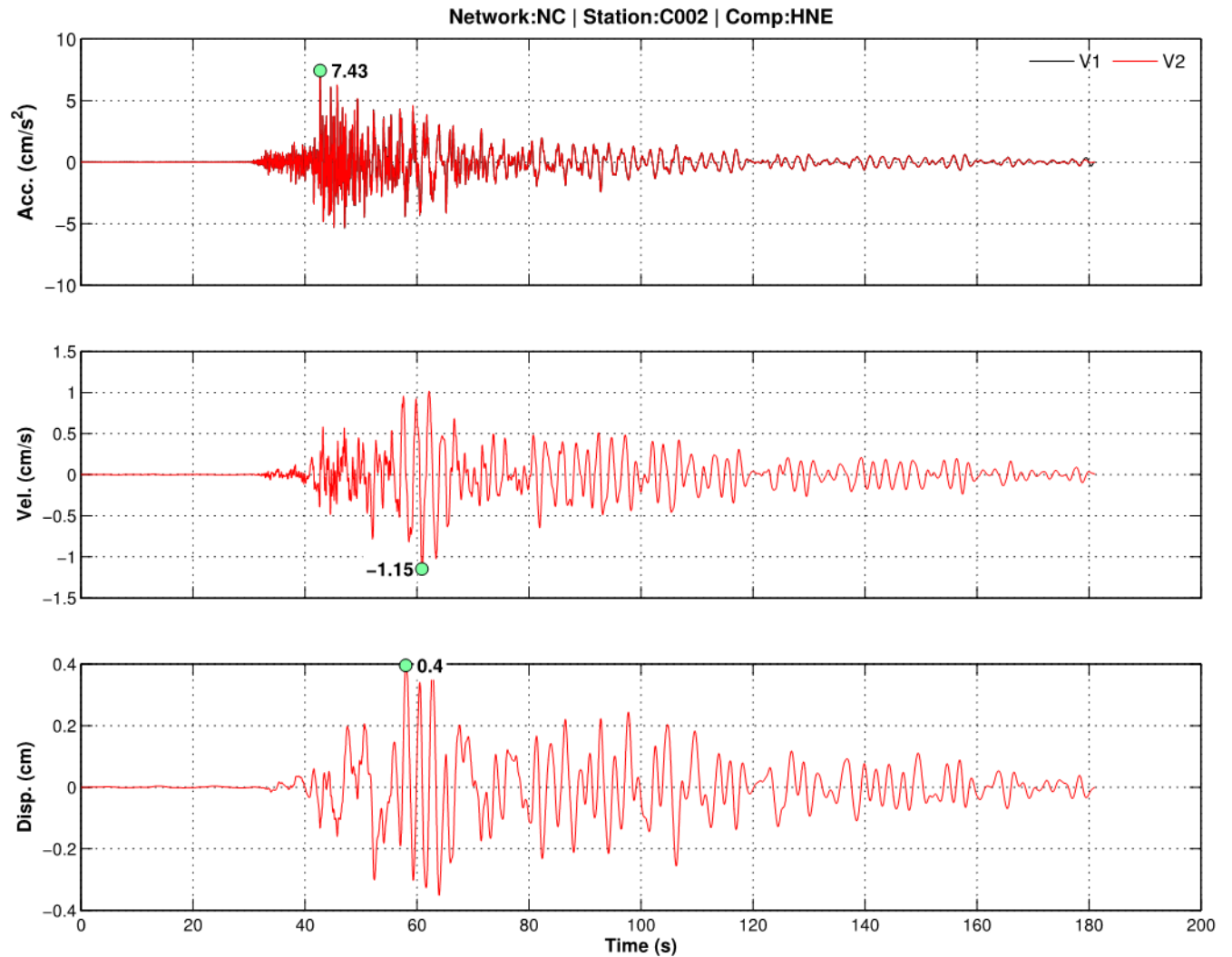


Figure 22. Graphs showing a final suite of acceleration (acc.), velocity (vel.), and displacement (disp.) time series (V2 products, red lines) for channel HNE at station C002 recorded with 200 samples-per-second from the 2014 *M*6.0 South Napa earthquake in California. Note that this channel of the record was processed without a need for adaptive baseline correction. Acceleration time series after V1 processing (black line) is also shown in the upper graph for comparison. Green dots indicate peak values of V2 products. cm, centimeters; cm/s, centimeters per second; cm/s², centimeters per second squared; s, seconds.

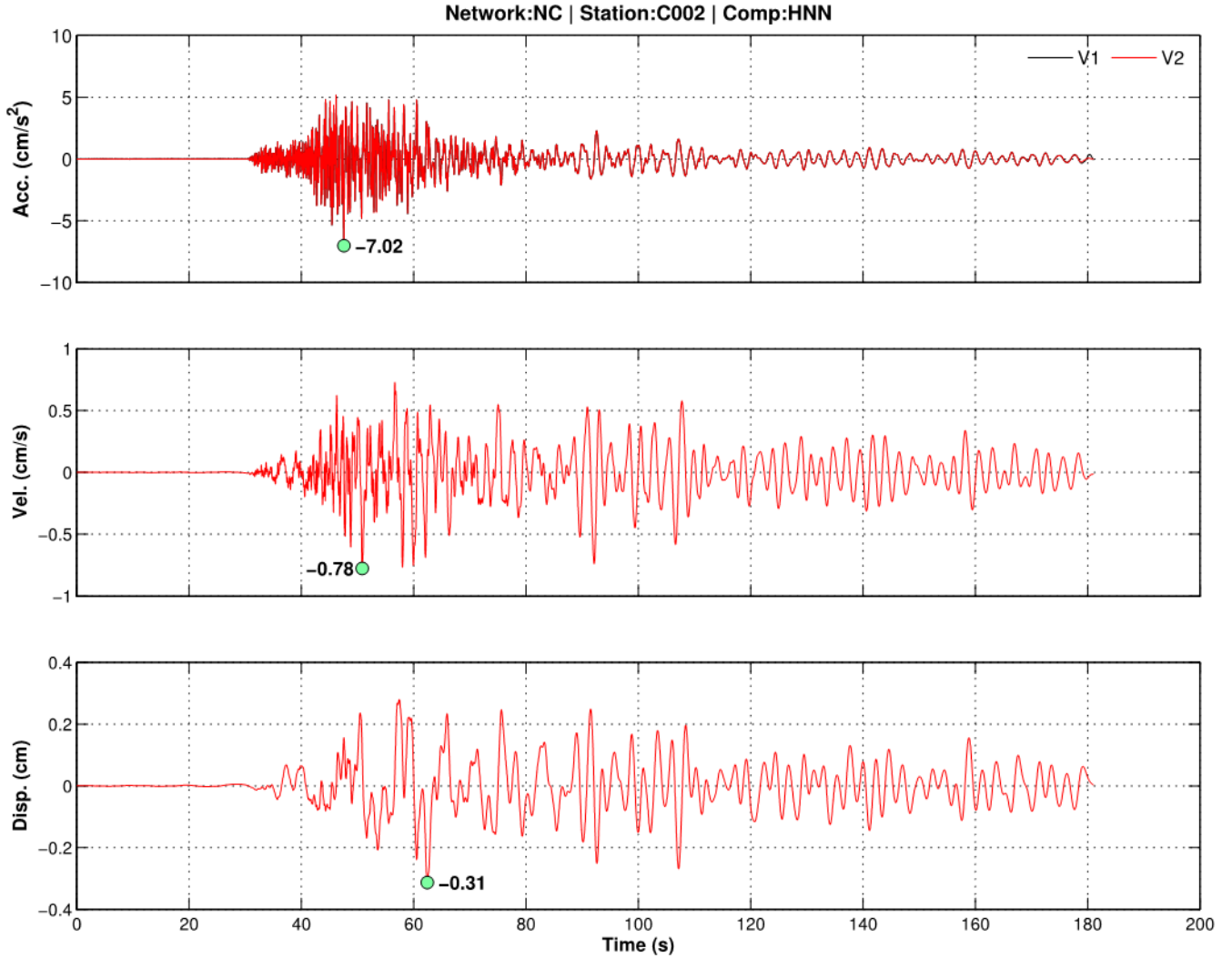


Figure 23. Graphs showing a final suite of acceleration (acc.), velocity (vel.), and displacement (disp.) time series (V2 products, red lines) for channel HNN at station C002 recorded with 200 samples-per-second from the 2014 *M*6.0 South Napa earthquake in California. Note that this channel of the record was processed without a need for adaptive baseline correction. Acceleration time series after V1 processing (black line) is also shown in the upper graph for comparison. Green dots indicate peak values of V2 products. cm, centimeters; cm/s, centimeters per second; cm/s^2 , centimeters per second squared; s, seconds.

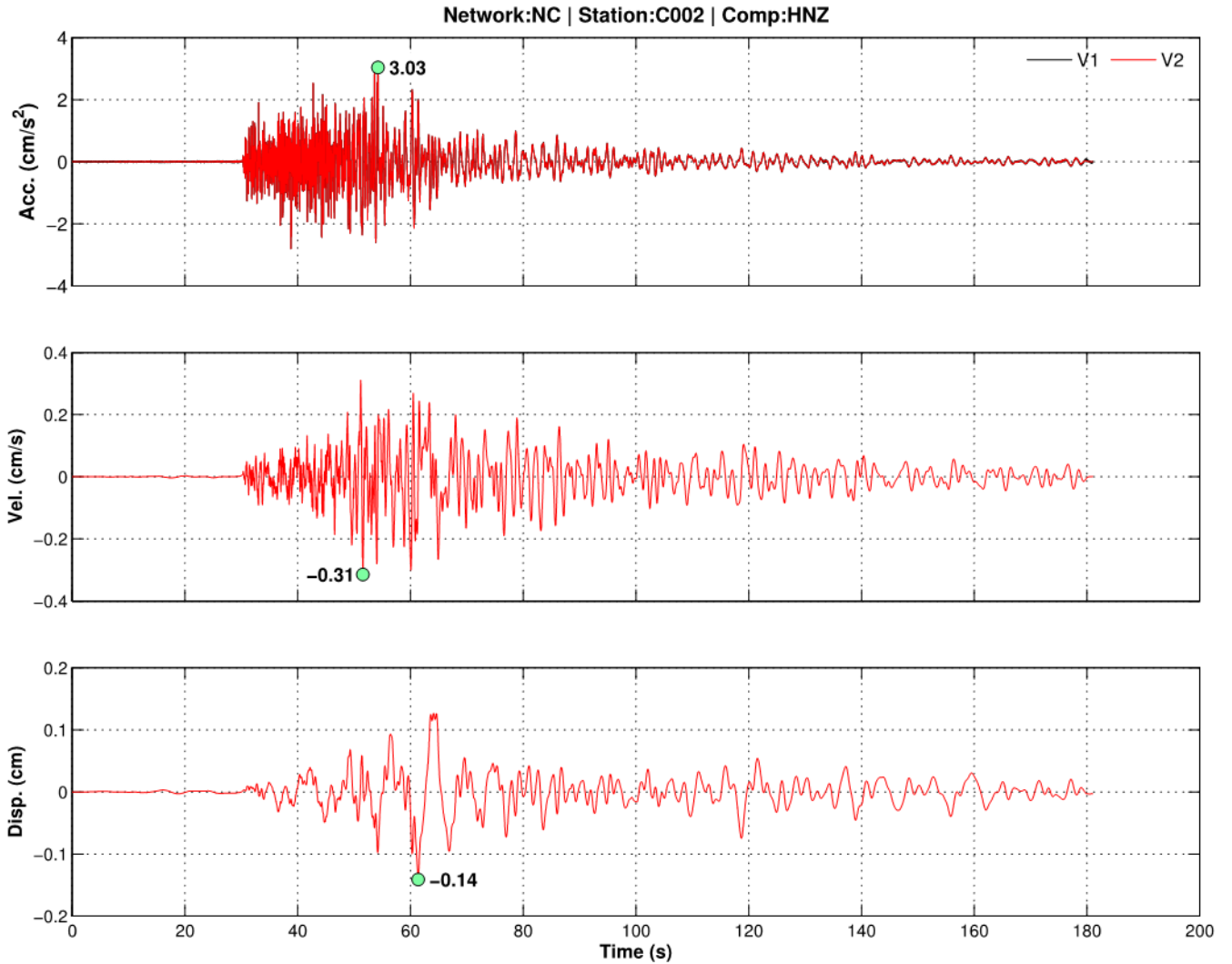


Figure 24. Graphs showing a final suite of acceleration (acc.), velocity (vel.), and displacement (disp.) time series (V2 products, red lines) for channel HNZ at station C002 recorded with 200 samples-per-second from the 2014 *M*6.0 South Napa earthquake in California. Note that this channel of the record was processed without a need for adaptive baseline correction. Acceleration time series after V1 processing (black line) is also shown in the upper graph for comparison. Green dots indicate peak values of V2 products. cm, centimeters; cm/s, centimeters per second; cm/s^2 , centimeters per second squared; s, seconds.

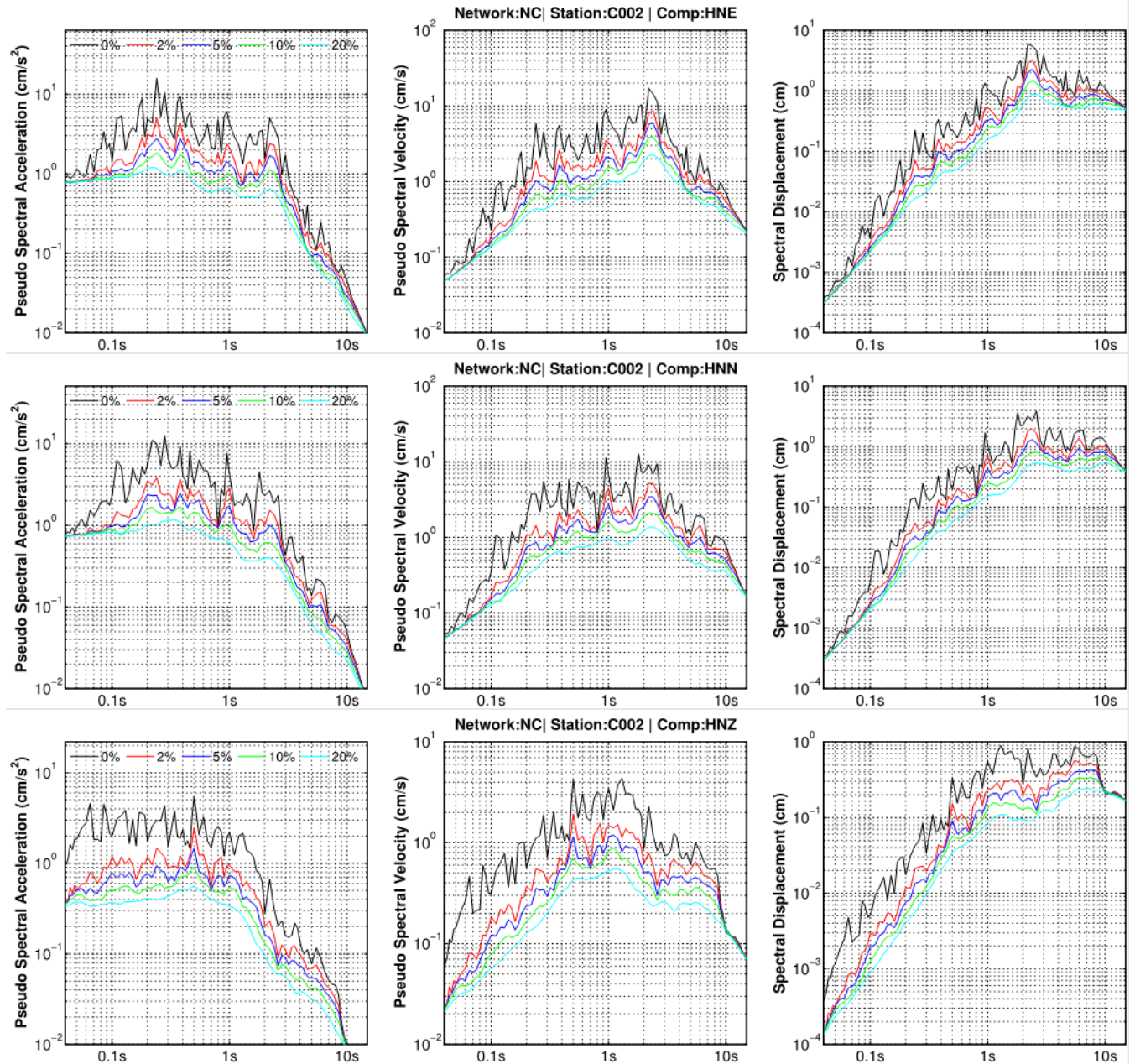


Figure 25. Graphs showing a final suite of pseudo-spectral acceleration, pseudo-spectral velocity, and spectral displacement spectra computed at different damping levels (0, 2, 5, 10, and 20 percent of critical) for three channels of C002 record with 200 samples-per-second from the 2014 *M*_{6.0} South Napa earthquake in California. cm, centimeters; cm/s, centimeters per second; cm/s², centimeters per second squared; s, seconds.

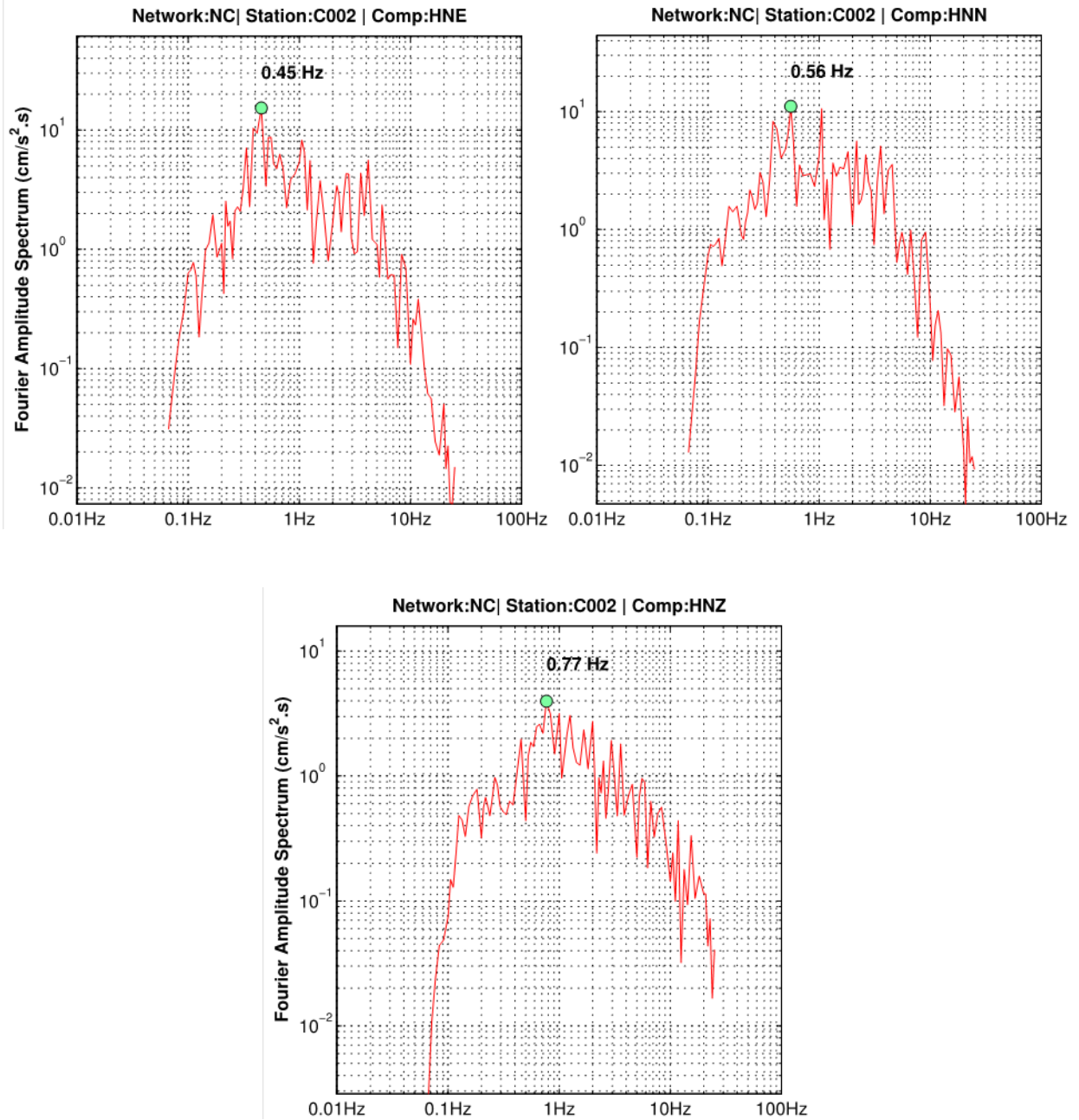


Figure 26. Graphs showing Fourier amplitude spectrum (V3 products, red lines) for three channels of C002 record with 200 samples-per-second from the 2014 *M*6.0 South Napa earthquake in California. Green dots indicate predominant frequency of signal. cm/s²·s, centimeters per second squared second; Hz, hertz.

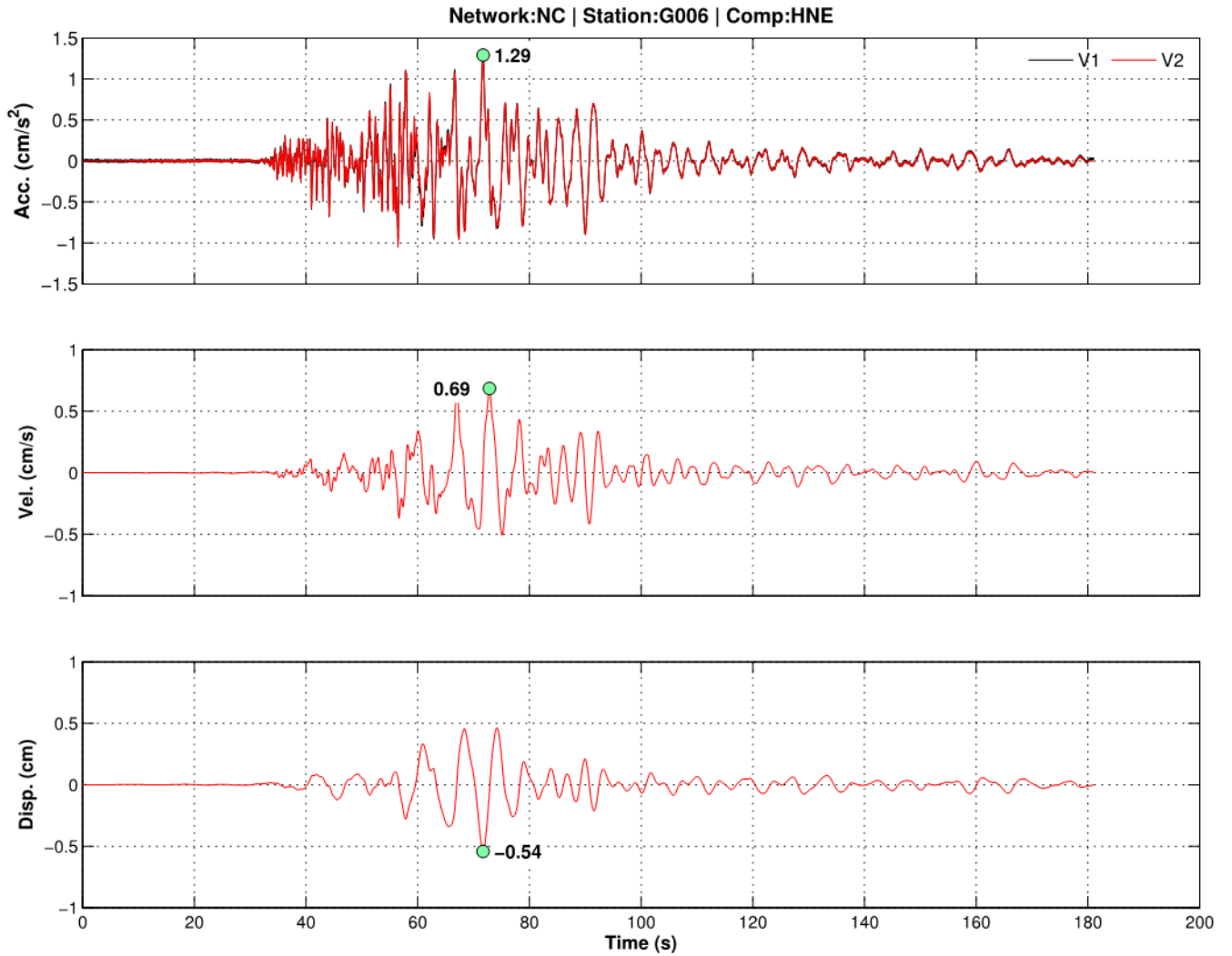


Figure 27. Graphs showing a final suite of acceleration (acc.), velocity (vel.), and displacement (disp.) time series (V2 products, red lines) for channel HNE at station G006 recorded with 200 samples-per-second from the 2014 *M*6.0 South Napa earthquake in California. Note that this channel of the record was processed without a need for adaptive baseline correction. Acceleration time series after V1 processing (black line) is also shown in the upper graph for comparison. Green dots indicate peak values of V2 products. cm, centimeters; cm/s, centimeters per second; cm/s^2 , centimeters per second squared; s, seconds.

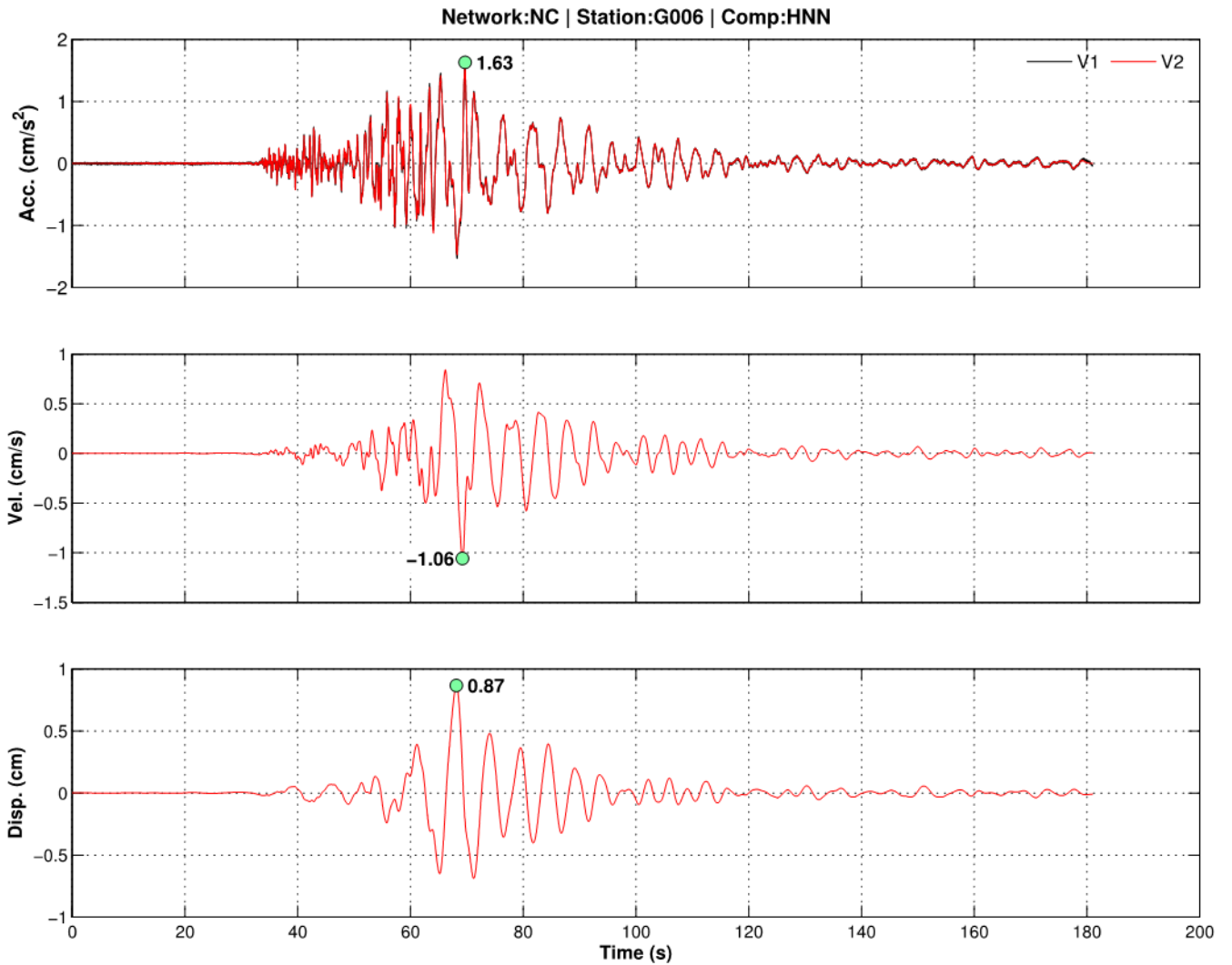


Figure 28. Graphs showing a final suite of acceleration (acc.), velocity (vel.), and displacement (disp.) time series (V2 products, red lines) for channel HNN at station G006 recorded with 200 samples-per-second from the 2014 *M*6.0 South Napa earthquake in California. Note that this channel of the record was processed without a need for adaptive baseline correction. Acceleration time series after V1 processing (black line) is also shown in the upper graph for comparison. Green dots indicate peak values of V2 products. cm, centimeters; cm/s, centimeters per second; cm/s², centimeters per second squared; s, seconds.

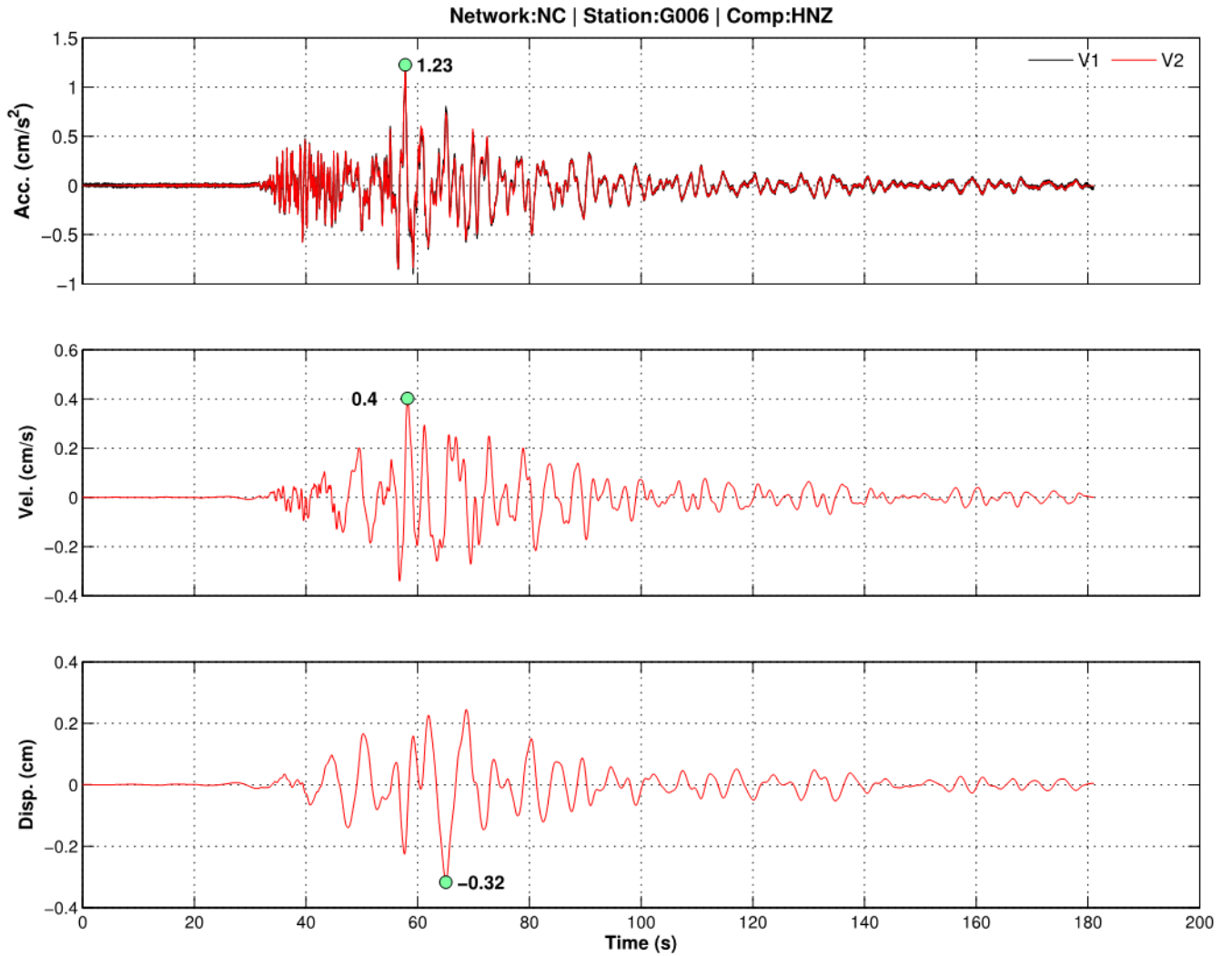


Figure 29. Graphs showing a final suite of acceleration (acc.), velocity (vel.), and displacement (disp.) time series (V2 products, red lines) for channel HNZ at station G006 recorded with 200 samples-per-second from the 2014 *M*6.0 South Napa earthquake in California. Note that this channel of the record was processed without a need for adaptive baseline correction. Acceleration time series after V1 processing (black line) is also shown in the upper graph for comparison. Green dots indicate peak values of V2 products. cm, centimeters; cm/s, centimeters per second; cm/s^2 , centimeters per second squared; s, seconds.

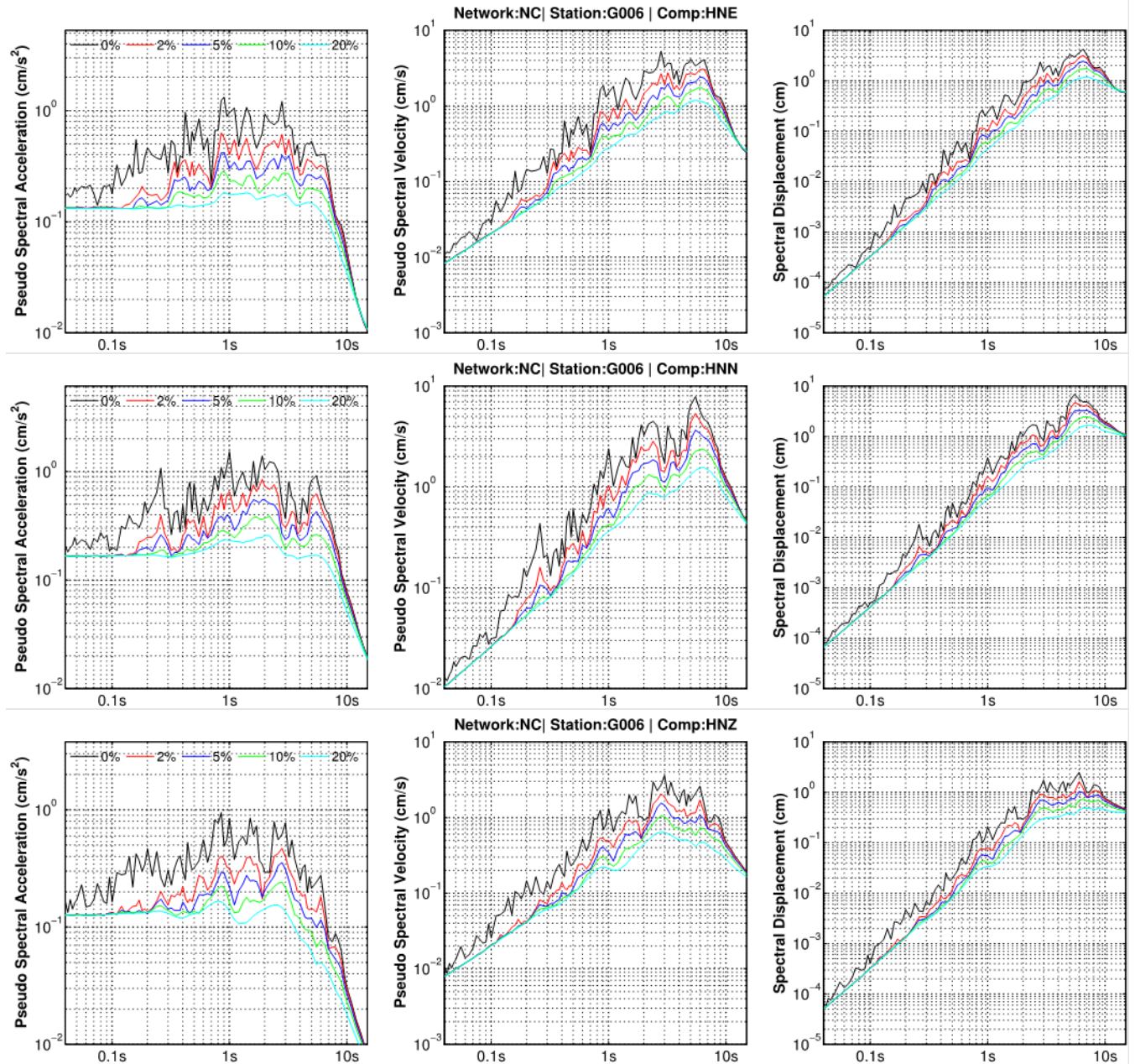


Figure 30. Graphs showing a final suite of pseudo-spectral acceleration, pseudo-spectral velocity, and spectral displacement spectra computed at different damping levels (0, 2, 5, 10, and 20 percent of critical) for three channels of G006 record with 200 samples-per-second from the 2014 *M*_{6.0} South Napa earthquake in California. cm, centimeters; cm/s, centimeters per second; cm/s², centimeters per second squared; s, seconds.

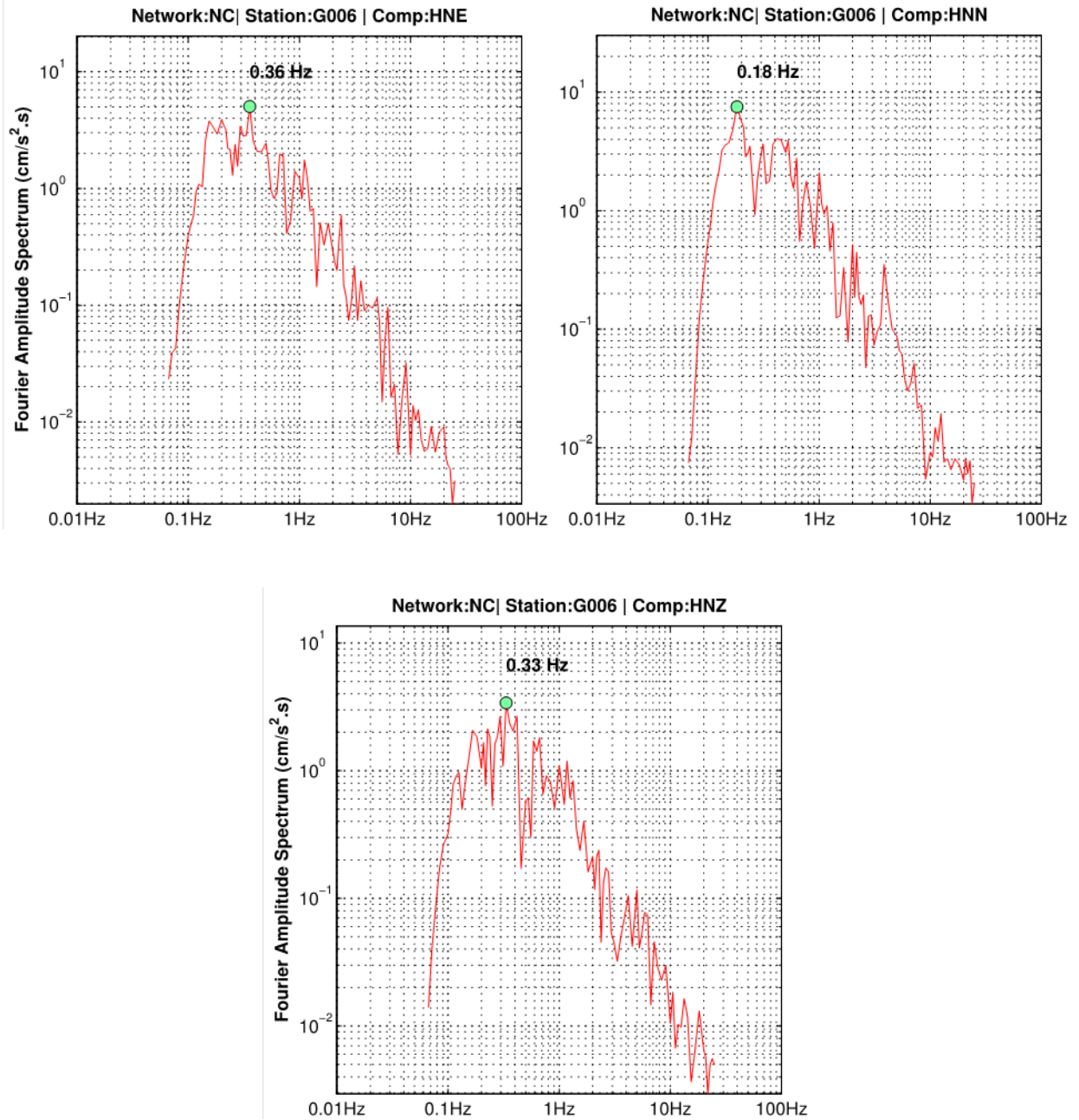


Figure 31. Graphs showing Fourier amplitude spectrum (V3 products, red lines) for three channels of G006 record with 200 samples-per-second from the 2014 *M*6.0 South Napa earthquake in California. Green dots indicate predominant frequency of the signal. cm/s²·s, centimeters per second squared second; Hz, hertz.

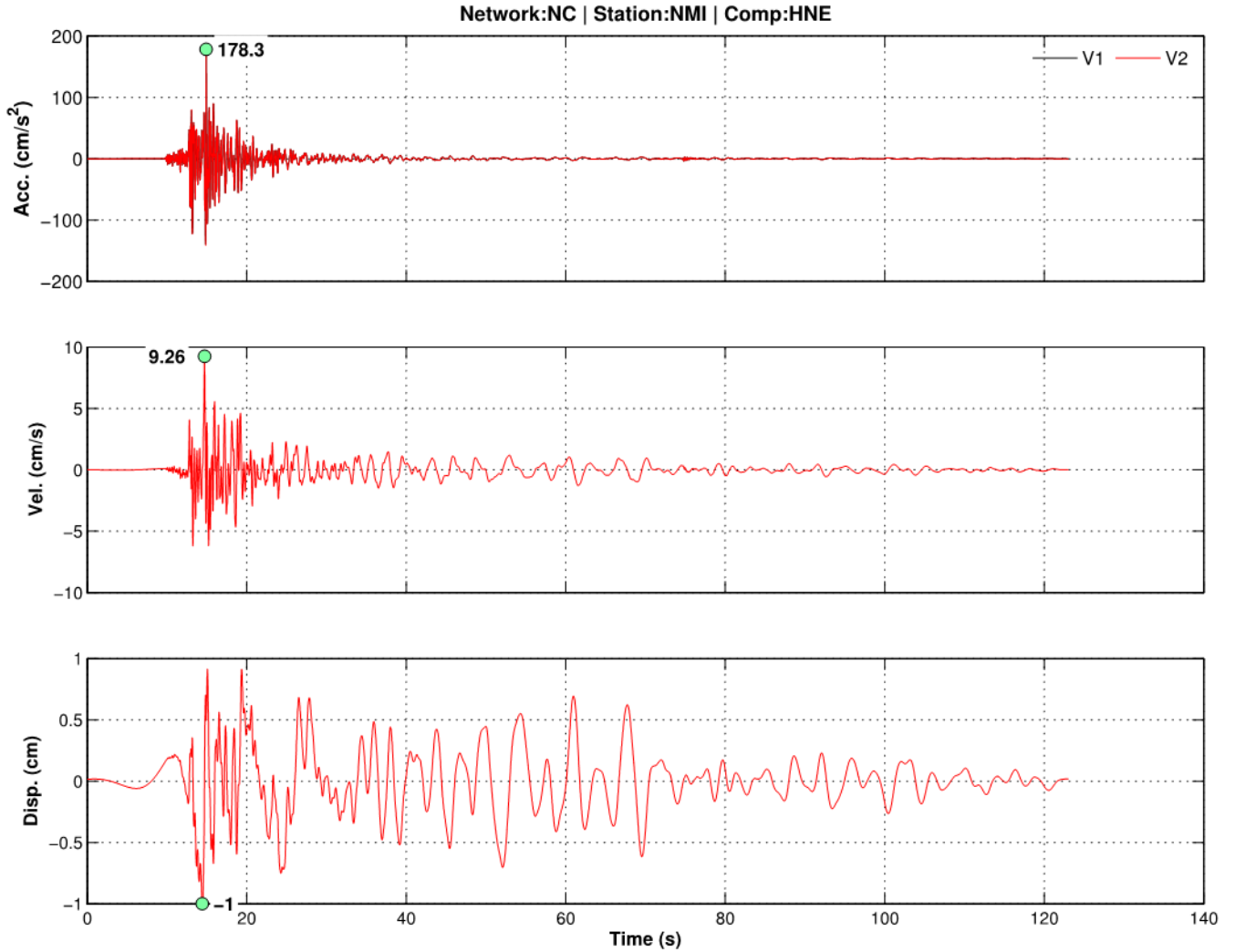


Figure 32. Graphs showing a final suite of acceleration (acc.), velocity (vel.), and displacement (disp.) time series (V2 products, red lines) for channel HNE at station NMI recorded with 100 samples-per-second from the 2014 *M*6.0 South Napa earthquake in California. Note that this channel of the record was processed with adaptive baseline correction. Acceleration time series after V1 processing (black line) is also shown in the upper graph for comparison. Green dots indicate peak values of V2 products. The transient on the displacement before the earthquake onset is a time-domain leakage, and it is a trade-off with using an acausal filter. cm, centimeters; cm/s, centimeters per second; cm/s^2 , centimeters per second squared; s, seconds.

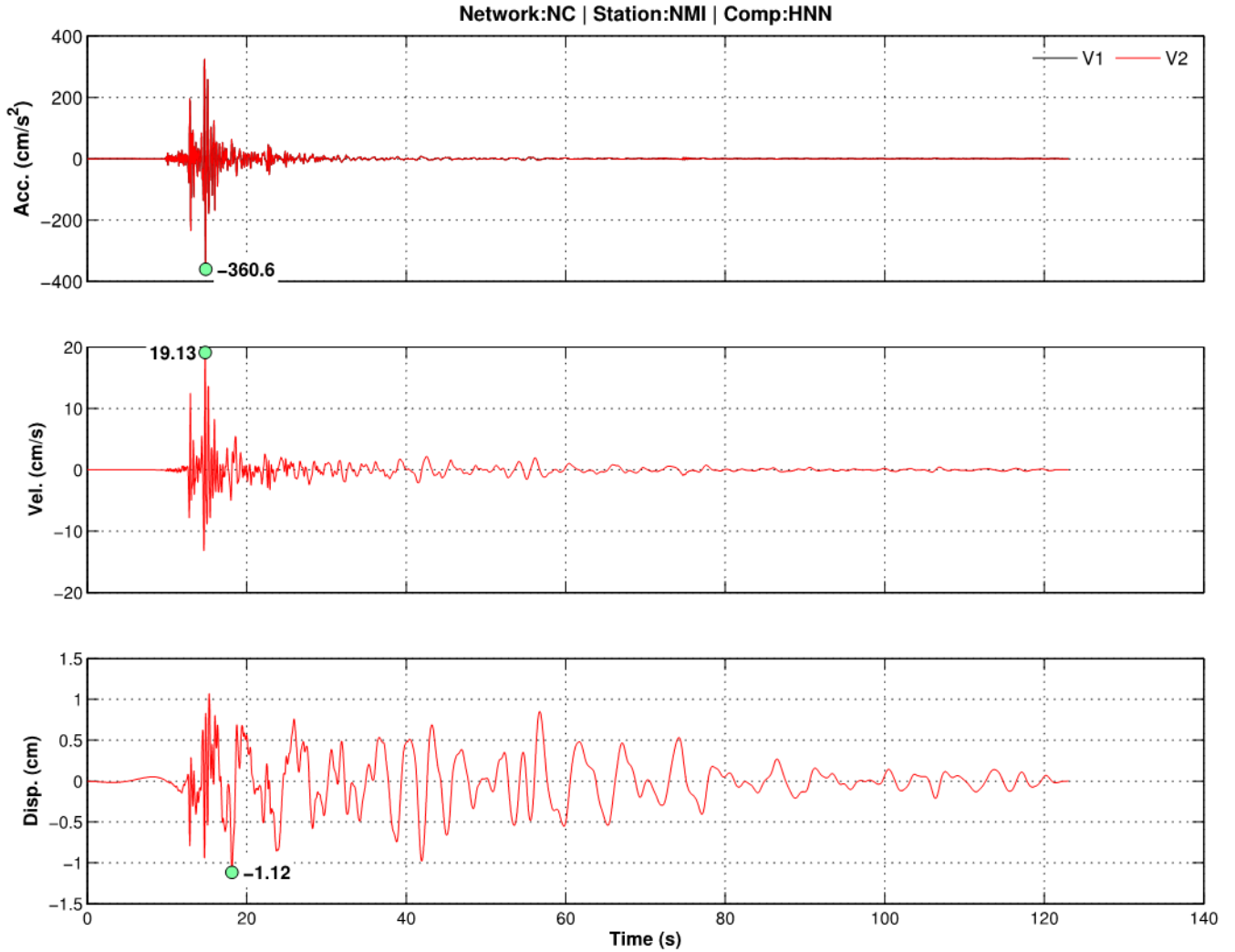


Figure 33. Graphs showing a final suite of acceleration (acc.), velocity (vel.), and displacement (disp.) time series (V2 products, red lines) for channel HNN at station NMI recorded with 100 samples-per-second from the 2014 *M*6.0 South Napa earthquake in California. Note that this channel of the record was processed with adaptive baseline correction. Acceleration time series after V1 processing (black line) is also shown in the upper graph for comparison. Green dots indicate the peak values of V2 products. The transient on the displacement before the earthquake onset is a time-domain leakage, and it is a trade-off with using an acausal filter. cm, centimeters; cm/s, centimeters per second; cm/s², centimeters per second squared; s, seconds.

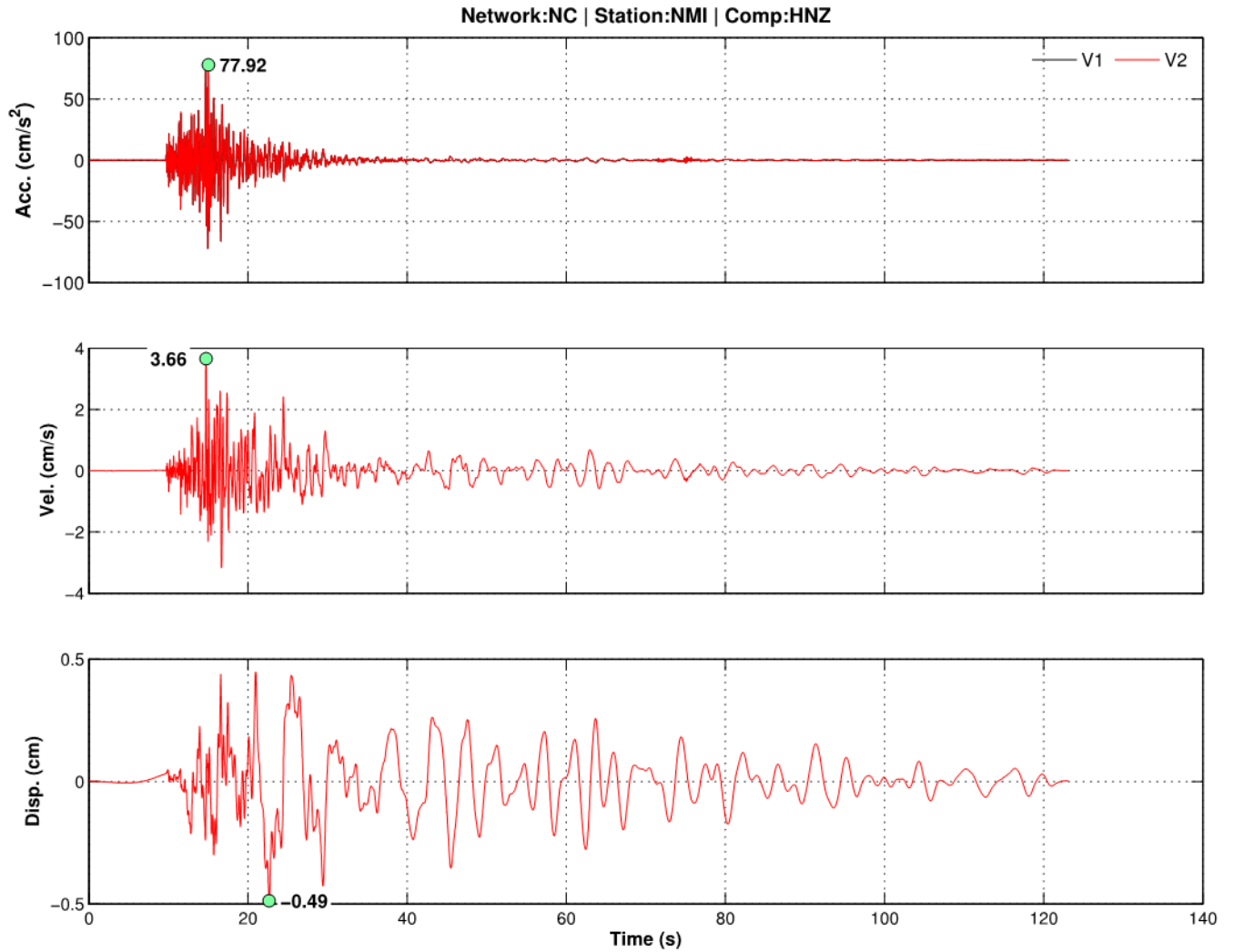


Figure 34. Graphs showing a final suite of acceleration (acc.), velocity (vel.), and displacement (disp.) time series (V2 products, red lines) for channel HNZ at station NMI recorded with 100 samples-per-second from the 2014 *M*6.0 South Napa earthquake in California. Note that this channel of the record was processed with adaptive baseline correction. Acceleration time series after V1 processing (black line) is also shown in the upper graph for comparison. Green dots indicate peak values of V2 products. The transient on the displacement before the earthquake onset is a time-domain leakage, and it is a trade-off with using an acausal filter. cm, centimeters; cm/s, centimeters per second; cm/s^2 , centimeters per second squared; s, seconds.

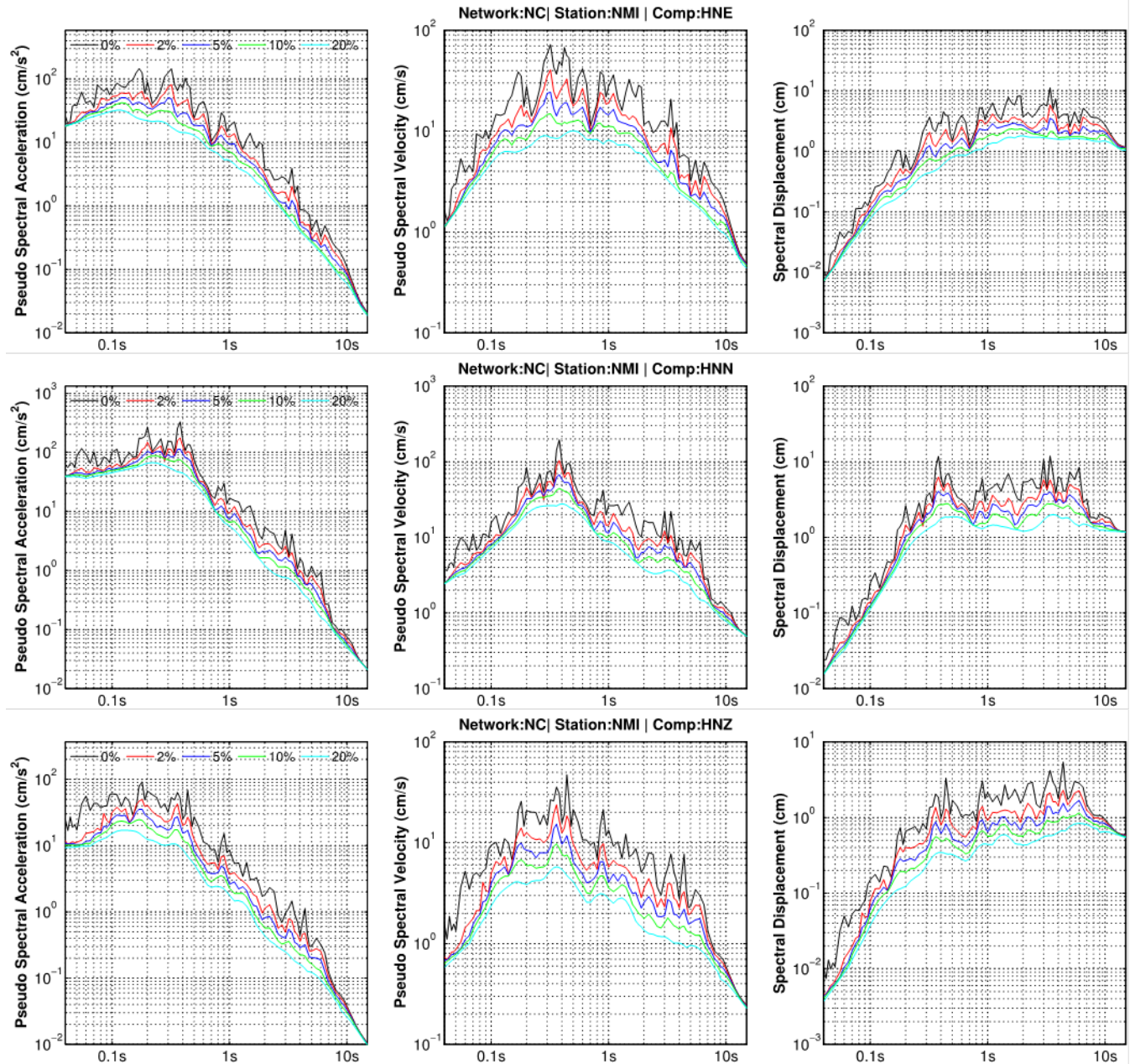


Figure 35. Graphs showing a final suite of pseudo-spectral acceleration, pseudo-spectral velocity, and spectral displacement spectra computed at different damping levels (0, 2, 5, 10, and 20 percent of critical) for three channels of NMI record with 100 samples-per-second from the 2014 *M*6.0 South Napa earthquake in California. cm, centimeters; cm/s, centimeters per second; cm/s², centimeters per second squared; s, seconds.

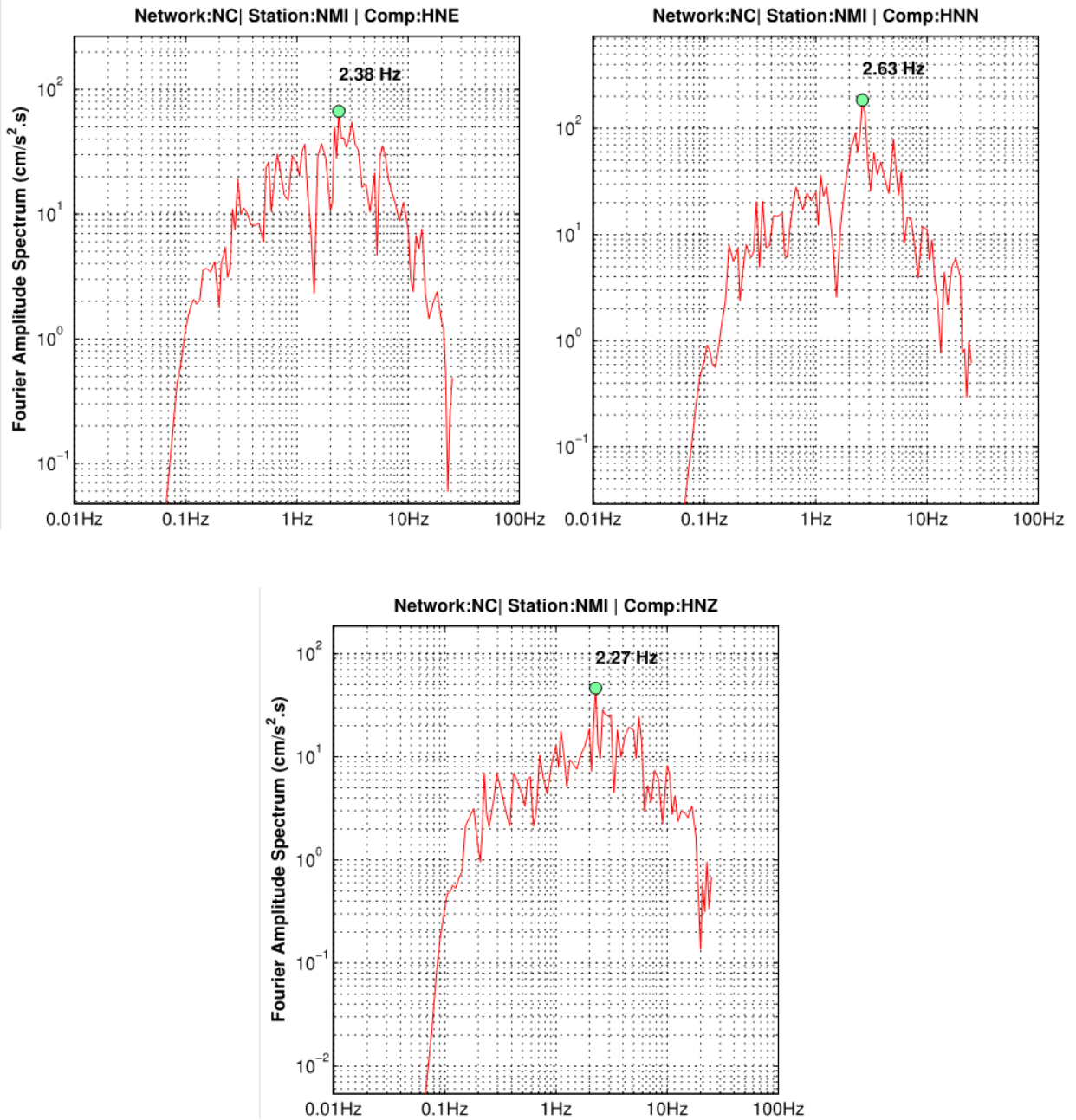


Figure 36. Graphs showing Fourier amplitude spectrum (V3 products, red lines) for three channels of NMI record with 100 samples-per-second from the 2014 *M*6.0 South Napa earthquake in California. Green dots indicate predominant frequency of the signal. cm/s²·s, centimeters per second squared second; Hz, hertz.

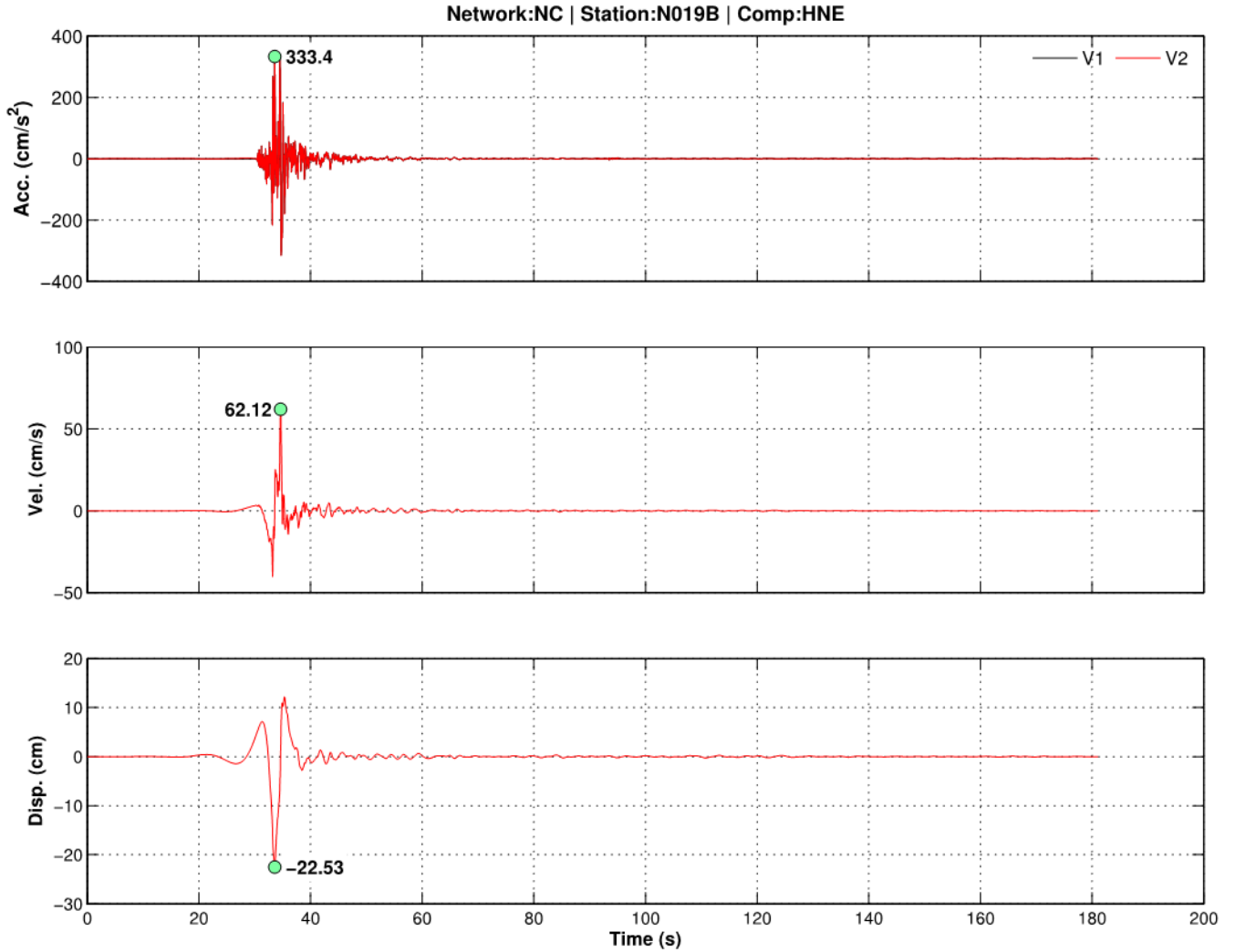


Figure 37. Graphs showing a final suite of acceleration (acc.), velocity (vel.), and displacement (disp.) time series (V2 products, red lines) for channel HNE at station N019B recorded with 200 samples-per-second from the 2014 *M*6.0 South Napa earthquake in California. Note that this channel of the record was processed with adaptive baseline correction. Acceleration time series after V1 processing (black line) is also shown in the upper graph for comparison. Green dots indicate peak values of V2 products. The transient on the displacement before the earthquake onset is a time-domain leakage, and it is a trade-off with using an acausal filter. cm, centimeters; cm/s, centimeters per second; cm/s², centimeters per second squared; s, seconds.

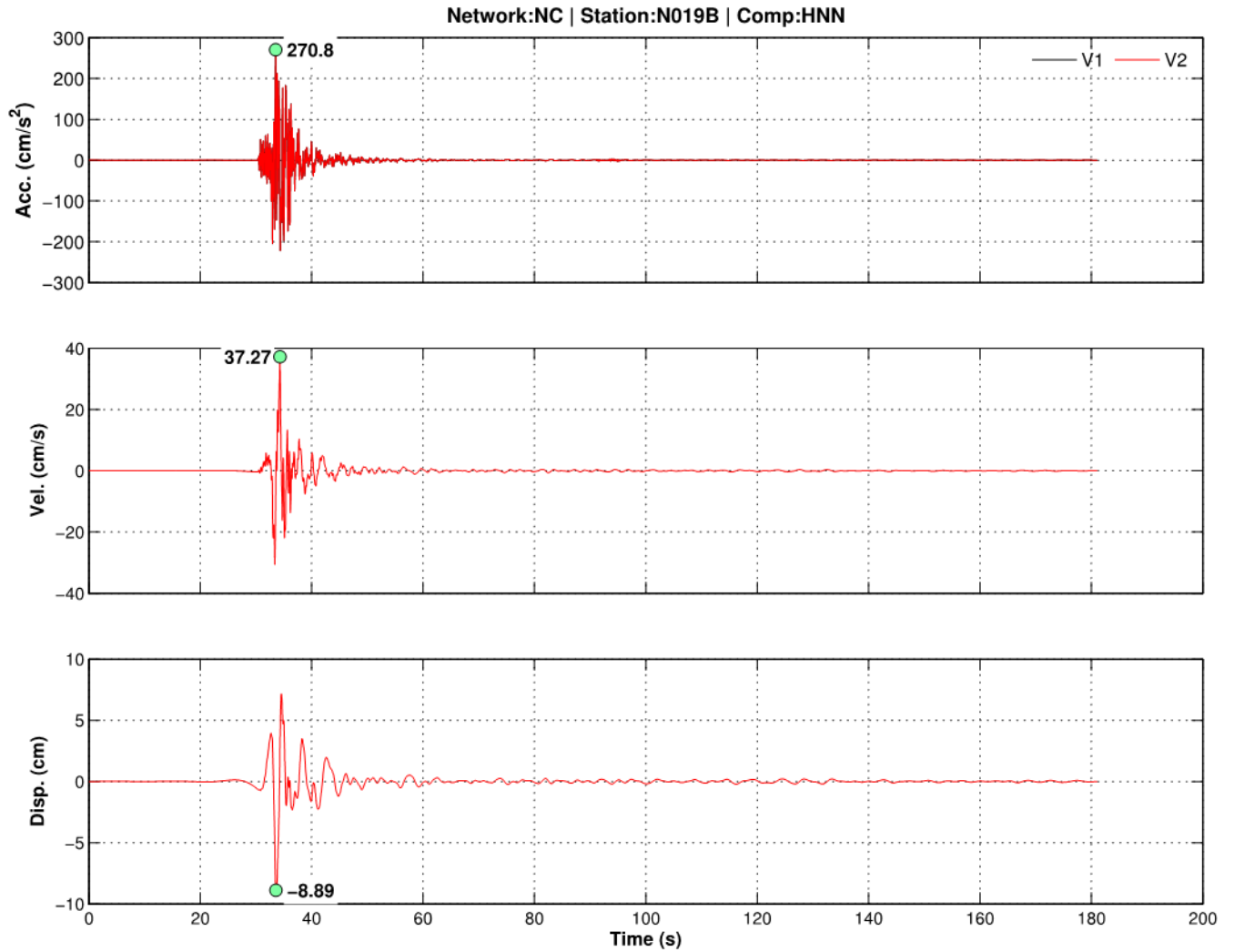


Figure 38. Graphs showing a final suite of acceleration (acc.), velocity (vel.), and displacement (disp.) time series (V2 products, red lines) for channel HNZ at station N019B recorded with 200 samples-per-second from the 2014 *M*6.0 South Napa earthquake in California. Note that this channel of the record was processed with adaptive baseline correction. Acceleration time series after V1 processing (black line) is also shown in the upper graph for comparison. Green dots indicate peak values of V2 products. cm, centimeters; cm/s, centimeters per second; cm/s², centimeters per second squared; s, seconds.

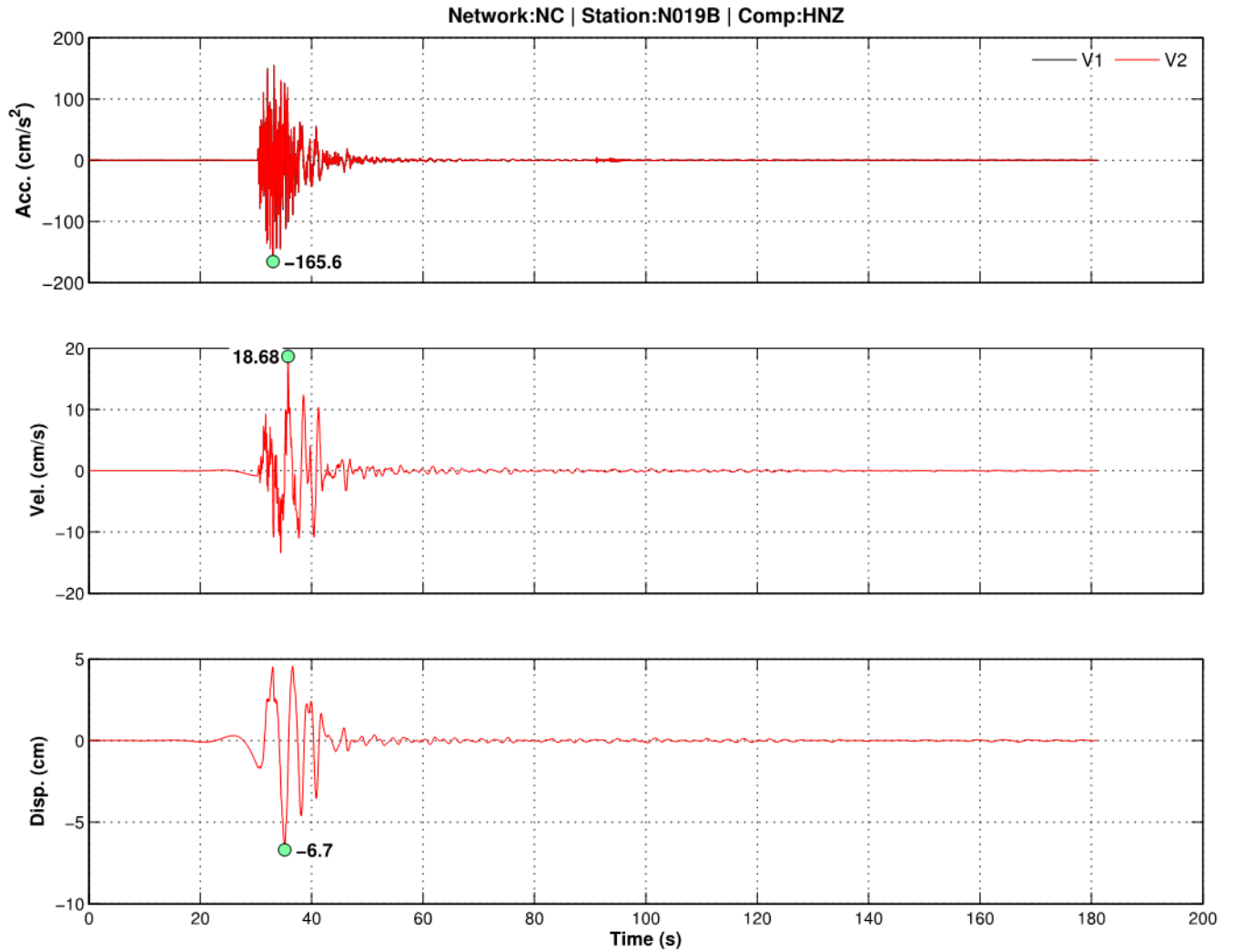


Figure 39. Graphs showing a final suite of acceleration (acc.), velocity (vel.), and displacement (disp.) time series (V2 products, red lines) for channel HNZ at station N019B recorded with 200 samples-per-second from the 2014 *M*6.0 South Napa earthquake in California. Note that this channel of the record was processed with adaptive baseline correction. Acceleration time series after V1 processing (black line) is also shown in the upper graph for comparison. Green dots indicate peak values of V2 products. The transient on the displacement before the earthquake onset is a time-domain leakage, and it is a trade-off with using an acausal filter. cm, centimeters; cm/s, centimeters per second; cm/s^2 , centimeters per second squared; s, seconds.

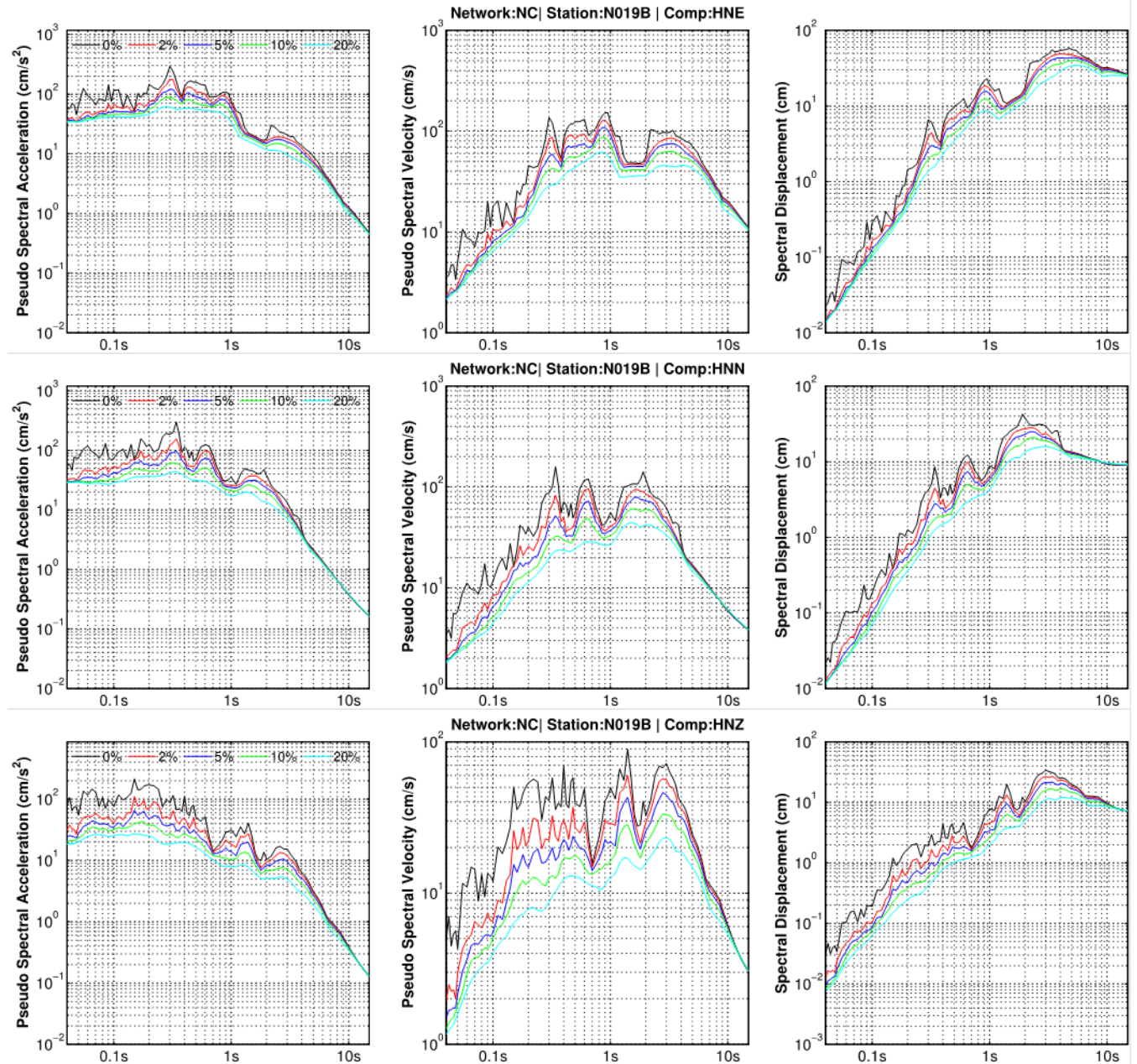


Figure 40. Graphs showing a final suite of pseudo-spectral acceleration, pseudo-spectral velocity, and spectral displacement spectra computed at different damping levels (0, 2, 5, 10, and 20 percent of critical) for three channels of N019B record with 200 samples-per-second from the 2014 *M*6.0 South Napa earthquake in California. cm, centimeters; cm/s, centimeters per second; cm/s², centimeters per second squared; s, seconds.

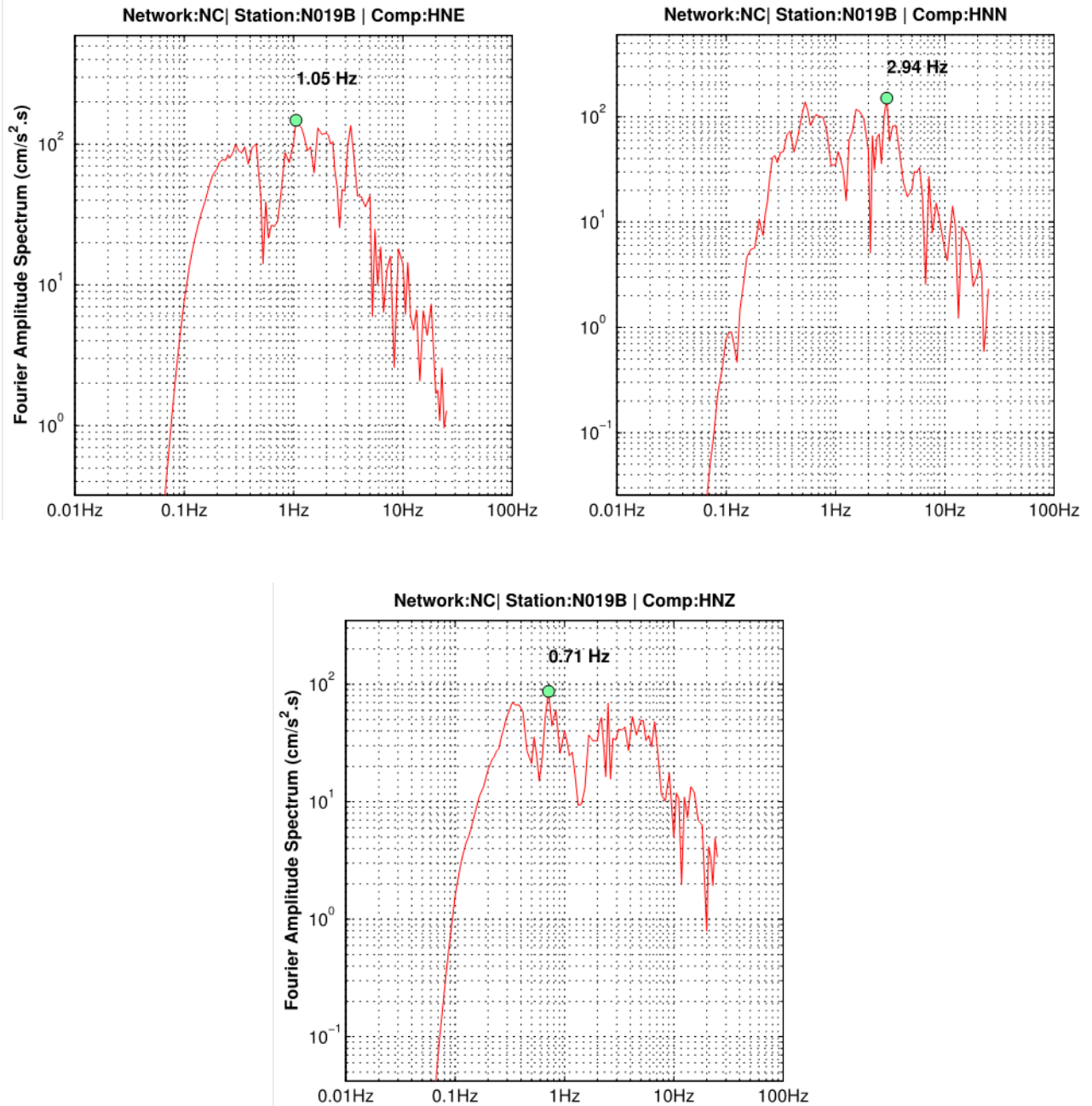


Figure 41. Graphs showing Fourier amplitude spectrum (V3 products, red lines) for three channels of N019B record with 200 samples-per-second from the 2014 *M*6.0 South Napa earthquake in California. Green dots indicate predominant frequency of the signal. cm/s²·s, centimeters per second squared second; Hz, hertz.

Run-Time Performance Assessment

The performance of PRISM is shown by using recordings from three recent events occurred in California as input—the *M*6.0 South Napa earthquake on August 24, 2014, the *M*4.4 South Dos Palos earthquake on September 28, 2014, and the *M*4.4 Greenfield earthquake on January 20, 2015. Table 3 lists the runtime statistics for each event, including the average processing time per channel and the number of channels that passed the QC tests. The ground-motion processing was conducted on a workstation with 2.6 gigahertz (GHz) processor and 16 gigabyte (GB) memory.

Table 3. Runtime statistics for three recent earthquake events
[PGA, peak ground acceleration; g, gravitational acceleration]

	South Napa earthquake	South Dos Palos earthquake	Greenfield earthquake
Moment magnitude	6.0	4.4	4.4
Number of channels	720	102	105
Pass rate (percent)	99	100	100
Number of products	4,312	608	630
Average processing time (second/channel)	0.84	0.48	0.43
Need adaptive baseline correction	105	10	4
Strong motion (PGA \geq 0.05 g)	51	0	0

PRISM generates output products (V1, V2, and V3) in a single-channel-per-file format, with separate files for acceleration, velocity, and displacement V2 products. PRISM also unbundles V0 records into a single-channel-per-file format for output. Thus, each channel successfully processed by PRISM produces one unbundled V0 file, one V1 file, three V2 files, and one V3 file for a total of six product files. For example, the 105 input records for Greenfield produced $105 \times 6 = 630$ products. Records that fail QC tests do not have V3 product files, and records with problems such as no detectable event onset do not have V2 or V3 product files. In the case of the South Napa earthquake processing, 720 records were processed successfully, 4 records failed the QC tests, and 1 record had no detectable event onset, resulting in $(715 \times 6) + (4 \times 5) + (1 \times 2) = 4,312$ products.

The average processing time for a set of input V0 files, each comprising three channels of data, depends on the length of the data arrays in each record, the number of channels that require resampling, and the number of records requiring ABC processing. Records for all three events shown in table 3 contained time series of about 18,000 to 36,000 samples. South Dos Palos earthquake data processing was completed at a rate of about 125 records per minute and it contained only 10 channels that needed ABC and 63 channels that needed to be resampled. Napa earthquake data processing was completed at an average rate of about 71 records per minute and contained 105 channels that needed ABC and 252 channels that needed to be resampled.

Strong-motion intensity measures are computed for records with a peak corrected acceleration magnitude greater than or equal to the strong-motion threshold defined in the configuration file. Approximately 7 percent of the Napa records had peak acceleration values meeting or exceeding the current threshold of 0.05 g, whereas no South Dos Palos or Greenfield records met the threshold. Calculation of the intensity measures increases processing time by a negligible amount.

Systematic Comparisons among PRISM, BAP, and CSMIP Processing

Systematic comparisons are made in time and frequency domains of records processed in PRISM and BAP, and in the California Strong Motion Instrumentation Program (CSMIP), by using a set of representative input motions with varying resolutions, frequency content, and amplitudes. Although the details of strong-motion records vary among the processing procedures, there are only minor differences among the waveforms for each component and within the frequency passband common to these procedures. A comprehensive statistical evaluation considering more than 1,800 ground-motion components demonstrates that differences in peak amplitudes of acceleration, velocity, and displacement time series obtained from PRISM and CSMIP processing are equal or less than 4 percent for 99 percent of data, and equal or less than 2 percent for 96 percent of data. Other statistical measures, including Euclidian distance (L^2 norm) and windowed root mean square levels of processed time series, also indicate that both processing schemes produce statistically similar products. The results of this comprehensive evaluation study are reported in Kalkan and Stephens (2017).

Running PRISM

PRISM is an application that is started from the command line. Written in Java version 8 (Oracle®), PRISM runs on any operating system with the Java programming language installed. The PRISM software has been tested on Windows7, Mac OS X 10.9.5, Linux CentOS 2.6.32, and Ubuntu 14.04 LTS.

PRISM takes three command-line arguments: the full path to the input directory containing the bundled or unbundled V0 files, the full path to the output directory to receive the product files, and the full path name to a configuration file. The input and output directories and the configuration file are required parameters. PRISM configuration file is an XML file, which is described in appendix 3 in details. To run PRISM from its JAR file, an example command line entry in the Windows7 operating system command line would look like the following:

```
>java -jar prism.jar D:\infolder D:\outfolder D:\config\prism_config.xml
```

On startup, PRISM gets a list of all files in the input directory with an extension containing “V0.” Some valid extensions are .V0, .v0, .V0C, and .v0c, where the data for all of these file extensions is expected to conform to the COSMOS V1.2 format. As the files are processed and the products written to the output folder, the input files are deleted from the input folder if the configuration file is set for input file deletion. Any files left in the input folder after application completion are records that PRISM was unable to process, most likely because of incomplete metadata in the headers. The specific reason for the failure can be found in the main log file “PrismLog.txt” (see appendix 4) in the Logs subdirectory of the output directory.

The output directory provided to PRISM on the command line becomes the topmost directory in a directory structure created by the software during execution, and is described in detail below. At the top level, PRISM creates a “Logs” subdirectory to hold the log files created during the processing run. Another subdirectory is created for each unique event found in the record identifier of the headers. If no event identifier (id) is found, an “Orphan” subdirectory is created to hold the product files. Debug text files are also written directly into the output directory if the WriteBaselineFunction option is set to “On” in the configuration file. Additional information on the various product file subdirectories is contained in the “Output Directory Structure” section of this report.

Output Directory Structure

PRISM builds a directory structure in the output directory based on event and station identifiers. Figure 42 shows the similar structure of the event/station and the Orphan/time directories.

For each event id (id = identifier) found in the records during processing, PRISM creates a new directory using the network code of the authoritative agency that located the event and the event id assigned by this agency. For each station found during processing, PRISM creates a subdirectory within the appropriate event directory using the station network code and the station code. PRISM looks for the event and station information after the RcrdId tag found either in the text header or comments of the input V0 file. For example, for this record id from a South Napa record, "RcrdId:NC.72282711.NC.NCC.HNE.--," the event directory name would be "NC.72282711" and the station directory name would be "NC.NCC."

The product files are placed in subdirectories within the station directory according to their volume numbers (V0, V1, ...), and the full path name for each file is written into the "PrismLog.txt" file. Before creating a new directory, the software checks to see if that directory already exists and, if so, uses the existing directory.

When PRISM is unable to successfully complete V2 processing on a record, it creates a subdirectory within the station directory named "Trouble" to hold the records that need manual processing. For example, in figure 42, one station directory has both the V0–V3 subdirectories for the channels that passed QC and a Trouble directory with its own V0–V2 subdirectories for the failed products. The full path name for each file that is written to a "Trouble" directory is recorded in the "TroubleLog.txt" file located in the Logs directory to aid the user in quickly locating these files.

When PRISM is unable to determine the event id in the input record, the software creates an Orphan directory for the products of these records. Instead of the station subdirectory, PRISM creates a subdirectory name from the date in the Record parameters section of the header metadata.

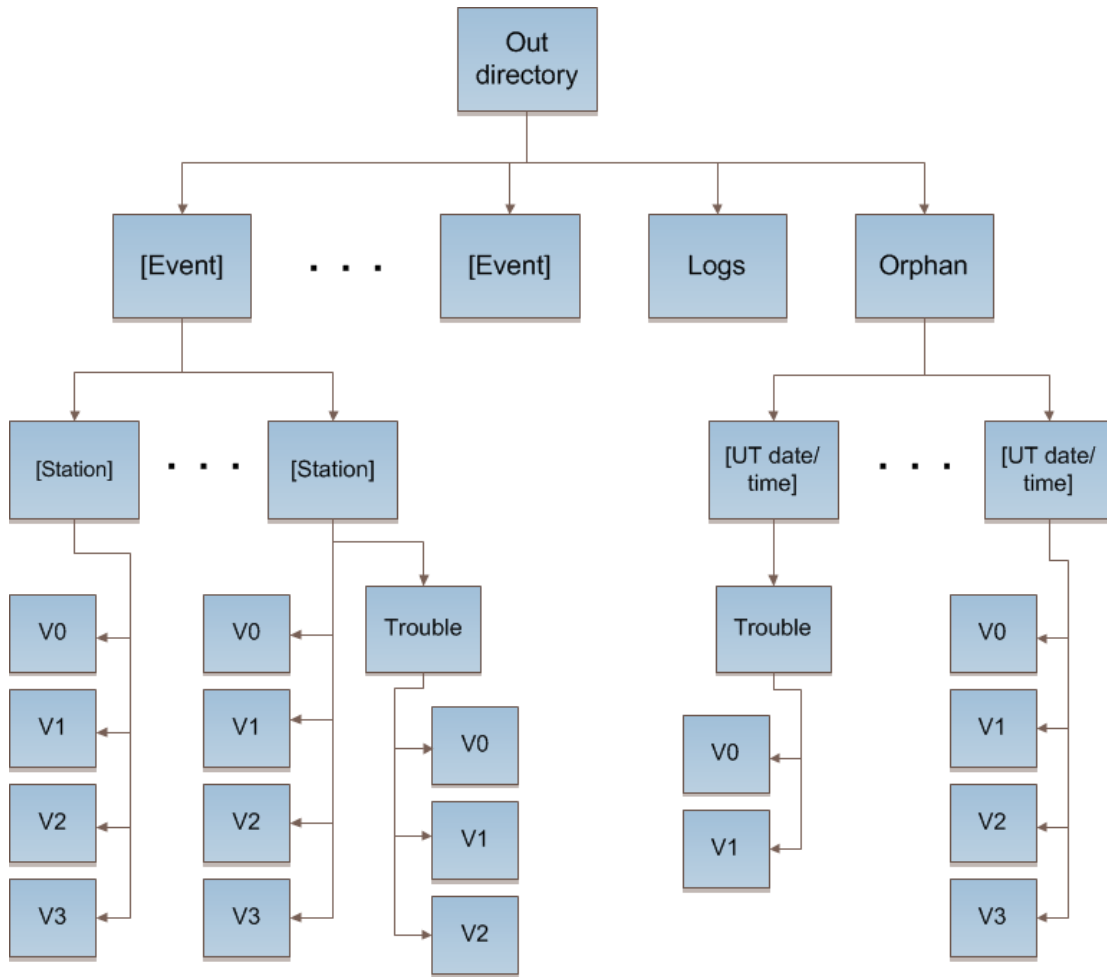


Figure 42. Illustration showing directory structure currently used in Processing and Review Interface for Strong Motion data (PRISM) software.

Concluding Remarks

A robust automated data processing procedure is essential to ensure high-quality accelerograms and derived products for immediate use in earthquake-engineering applications and for seismological studies. This report describes the automated Processing and Review Interface for Strong Motion data (PRISM) software developed at the U.S. Geological Survey. Although there is no unique procedure for processing strong-motion data, PRISM utilizes techniques accepted worldwide (for example, Boore and others, 2002; Boore and Bommer, 2005; Shakal and others, 2003, 2004) that are designed to remove low- and high-frequency noise in order to provide reliable estimations of velocity and displacement time series.

A comprehensive benchmark test, conducted by comparing processing results of PRISM to BAP and to California Strong-Motion Instrument Program processing, shows that there are only minor differences among the waveforms for each component and within the frequency passband common to these procedures (Kalkan and Stephens, 2017).

All essential steps applied in PRISM, whether automatic or manual, are documented in the ASCII file headers of the processed time series so that users can evaluate the suitability of the data for their intended application.

Complementary to the California Integrated Seismic Network (<http://www.cisn.org/>, last accessed January 2017), in which automated processing of records provides metadata that are used as input for products such as ShakeMaps, PRISM processing engine was designed to automatically and rapidly generate preliminary products of earthquake-engineering interest to include in Internet Quick Reports issued by the Center for Engineering Strong-Motion Data (<http://strongmotioncenter.org>, last accessed January 2017).

Data and Resources

PRISM software for both the processing engine and the review tool is available at <http://earthquake.usgs.gov/research/software/#prism> (last accessed January 2017). Users are encouraged to e-mail the authors, Jeanne Jones (jmjones@usgs.gov), Erol Kalkan (ekalkan@usgs.gov), Christopher Stephens (cdstephens@usgs.gov), and Peter Ng (png@usgs.gov) with evidence of any problems or errors encountered while running PRISM.

The unprocessed ground-motion data from the *M*6.0 South Napa earthquake on August 24, 2014, in California, the *M*4.4 South Dos Palos earthquake on September 28, 2014, in California, the *M*5.1 La Habra earthquake on March 29, 2014, in California, and the *M*4.4 Greenfield earthquake on January 20, 2015, in California, used in demonstration of PRISM are available at Center for Engineering Strong-Motion Data (<http://www.strongmotioncenter.org>, last accessed January 2017). The unprocessed ground-motion records from the *M*6.1 earthquake occurred on May 05, 2014, in Thailand are available from the National Strong-Motion Project (GS-G-WR_ESC_NSMP@usgs.gov) upon request.

References Cited

- Ancheta, T.D., Darragh, R.B., Stewart, J.P., Seyhan, E., Silva, W.J., Chiou, B.S.J., Wooddell, K.E., Graves, R.W., Kottke, A.R., Boore, D.M., Kishida, T., and Donahue, J.L., 2013, PEER NGA-West database: Berkeley, Calif., University of California, Pacific Earthquake Engineering Research Center, PEER Report 2014/17, 136 p.
- Arias, A., 1970, A measure of earthquake intensity *in* Hansen, R.J., ed., Seismic Design for Nuclear Power Plants: Cambridge, Mass., MIT Press, 438–483.
- Bazzurro, P., Sjoberg, B., Luco, N., Silva, W., and Darragh, R., 2005, Effects of strong motion processing procedures on time histories, elastic and inelastic spectra: COSMOS publication no CP-2005/02, 39 p., accessed January 2017 at <http://www.cosmos-eq.org/publications/reports/CP-2005-02.pdf>.
- Bolt, B.A., 1969, Duration of strong motion: Proceedings of the 4th World Conference on Earthquake Engineering, Santiago, Chile, p. 1304–1315.
- Boore, D., 2001, Effect of baseline correction on displacements and response spectra for several recordings of the 1999 Chi-Chi, Taiwan, earthquake: Bulletin of the Seismological Society of America, v. 91, no. 5, p. 1199–1211.
- Boore, D.M., Stephens, C.D., and Joyner, W.B., 2002, Comments on baseline correction of digital strong motion data—Examples from the 1999 Hector Mine California earthquake: Bulletin of the Seismological Society of America, v. 92, no. 4, p. 1543–1560.
- Boore, D.M., 2005, On pads and filters—Processing strong-motion data: Bulletin of the Seismological Society of America, v. 95, no. 2, p. 745–750.
- Boore, D.M., and Akkar, S., 2003, Effect of causal and acausal filters on elastic and inelastic response spectra: Earthquake Engineering and Structural Dynamics, v. 32, p. 1729–1748.

- Boore, D.M., and Bommer, J.J., 2005, Processing of strong-motion accelerograms—Needs, options and consequences: *Soil Dynamics and Earthquake Engineering*, v. 25, p. 93–115.
- Boore, D.M., Sisi, A.A., and Akkar, S., 2012, Using pad-stripped acausally filtered strong-motion data: *Bulletin of the Seismological Society of America*, v. 102, no. 2, p. 751–760.
- Boroschek, R.L., and Legrand, D., 2006, Tilt motion effects on the double-time integration of linear accelerometers—An experimental approach: *Bulletin of the Seismological Society of America*, v. 96, no. 6, p. 2072–2089.
- Brune, J.N., 1970, Tectonic stress and the spectra of seismic shear waves from earthquakes: *Journal of Geophysical Research*, v. 75, no. 26, p. 4997–5009.
- Brune, J.N., 1971, Correction [to ‘Tectonic stress and the spectra of seismic shear waves from earthquakes’]: *Journal of Geophysical Research*, v. 76, issue 20, p. 5002.
- Chiou, B.S.J., Darragh, R.B., Gregor, N.J., and Silva, W.J., 2008, NGA project strong-motion database: *Earthquake Spectra*, v. 24, p. 23–44.
- Consortium of Organizations for Strong-Motion Observation Systems, 2001, COSMOS Strong motion data format: Cosmos Strong Motion Programs Board, 16 p., accessed January 2017 at http://www.strongmotioncenter.org/vdc/cosmos_format_1_20.pdf.
- Converse, A.M., and Brady, A.G., 1992, BAP—Basic strong-motion accelerogram processing software, version 1.0: U.S. Geological Survey Open-File Report 92–296A, 174 p., accessed January 2017 at <https://pubs.er.usgs.gov/publication/ofr92296A>.
- Darragh, R.B., Silva, W.J., and Gregor, N., 2004, Strong motion record processing procedures for the PEER Center: *Proceedings of COSMOS Workshop on Strong-Motion Record Processing*, Richmond, Calif., p. 1–12.
- Electric Power Research Institute (EPRI), 1991, Standardization of the cumulative absolute velocity: report prepared by Yankee Atomic Electric Company, no. EPRI TR-100082-T2, accessed January 2017 at <http://www.epri.com/abstracts/Pages/ProductAbstract.aspx?ProductId=TR-100082-T2>.
- Goulet, C.A., Kishida, T., Ancheta, T.D., Cramer, C.H., Darragh, R.B., Silva, W.J., Hashash, Y.M.A., Harmon, J., Stewart, J. P., Wooddell, K.E., and Youngs, R.R., 2014, PEER NGA-East database: Berkeley, Calif., University of California, Pacific Earthquake Engineering Research Center, PEER Report 2014/17, 68 p.
- Graizer, V.M., 1979, Determination of the true ground displacement by using strong motion records: *Izvestiya, Earth Physics*, v. 15, no. 12, p. 875–85.
- Graizer, V.M., 2005, Effect of tilt on strong motion data processing: *Soil Dynamics and Earthquake Engineering*, v. 25, no. 3, p. 197–204.
- Graizer, V.M., 2010, Strong motion recordings and residual displacements—What are we actually recording in strong motion seismology?: *Seismological Research Letters*, v. 81, p. 635–639.
- Hamming, R.W., 1989, *Digital filters*, third edition: Dover Publications, Inc., Mineola, New York, 284 p., ISBN 0-486-65088-X (pbk.)
- Housner, G.W., 1959, Behavior of structures during earthquakes: *Journal of the Engineering Mechanics Division*, v. 85, p. 109–130.
- Iwan, W.D., Moser, M.A., and Peng, C.Y., 1985, Some observations on strong-motion earthquake measurements using a digital accelerograph: *Bulletin of the Seismological Society of America*, v. 75, p. 1225–1246.
- Kalkan, E., 2016, An automatic *P*-phase arrival time picker: *Bulletin of the Seismological Society of America*, v. 106, no. 3, p. 971–986, doi:10.1785/0120150111.
- Kalkan, E., and Graizer, V., 2007a, Coupled tilt and translational ground motion response spectra: *Journal of Structural Engineering*, v. 133, issue 5, p. 609–619.

- Kalkan, E., and Graizer, V., 2007b, Multi-component ground motion response spectra for coupled horizontal, vertical, angular accelerations, and tilt: *ISET Journal of Earthquake Technology*, v. 44, no. 1, p. 259–284.
- Kalkan, E., and Kunnath, S.K., 2006, Effects of fling step and forward directivity on the seismic response of buildings: *Earthquake Spectra*, v. 22, no. 2, p. 367–390.
- Kalkan, E., and Stephens, C., 2017, Systematic comparisons between PRISM version 1.0.0, BAP, and CSMIP ground-motion processing: U.S. Geological Survey Open-File Report 2017–1020, 108 p., <https://doi.org/10.3133/ofr20171020>.
- Kanasewich, E.R., 1975, Time sequence analysis in geophysics, second edition: University of Alberta Press, p. 365.
- Kramer, S.L., 1996, Geotechnical earthquake engineering: New Jersey, Prentice Hall International Inc., 652 p.
- Maeda, N., 1985, A method for reading and checking phase times in auto-processing system of seismic wave data: *Zisin (Journal of the Seismological Society of Japan)*, v. 38, no. 3, p. 365–379.
- Massa, M., Pacor, F., Luzi L., Bindi, D., Milana, G., Sabetta, F., Gorini, A., and Marcucci, S., 2010, The Italian ACcelerometric Archive (ITACA)—Processing of strong-motion data: *Bulletin of Earthquake Engineering*, v. 8, issue 5, p. 1175–1187.
- Nigam, N.C., and Jennings, P.C., 1969, Calculation of response spectra from strong-motion earthquake records: *Bulletin of the Seismological Society of America*, v. 59, no. 2, p. 909–922.
- Shakal, A.F., and Ragsdale, J.T., 1984, Acceleration, velocity and displacement noise analysis for the CSMIP accelerogram digitization system: *Proceedings of the 8th World Conference on Earthquake Engineering*, v. 2, p. 111–118.
- Shakal, A.F., Huang, M.J., and Graizer, V.M., 2003, Strong-Motion Data Processing, Lee, W.H.K., Kanamori, H., Jennings, P.C., and Kisslinger, C., eds., *in International Handbook of Earthquake and Engineering Seismology*, B: Amsterdam, Academic Press, p. 967–981.
- Shakal, A.F., Huang, M.J., and Graizer, V.M., 2004, California Strong-Motion Instrumentation Program processing methods and procedures, *Proceedings of COSMOS Invited Workshop on Strong-Motion Processing: COSMOS Pub. CP-2004/02*, p. 111–122.
- Trifunac, M.D., 1971, Zero baseline correction of strong-motion accelerograms: *Bulletin of the Seismological Society of America*, v. 61, p. 1201–1211.
- Trifunac, M.D., and Brady, A.G., 1975, A study on duration of strong earthquake ground motion: *Bulletin of the Seismological Society of America*, v. 65, p. 581–626.
- Trifunac, M.D., 1977, Uniformly processed strong earthquake ground accelerations in the Western United States of America for the period from 1933 to 1971—Pseudo relative velocity spectra and processing noise: Los Angeles, University of Southern California Faculty Research and Publications, no. 77-04, p. 35, accessed January 2017 at <http://digitalibrary.usc.edu/cdm/ref/collection/p15799coll84/id/2798>.
- Wang, L.J., 1996, Processing of near-field earthquake accelerograms: Pasadena, California Institute of Technology, accessed January 2017 at <http://resolver.caltech.edu/CaltechEERL:1996.EERL-96-04>.

Appendix 1. Frequency-Domain Zero-Padding Resampling

Interpolating a time series is an important task in ground-motion processing and in computing response spectra. There are many time-domain resampling methods (for example, curve fitting) in the literature. An acceleration time series sampled at N samples-per-second (sps) should have no energy beyond the Nyquist frequency (f_{Nyquist}). Ideally, any interpolation method should not introduce energy at frequencies beyond f_{Nyquist} of the original time series. Linear interpolating to a higher sampling rate in time domain with an anti-aliasing filter violates this condition, and such resampled records are expected to lead to errors in the Fourier spectra and response spectra (Boore and Goulet, 2014). Other approaches for interpolation include zero-padding in the frequency-domain (Fraser, 1989), windowed sinc interpolation in the time-domain (Shannon, 1998), and resampling using poly-phase filter implementation (Schafer and Rabiner, 1973).

In the Processing and Review Interface for Strong Motion data (PRISM) software, we implemented the frequency-domain zero padding (FDZP) approach for resampling from N samples to $N \times M$ samples. The procedure consists of following steps (Lyons, 2014):

1. Compute an N -point (where N is a power of 2) fast Fourier transform (FFT) on N -point $x(n)$ time series, yielding N complex frequency samples $X(n)$.
2. Form the $N \times M$ -point split and zero-padded stretched transform. The number of additional zero-valued complex points is $N \times (M - 1)$. For example, to double the sampling rate, the required number of additional z -valued points is $N \times (2 - 1) = N$ (for a total of $2N$ complex frequencies). Then, the new frequency domain vector is constructed using the first $N/2 + 1$ points from $X(n)$, then appending the N additional zeros, and finally affixing the last $N/2 - 1$ points from $X(n)$. The zero padding is inserted “in the middle,” to preserve the conjugate symmetry in the transform domain.
3. Compute the real part of the $N \times M$ -point inverse FFT (IFFT) and scale by M to compensate for the $1/M$ amplitude loss introduced by the method resampling.

The procedure is tested using a chirp signal 20 s in duration starting at a frequency of 0.1 Hz ending at 50 Hz. The signal is interpolated from 100 to 200 sps. Figure 1–1 shows the spectrograms of the analytical linear chirp signal with 100 sps, the analytical linear chirp signal with 200 sps, and the interpolated linear chirp signal. In order to maintain the 20-s duration and make sure that both analytical chirp signals reach 50 Hz at 10 s, the analytical chirp signal with 100 sps folds at 50 Hz (figure 1–1A) in contrast to the linear chirp signal with 200 sps (figure 1–1B). Note that the energy of the interpolated signal (figure 1–1C) is bounded at 50 Hz, which meets the condition that the interpolation process should not introduce energy beyond the original f_{Nyquist} .

Figure 1–2A shows the comparison of analytical linear chirp signal with 200 sps in blue with resampled chirp signal from 100 sps to 200 sps in red, and the difference in analytical and resampled chirp signals. Overall, the resampled signal matches well with the analytical signal within a wide range of frequencies. Some discrepancies at high frequencies close to f_{Nyquist} (figure 1–2B) result from discontinuities in the time domain. When we try to approximate discontinuities in the time-domain, with a finite number of values in frequency-domain, ripples take place before and after the interpolated discontinuity.

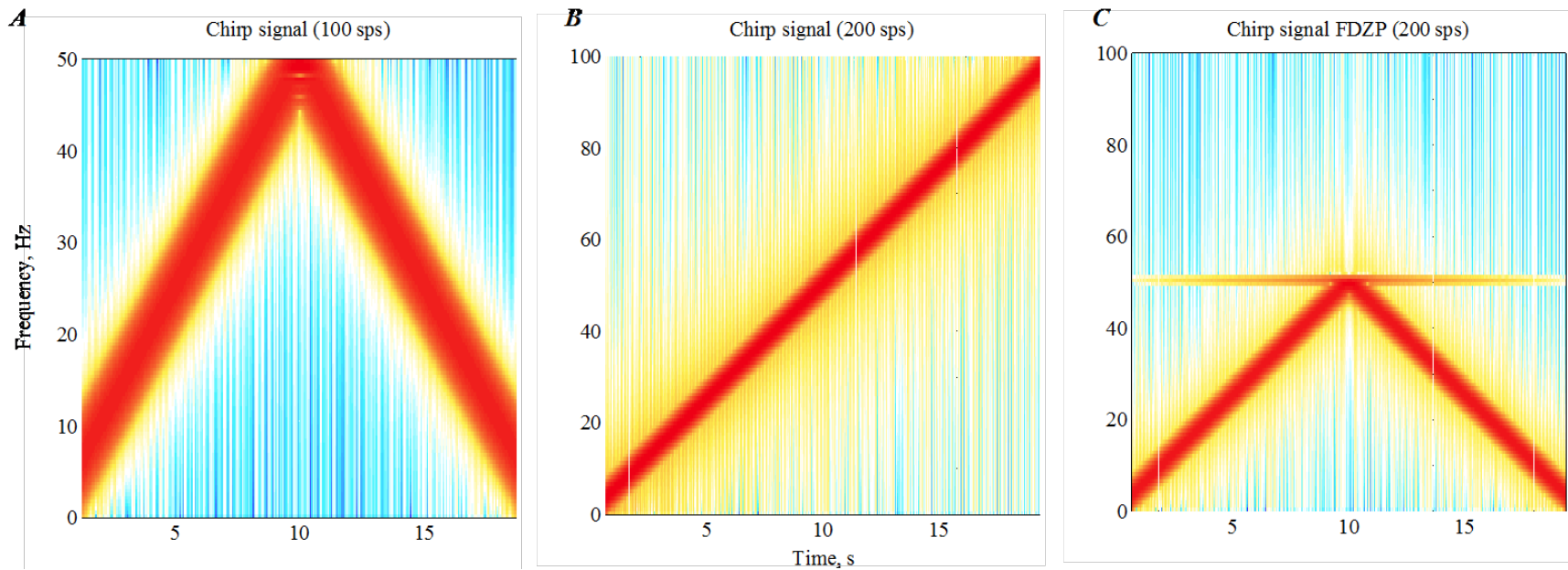


Figure 1–1. Graphs showing spectrograms. *A*, Analytical linear chirp signal with 100 samples-per-second (sps) with the frequency range of 0.1 to 50 hertz (Hz). *B*, Analytical linear chirp signal with 200 sps with the frequency range of 0.1 to 100 Hz. *C*, Interpolated linear chirp signal (from 100 to 200 sps by frequency-domain zero-padding [FDZP] resampling). The power spectral density of each segment of a linear chirp starts at 0 and crosses 50 Hz at 10 seconds. s, seconds.

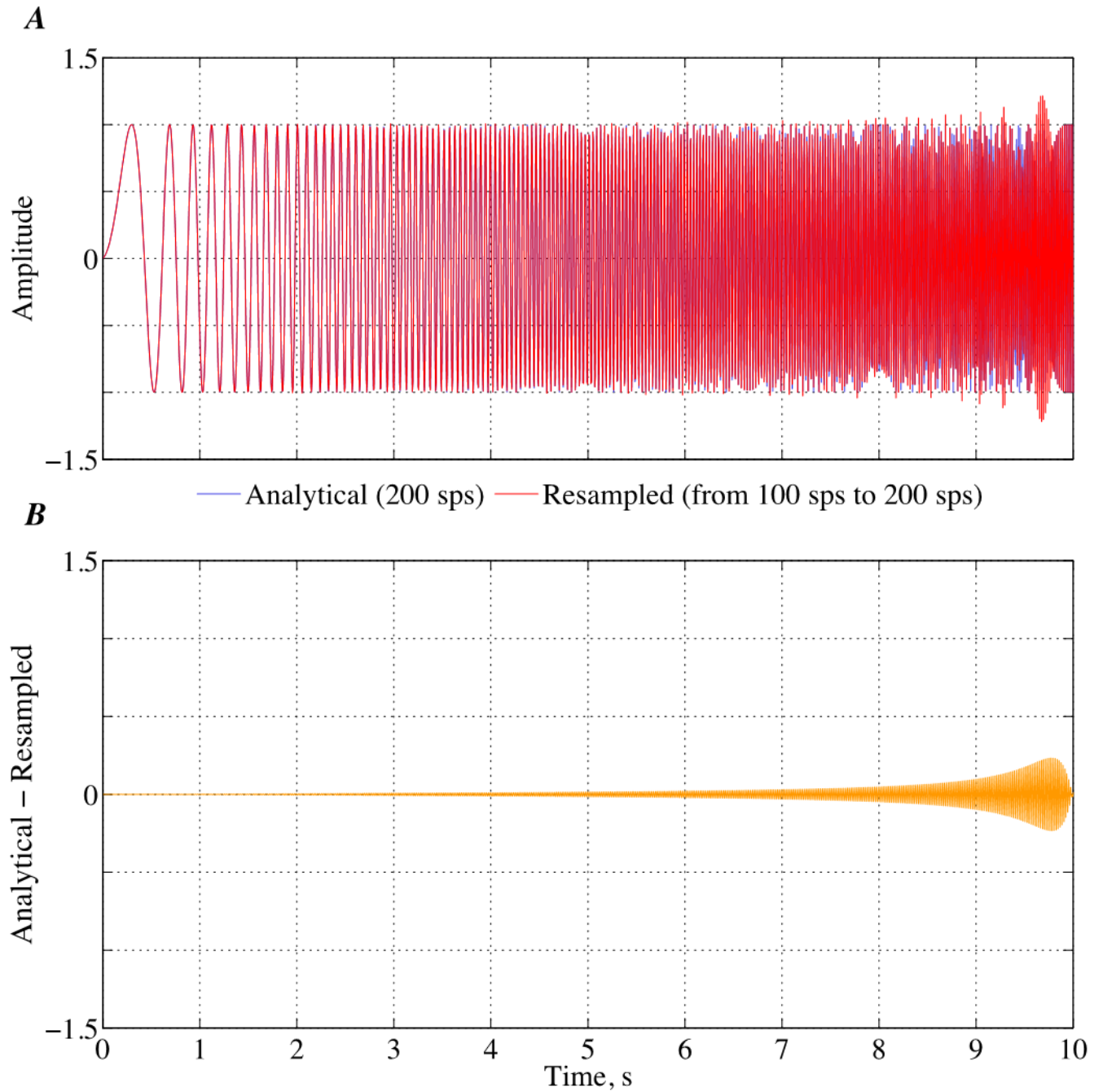


Figure 1-2. Graphs showing analytical and resampled chirp signals. *A*, Comparison of analytical linear chirp signal with 200 samples-per-second (sps) in blue with resampled chirp signal from 100 sps to 200 sps in red. *B*, Difference in analytical and resampled chirp signals. s, seconds.

References Cited

- Boore, D.M., and Goulet, C.A., 2014, The Effect of sampling rate and anti-aliasing filters on high-frequency response spectra: *Bulletin of Earthquake Engineering*, v. 12, p. 203–216.
- Fraser, D., 1989, Interpolation by the FFT revisited—An experimental investigation: *IEEE Transactions on Acoustics, Speech, and Signal Processing*, v. 37, p. 665–675, doi:10.1109/29.17559.
- Lyons, R.G., 2014, *Understanding digital signal processing*, third edition: Indiana, Prentice Hall, 954 p.
- Schafer, R.W., and Rabiner, L.R., 1973, A digital signal processing approach to interpolation: *Proceedings of the Institute of Electrical and Electronics Engineers (IEEE)*, v. 61, p. 692–702.
- Shannon, C.E., 1998, *Communication in the presence of noise* (a reprint of the classic 1949 paper): *Proceedings of the Institute of Electrical and Electronics Engineers (IEEE)*, v. 86, p. 447–457.

Appendix 2. Event-Onset Detection

Two event-onset detection algorithms have been implemented in the Processing and Review Interface for Strong Motion data (PRISM) software; these are $P_{PHASEPICKER}$ and Akaike information criterion (AIC) picker. While both pickers work well with ground-motion acceleration records, $P_{PHASEPICKER}$ provides more accurate picks (Kalkan, 2016). The theory behind these pickers is explained briefly in the following.

$P_{PHASEPICKER}$

$P_{PHASEPICKER}$ (also abbreviated as PWD) is an automated P -phase onset time picking algorithm without requiring any detection interval or threshold settings (Kalkan, 2016). This picker transforms the seismic signal into the response domain of a linear-elastic single-degree-of-freedom (SDF) oscillator with viscous damping (figure 2–1), and then tracks the rate of change (power) of dissipated energy in order to pick the event onset time (that is, P -wave phase). The SDF oscillator has a short natural period and a correspondingly high resonant frequency, which is higher than most frequencies in a seismic wave. The damping ratio is 60 percent of critical, which is similar to the short-period seismometers used to study body waves. At this damping level, the response of the oscillator very closely approaches the Butterworth “maximally flat” magnitude filter. This way the frequency content of the input signal is preserved in response of the oscillator—an important factor for accurate picking of the onset of the P -wave phase on time series.

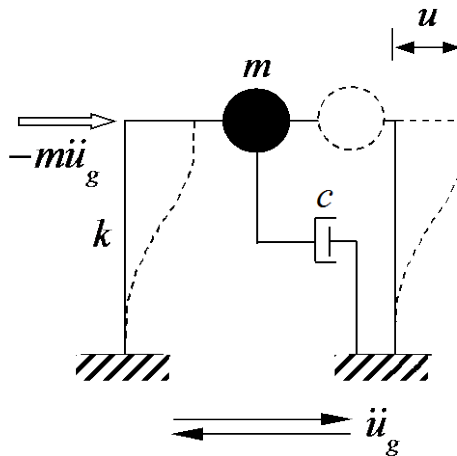


Figure 2–1. Illustration showing idealized fixed-base single-degree-of-freedom oscillator with viscous damping used for P -wave phase picking. c , damping; k , stiffness, m , mass; u , relative displacement of mass with respect to base; \ddot{u}_g , ground-motion acceleration.

The input energy imparted to the SDF oscillator by the seismic signal (that is, base excitation) is stored as elastic-strain energy and dissipated by damping energy. This is shown in figure 2–2 where the SDF oscillator is subjected to a raw acceleration record in trace (A), and the resultant energy parameters are plotted in trace (B) through trace (E). The relative-input energy is the summation of relative-kinetic energy, elastic-strain energy, and damping energy. The kinetic energy of the oscillator is negligibly small, because the mass barely moved with respect to the base owing to the short-vibration period and high damping ratio of the SDF oscillator. The relative velocity of the mass is small, yet it preserves the frequency characteristics of the input acceleration. The damping energy is a cumulative function (proportional to square of the relative velocity of the mass—as will be shown in equation [A2]);

therefore, it yields a smooth dissipation envelope over time. The damping energy is zero in the beginning of the signal, zero or near zero before the *P*-phase arrival, and builds up rapidly with the *P*-wave. Because the damping energy function changes considerably at the onset of the signal, it is a convenient metric to track and detect the *P*-phase arrival time.

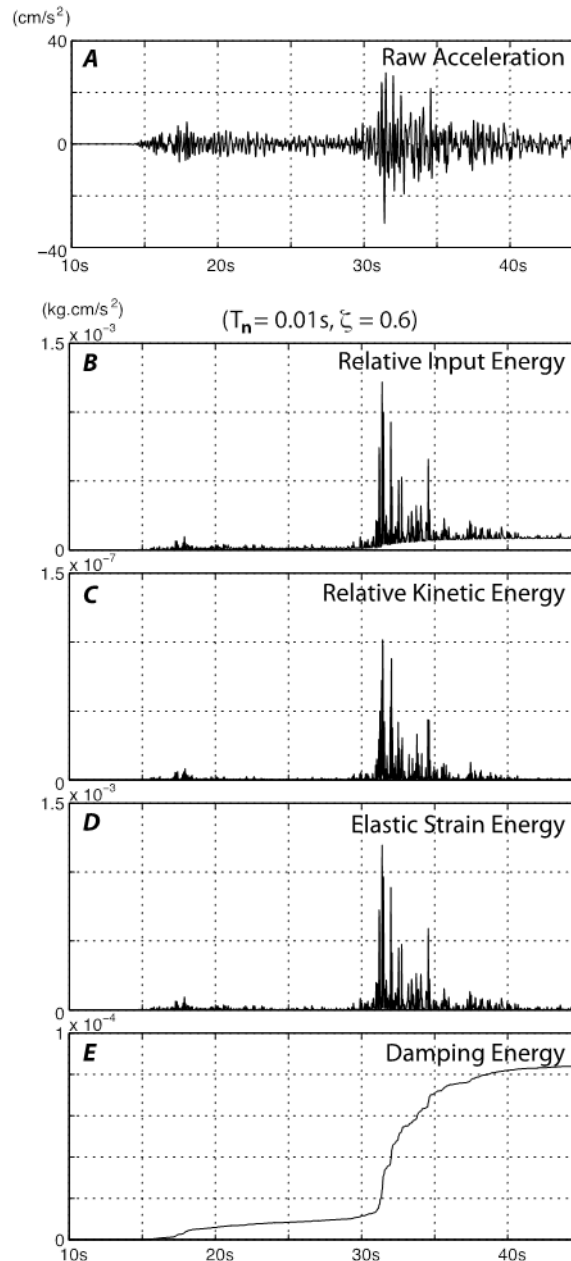


Figure 2-2. Graphs showing raw acceleration record of AZ-BZN station with 100 samples-per-second from 03/29/2014 *M*5.1 La Habra earthquake in southern California used to demonstrate the energy metrics for idealized single-degree-of-freedom (SDF) oscillator as fixed-base with a short period and high damping ratio ($T_n = 0.01 \text{ s}$, $\zeta = 0.6$). *A*, Raw acceleration signal. *B*, Relative-input energy imparted to the SDF oscillator. *C*, Relative-kinetic energy of the moving mass with respect to base. *D*, Elastic-strain energy. *E*, Energy dissipated by viscous damping. Energy is in units of kilograms centimeters per second squared ($\text{kg}\cdot\text{cm}/\text{s}^2$). Note the smoothness of damping energy in *E*.

As an example, the $P_{PHASEPICKER}$ is applied to a three-component raw acceleration record in figure 2–3. This record, obtained from a $M6.1$ earthquake occurred on May 05, 2014 in Thailand, is chosen because its HN1 component is much noisier than the other two components. The $P_{PHASEPICKER}$ picks the P -phase onset (P0-) at 61.55, 61.08, and 61.80s respectively for HN1, HN2, and UP components (marked by vertical red line) where there is a noticeable change in the energy content at the onset of the signal. To facilitate comparisons, the damping energy and its power are normalized in each panel by the corresponding peak values. The manual picks are 60.65 s, 61.00 s, and 61.70 s. The maximum discrepancy between the manual picks and the picks by $P_{PHASEPICKER}$ is 0.09 s.

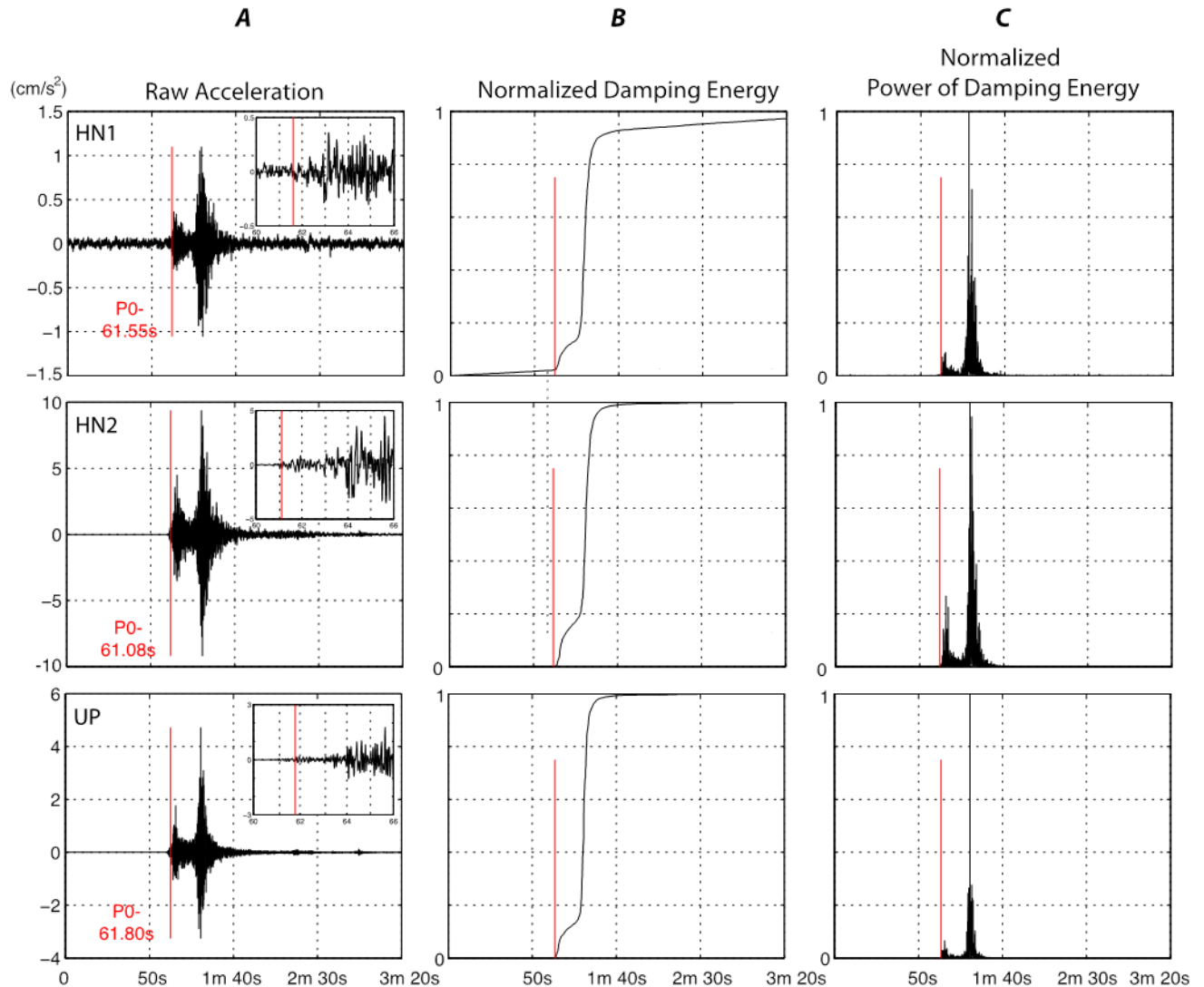


Figure 2–3. Graphs showing P -phase detection results for three-component acceleration records obtained from a $M6.1$ earthquake on 05/05/2014 in Thailand with 100 samples-per-second. *A*, Raw acceleration components (with mean removed). *B*, Normalized damping energy. *C*, Normalized power of damping energy dissipated. Damping energy and power plots, normalized by their associated peak values, correspond to bandpass filtered input signal with corner frequencies: high-cut = 20 hertz (Hz) and low-cut = 0.1 Hz. Emergent P -phase onset is shown by vertical red line and is repeated in close up views on left panels. Manual pick times are 60.65 seconds (s), 61.00 s, and 61.70 s, consistent with picking results from $P_{PHASEPICKER}$. cm/s^2 , centimeters per second squared; m, minutes.

Akaike Information Criterion (AIC) Picker

Autoregressive (AR) techniques are commonly used for phase picking in seismology. These techniques are based on the assumption that the seismic signal can be divided into locally stationary segments each modeled as an AR process, and the intervals before and after the onset time are two different stationary processes with different statistical properties (Sleeman and van Eck, 1999; Rastin and others, 2013). To detect an ideal time instant that splits statistical properties of the sub-window before the onset (signal containing background noise) from those of the sub-window (signal containing seismic waves and background noise) after the onset, AR techniques analyze different windows of time series. For example, typical seismic noise is well represented by a relatively low order AR process, whereas seismic signals are usually represented by a higher order AR process (Leonard and Kennett, 1999).

The Akaike information criterion (AIC) helps to determine the order of the AR process when fitting a time series with an AR process, which indicates the model misfit as well as the unreliability (Akaike, 1974). This method has been used in onset estimation by analyzing the variation in AR coefficients representing both multi-component and single-component traces of broadband and short-period seismograms (Takanami and Kitagawa, 1988; Leonard and Kennett, 1999). When the order of the AR process is fixed, the AIC function is a measure for the model fit. The point where the AIC is minimized determines the optimal separation of the two stationary time series in the least squares sense, and thus is interpreted as the phase onset (Sleeman and van Eck, 1999); this picker is known as AR-AIC picker (Leonard, 2000). Different than AR-AIC picker, Maeda (1985) calculates the AIC function directly from the seismogram without using the AR coefficients. For time series x of length N , the AIC is defined as

$$\text{AIC}(k) = k \log(\text{var}(x[1, k])) + (N - k - 1) \log(\text{var}(x[k + 1, N])) \quad (2-1)$$

where k is range through all times of the time series.

The AIC picker finds the onset point as the global minimum. For the accelerogram with a very clear onset, AIC values have a very clear global minimum, which corresponds to the P -phase arrival as shown in figure 2–4. For the accelerogram with a relatively low signal-to-noise ratio (SNR), there are a few local minima in AIC values and global minimum cannot guarantee to indicate the P -phase onset (figure 2–5A). When there is more noise in the accelerogram and associated multiple local minima in AIC values, even filtering and detrending may not be sufficient to get the accurate P -phase onset (figure 2–5B). When there are more seismic phases in a time window, AIC picker will choose the stronger phase. For this reason, it is necessary to choose a time window especially for those records with low SNR that includes only the segment of accelerogram of interest. If the time window is chosen properly, AIC picker can find the P -phase arrival more accurately (figure 2–5C). On the other hand, AIC picker is not “smart” enough so that it will usually pick an “onset” for any segment of data no matter whether there is a true phase arrival in the time window or not (figure 2–6).

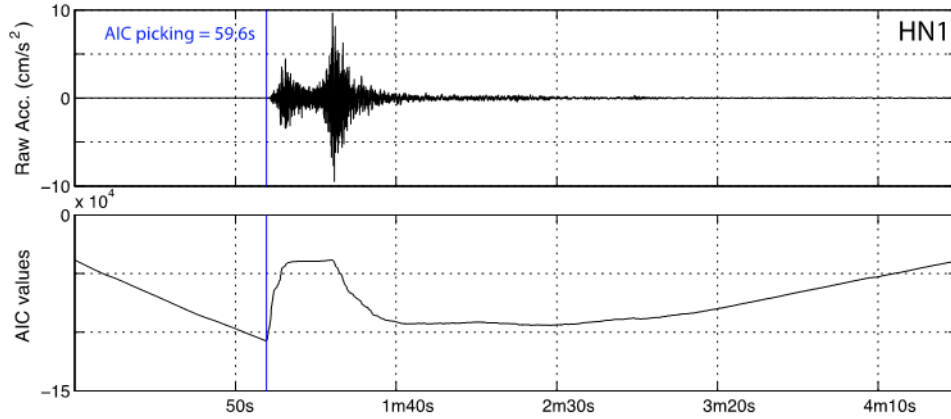


Figure 2–4. Graphs showing HN1 component of acceleration record obtained from a *M*6.1 earthquake on 05/05/2014 in Thailand with 100 samples-per-second, and its corresponding Akaike information criterion (AIC) values. For an accelerogram with a clear *P*-wave arrival, AIC value has a very clear minimum point. cm/s², centimeters per second squared; m, minutes; s, seconds.

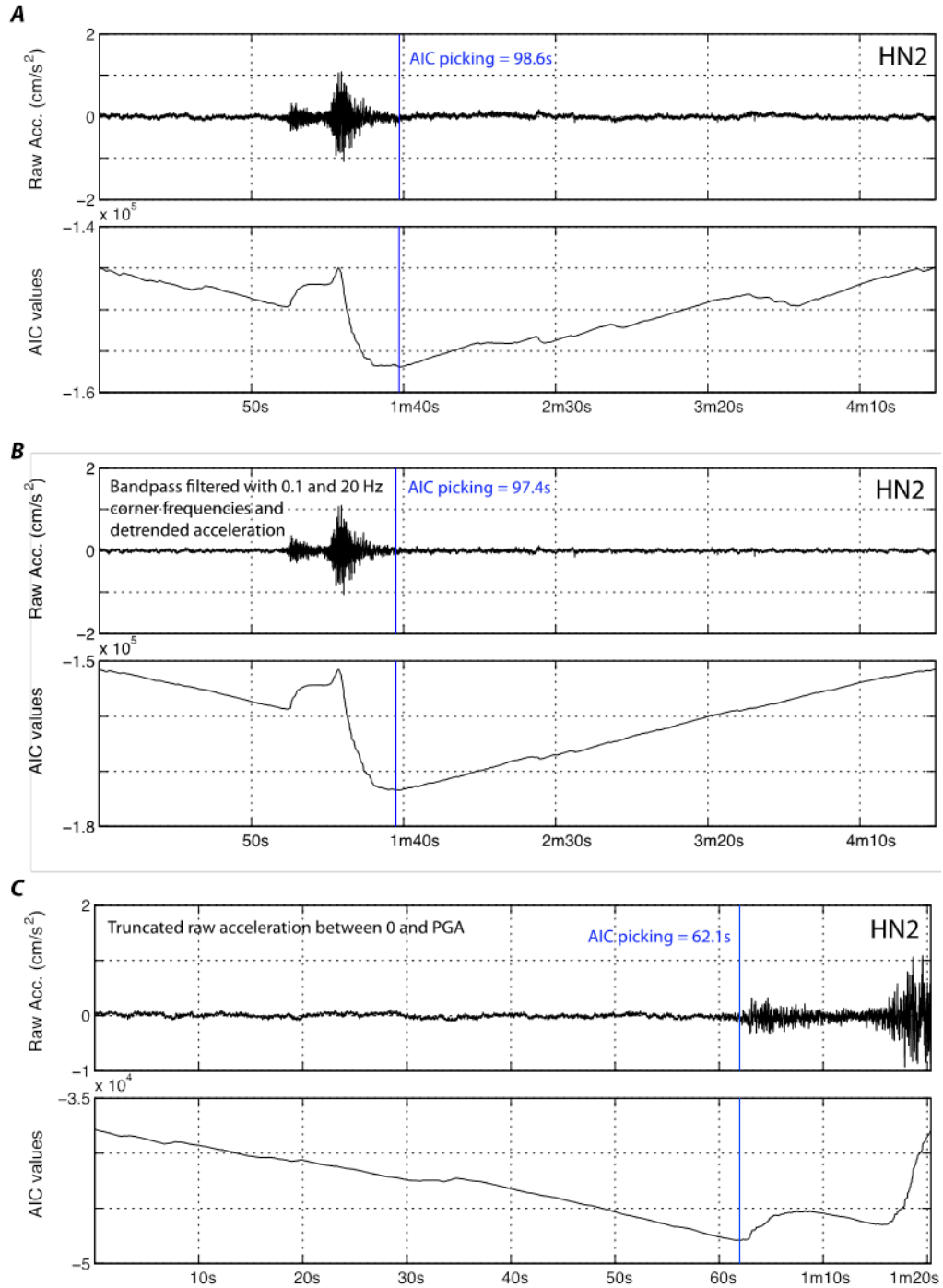


Figure 2-5. Graphs showing HN2 component of acceleration record from a $M6.1$ earthquake on 05/05/2014 in Thailand with 100 samples-per-second, and its corresponding Akaike information criterion (AIC) values. A, For raw accelerogram with relatively lower signal-to-noise ratio, AIC function has many local minima, and the global minima cannot be guaranteed to be the P -phase onset. B, For accelerogram bandpass filtered, AIC function picks the global minima not corresponding to P -phase arrival. C, For raw accelerogram truncated between 0 and peak-ground acceleration, local minima corresponds to P -phase onset. cm/s², centimeters per second squared; Hz, hertz; m, minutes; PGA, peak ground acceleration; s, seconds.

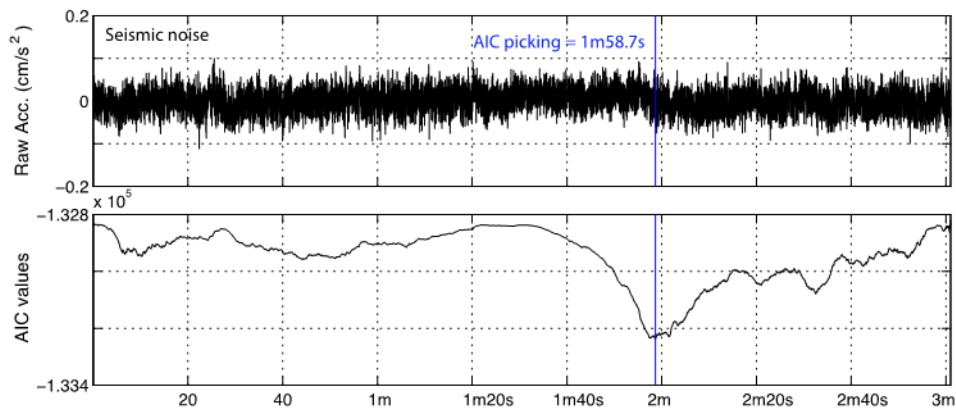


Figure 2-6. Graph showing seismic noise data and its Akaike information criterion (AIC) values. The minimum AIC value does not indicate any phase arrival although it divides the data into two different stationary segments. cm/s^2 , centimeters per second squared; m, minutes; s, seconds.

References Cited

- Kalkan, E., 2016, An automatic P-phase arrival time picker: *Bulletin of the Seismological Society of America*, v. 106, no. 3, p. 971–986, doi:10.1785/0120150111.
- Leonard, M., 2000, Comparison of manual and automatic onset time picking: *Bulletin of the Seismological Society of America*, v. 90, no. 6, p. 1384–1390.
- Leonard, M., and Kennett, B.L.N., 1999, Multi-component autoregressive techniques for the analysis of seismograms: *Physics of the Earth and Planetary Interiors*, v. 113, p. 247–263.
- Maeda, N., 1985, A method for reading and checking phase times in auto-processing system of seismic wave data: *Zisin (Journal of the Seismological Society of Japan)*, v. 38, no. 3, p. 365–379.
- Rastin, S.J., Unsworth, C.P., Benites, R., and Gledhill, K.R., 2013, Using real and synthetic waveforms of the Matata Swarm to assess the performance of New Zealand GeoNet phase pickers: *Bulletin of the Seismological Society of America*, v. 103, p. 2173–2187.
- Sleeman, R., and Van Eck, T., 1999, Robust automatic P-phase picking—An on-line implementation in the analysis of broadband seismogram recordings: *Physics of the Earth and Planetary Interiors*, v. 113, p. 265–275.
- Takanami, T., and Kitagawa, G., 1988, A new efficient procedure for the estimation of onset times of seismic waves: *Journal of Physics of the Earth*, v. 36, p. 267–290.

Appendix 3. PRISM Configuration XML File

PRISM uses XML file format for the configuration file. XML is a file extension, which stands for extensible markup language. The details of the PRISM configuration XML file are as follows:

```
<?xml version="1.0" encoding="UTF-8"?>
<PRISM>
  <!-- Entries taken from Table 4. Strong Motion Network Codes, in the
  COSMOS Strong Motion Data Format spec. -->
  <ProcessingAgency>
    <StrongMotionNetworkCode>
      <AgencyFullName>U.S. Geological Survey</AgencyFullName>
      <AgencyAbbreviation>USGS</AgencyAbbreviation>
      <AgencyCode>2</AgencyCode>
      <AgencyIRISCode>NP</AgencyIRISCode>
    </StrongMotionNetworkCode>
  </ProcessingAgency>

  <!-- Units to use for conversion from counts in V1 processing. Entries
  taken from Table 2. Data Units Codes, in the COSMOS Strong Motion
  Data Format spec. Currently supported are cm/sec/sec and g. -->
  <DataUnitsForCountConversion>
    <DataUnitCodes>
      <DataUnitCode>04</DataUnitCode>
      <DataUnitName>cm/sec2</DataUnitName>
    </DataUnitCodes>
  </DataUnitsForCountConversion>

  <!-- There are 2 different algorithms for event detection:
  AIC (modified Akaike Information Criterion) or PWD (P-wave Detector). -->
  <EventDetectionMethod>PWD</EventDetectionMethod>

  <!--The Event Onset algorithm estimates the start of the event onset and
  returns the time that the onset occurred in the time series, assuming time = 0
  at the start of the data array. The event onset buffer parameter
  extends the returned time earlier in the array by the buffer
  value. The buffer value is in seconds. The default is 0.0 seconds. -->

  <EventOnsetBufferAmount>0.0</EventOnsetBufferAmount>

  <!-- The QC parameters are used during V2 processing as acceptable limits
  for the initial and residual velocity and the residual displacement. If
  the array values during QC tests are less than or equal to these parameters,
  then the record passes on to V3 processing. -->
  <QCparameters>
    <InitialVelocity>0.1</InitialVelocity>
    <ResidualVelocity>0.1</ResidualVelocity>
```

```
<ResidualDisplacement>0.1</ResidualDisplacement>
</QCparameters>
```

<!-- The Butterworth band pass filter implementation expects the filter order to be an even number. If an odd number is entered here for the filter order, it will be truncated by integer division to the next lower multiple of 2. The taper length is defined in seconds, and defines the number of elements at the beginning and end of the array over which the half cosine taper is applied. -->

```
<BandPassFilterParameters>
  <BandPassFilterOrder>4</BandPassFilterOrder>
  <BandPassTaperLength>3.0</BandPassTaperLength>
  <BandPassFilterCutoff>
    <CutoffLow>0.1</CutoffLow>
    <CutoffHigh>20.0</CutoffHigh>
  </BandPassFilterCutoff>
</BandPassFilterParameters>
```

<!--If a filename is given here, it will be read in and used to configure the filters to be used for given station numbers. Currently not used -->

```
<StructuresFilterTable></StructuresFilterTable>
```

<!--The Adaptive Baseline Correction algorithm uses 3 segments to try and construct a baseline correction function. The first segment, from the start of the velocity array until the event onset, is fitted with a polynomial whose order is defined with the FirstPolyOrder tag. The third segment, whose start is determined by an iterative process, is fitted with a polynomial whose order is defined with the ThirdPolyOrder tag. The middle segment, starting at the event onset, is fitted with a polynomial spline function that interpolates between the 1st and 3rd segments.-->

```
<AdaptiveBaselineCorrection>
  <FirstPolyOrder>
    <LowerLimit>1</LowerLimit>
    <UpperLimit>2</UpperLimit>
  </FirstPolyOrder>
  <ThirdPolyOrder>
    <LowerLimit>1</LowerLimit>
    <UpperLimit>3</UpperLimit>
  </ThirdPolyOrder>
</AdaptiveBaselineCorrection>
```

<!-- The strong motion threshold parameter determines the %g that the corrected acceleration needs to meet or exceed to have computed parameters calculated and the strong motion flag set. This value should be a percentage, such as 5 for strong

```

motion records >= 5%g -->
<StrongMotionThreshold>5</StrongMotionThreshold>
<!-- The differentiation order parameter: values 3,5,7,9 -->
<DifferentiationOrder>5</DifferentiationOrder>
<!-- Tags for output data array format are SingleColumn and Packed.
SingleColumn will write one data value per line, and Packed will pack
multiple values per line to fill up the 80-character line width. -->
<OutputArrayFormat>SingleColumn</OutputArrayFormat>
<!-- The DeleteInputV0 flag controls the deletion of the files from the input folder
as they are processed. If flag is set to 'Yes', the input files that are successfully
processed will be deleted from the input folder. This option is for an automated
processing configuration. To leave the input files in the input folder after execution
is complete, set this flag to 'No'. -->
<DeleteInputV0>No</DeleteInputV0>
<!-- The DebugToLog flag controls the amount of information that is written to the
ErrorDebugLog text file during processing. If this flag is set to Off, only information
about records that fail to pass V2 processing will be written to the log. If the
value is set to On, debug information about all records processed gets written to the log.
The WriteBaselineFunction flag, if set to 'On', will cause the baseline functions created
during adaptive baseline correction (ABC) to be written as text files into the
output folder.
It will also write the velocity array just before baseline correction.
The name of the files will be the V0 file name with either "baseline.txt" or
"afterIntegrationToVel" appended to it. If
the flag is set to 'On' and no baseline text files are output, then ABC was not used for any
processing.
-->
<DebugToLog>On</DebugToLog>
<WriteBaselineFunction>On</WriteBaselineFunction>
</PRISM>

```

Appendix 4. Logging and Parametric Data

PrismLog

The “PrismLog.txt” file contains the full path name of every product file generated during a Processing and Review Interface for Strong Motion data (PRISM) software processing run as well as a copy of the configuration file parameters used during processing. PRISM appends the results of each processing run to the end of an existing “PrismLog.txt” file found in the “Logs” directory under the output directory, and writes the date and time at the start of each run. Since the input V0 files are unbundled and moved to the output directory, the name of each V0 file is also recorded as a product. Any errors that PRISM encounters during processing are also written to this log file. The error messages should contain the name of the V0 file that caused the error as well as the error condition itself. PRISM tries to complete processing on all files in the input directory, and the software will log non-fatal errors and continue to completion. A portion of the PrismLog from the 2014 M4.4 Greenfield earthquake ground-motion processing, showing a recorded error message for missing header metadata in a record is shown as follows:

```
Prism Log Entry: 2015-04-01 21:37:32 GMT
D:\PRISM\smtesting\new_Greenfield\out\NC.72383481\BK.SAO\V0\BKSAO--n.481.HNE.00.V0
D:\PRISM\smtesting\new_Greenfield\out\NC.72383481\BK.SAO\V0\BKSAO--n.481.HNN.00.V0
D:\PRISM\smtesting\new_Greenfield\out\NC.72383481\BK.SAO\V0\BKSAO--n.481.HNZ.00.V0
D:\PRISM\smtesting\new_Greenfield\out\NC.72383481\BK.SAO\V1\BKSAO--n.481.HNE.00.V1
D:\PRISM\smtesting\new_Greenfield\out\NC.72383481\BK.SAO\V1\BKSAO--n.481.HNN.00.V1
D:\PRISM\smtesting\new_Greenfield\out\NC.72383481\BK.SAO\V1\BKSAO--n.481.HNZ.00.V1
D:\PRISM\smtesting\new_Greenfield\out\NC.72383481\BK.SAO\V2\BKSAO--n.481.HNE.00.acc.V2
D:\PRISM\smtesting\new_Greenfield\out\NC.72383481\BK.SAO\V2\BKSAO--n.481.HNE.00.vel.V2
D:\PRISM\smtesting\new_Greenfield\out\NC.72383481\BK.SAO\V2\BKSAO--n.481.HNE.00.dis.V2
D:\PRISM\smtesting\new_Greenfield\out\NC.72383481\BK.SAO\V2\BKSAO--n.481.HNN.00.acc.V2
D:\PRISM\smtesting\new_Greenfield\out\NC.72383481\BK.SAO\V2\BKSAO--n.481.HNN.00.vel.V2
D:\PRISM\smtesting\new_Greenfield\out\NC.72383481\BK.SAO\V2\BKSAO--n.481.HNN.00.dis.V2
D:\PRISM\smtesting\new_Greenfield\out\NC.72383481\BK.SAO\V2\BKSAO--n.481.HNZ.00.acc.V2
D:\PRISM\smtesting\new_Greenfield\out\NC.72383481\BK.SAO\V2\BKSAO--n.481.HNZ.00.vel.V2
D:\PRISM\smtesting\new_Greenfield\out\NC.72383481\BK.SAO\V2\BKSAO--n.481.HNZ.00.dis.V2
D:\PRISM\smtesting\new_Greenfield\out\NC.72383481\BK.SAO\V3\BKSAO--n.481.HNE.00.V3
D:\PRISM\smtesting\new_Greenfield\out\NC.72383481\BK.SAO\V3\BKSAO--n.481.HNN.00.V3
D:\PRISM\smtesting\new_Greenfield\out\NC.72383481\BK.SAO\V3\BKSAO--n.481.HNZ.00.V3
Unable to process file D:\PRISM\smtesting\new_Greenfield\in\BKTCHL-n.481.v0c
Real header #42, sensor sensitivity, is invalid: 0.0
```

TroubleLog

The “TroubleLog.txt” file contains the full path name of every product file written into a “Trouble” directory. Files are sent to a “Trouble” directory when PRISM is unable to complete V2 processing or when the processed V2 time series fail the QC tests. Specific information on the problem can be found in the Debug files described below. The TroubleLog file names are appended with the processing date and time, so each PRISM processing run will create a new TroubleLog file. An example of the TroubleLog file from the South Napa processing is given as follows:

D:\PRISM\smtesting\new_Napa\out\NC.72282711\NC.CUSLD\Trouble\V0\NCCUSLDn.711.10.V0
 D:\PRISM\smtesting\new_Napa\out\NC.72282711\NC.CUSLD\Trouble\V1\NCCUSLDn.711.10.V1
 D:\PRISM\smtesting\new_Napa\out\NC.72282711\NC.HMOB\Trouble\V0\NCHMOB-n.711.HNZ.--.V0
 D:\PRISM\smtesting\new_Napa\out\NC.72282711\NC.HMOB\Trouble\V1\NCHMOB-n.711.HNZ.--.V1
 D:\PRISM\smtesting\new_Napa\out\NC.72282711\NC.N016\Trouble\V0\NCN016-n.711.HNN.01.V0
 D:\PRISM\smtesting\new_Napa\out\NC.72282711\NC.N016\Trouble\V1\NCN016-n.711.HNN.01.V1
 D:\PRISM\smtesting\new_Napa\out\NC.72282711\NC.N016\Trouble\V2\NCN016-n.711.HNN.01.acc.V2
 D:\PRISM\smtesting\new_Napa\out\NC.72282711\NC.N016\Trouble\V2\NCN016-n.711.HNN.01.vel.V2
 D:\PRISM\smtesting\new_Napa\out\NC.72282711\NC.N016\Trouble\V2\NCN016-n.711.HNN.01.dis.V2
 D:\PRISM\smtesting\new_Napa\out\NC.72282711\NP.1765\Trouble\V0\NP1765-n.711.2.V0
 D:\PRISM\smtesting\new_Napa\out\NC.72282711\NP.1765\Trouble\V1\NP1765-n.711.2.V1
 D:\PRISM\smtesting\new_Napa\out\NC.72282711\NP.1765\Trouble\V2\NP1765-n.711.2.acc.V2
 D:\PRISM\smtesting\new_Napa\out\NC.72282711\NP.1765\Trouble\V2\NP1765-n.711.2.vel.V2
 D:\PRISM\smtesting\new_Napa\out\NC.72282711\NP.1765\Trouble\V2\NP1765-n.711.2.dis.V2

DebugLog

The “DebugLog.txt” file contains detailed information on processing parameters for each record. These processing parameters include such information as the event detection method, the event onset time, and the value of the pre-event mean removed from acceleration, as well as the expected and actual QC parameters. If the DebugToLog flag in the configuration file is set to “Off”, only processing parameters for records that are sent to Trouble directories are written to “DebugLog.txt”. If the flag is set to “On”, then the parameters for all records are written to the file. The DebugLog file names are appended with the processing date and time, so each PRISM processing run will create a new DebugLog file. An example of one entry in the DebugLog file for the South Napa processing is as follows:

Prism Error/Debug Log Entry: 2015-04-07 15:51:56 GMT

Start of V2 processing for D:\PRISM\smtesting\new_Napa\in\NCN016-n.711.v0c and channel HNN.01

EventID: 72282711

time per sample in sec 0.005

sample rate (samp/s): 200.0

length of acceleration array: 36200

Event detection: remove linear trend, filter, event onset detection

filtering before event onset detection, taperlength: 400

Event Detection algorithm: PwD method

pick index: 6178, start index: 6178

pick time in seconds: 30.890, buffered time: 30.890

Acausal bandpass filter:

earthquake magnitude is 6.02 and M used is MOMENT

adjusted lowcut: 0.10 and adjusted highcut: 40.00 Hz

Pre-event mean of -7.111225e-02 removed from uncorrected acceleration

acceleration integrated to velocity

Velocity QC1 failed:

initial velocity: 0.103919, limit 0.100000
final velocity: 0.001318, limit 0.100000
Adaptive baseline correction beginning
length of ABC params: 312
ABC: final status: FAILQC
ABC: rank: 0
ABC: poly1 order: 2
ABC: poly2 order: 1
ABC: start: 6178 stop: 8178
ABC: velstart: 0.152344, limit 0.100000
ABC: velend: 0.002621, limit 0.100000
ABC: disend: 0.002350, limit 0.100000
ABC: calc. taperlength: 6072
Final QC failed - V2 processing unsuccessful:
initial velocity: 0.103919, limit 0.100000
final velocity: 0.001318, limit 0.100000
final displacement,: 0.000000, limit 0.100000
V2process: exit status = FAILQC
Peak Velocity: -46.475859

ParameterLog

The ParameterLog contains the same information as the DebugLog only written in comma-separated value (CSV) format for viewing in a spreadsheet application. It follows the same convention as the DebugLog, with the type of information written to it controlled by the DebugToLog configuration file parameter. The ParameterLog file names are appended with the processing date and time, so each PRISM processing run will create a new ParameterLog file. An example ParameterLog file for few entries is shown in table 4–1 for the South Napa earthquake processing.

aphtable

The aphtable is a CSV file that records parametric data about each record that was successfully processed. It contains station-orientation information as well as peak ground motion and response values (see table 4–2). The aphtable file names are appended with the processing date and time, so each PRISM processing run will create a new aphtable file.

Table 4-1. Example of ParameterLog comma-separated value (CSV) file for the 2014 moment magnitude 6.0 South Napa earthquake ground-motion processing.

[ABC, adaptive baseline correction; ACC, acceleration; CM, centimeters; CM/SEC, centimeters per second; DIS, displacement; G, gravitational acceleration; MAG, magnitude; PARM, parameter; POLY1, first polynomial; POLY2, second polynomial; SAMP, sampling; SEC, seconds; VEL, velocity; WIN, winning rank]

| EVENT | MAG | NAME | CHANNEL | ARRAY LENGTH | SAMP INTERVAL(SEC) | PICK INDEX | PICK TIME(SEC) | PEAK VEL(CM/SEC) | TAPERLENGTH | PRE-EVENT MEAN | PEAK ACC(G) | STRONG MOTION |
|----------|------|------------------|---------|--------------|--------------------|------------|----------------|------------------|-------------|----------------|-------------|---------------|
| 72282711 | 6.02 | NCCRH--n.711.v0c | HNE.-- | 18100 | 0.01 | 3274 | 32.74 | -2.45062 | 3261 | -0.098617 | 0.0222 | NO |
| 72282711 | 0 | NCCUSLDn.711.v0c | 10 | 36200 | 0.005 | 0 | 0 | 0 | 0 | 0 | 0 | -- |
| 72282711 | 6.02 | NCG005-n.711.v0c | HNE.01 | 36200 | 0.005 | 6546 | 32.73 | -1.33834 | 6343 | -0.016673 | -0.0116 | NO |
| 72282711 | 6.02 | NCG005-n.711.v0c | HNN.01 | 36200 | 0.005 | 6771 | 33.855 | 1.23331 | 6689 | 0.00273 | -0.0117 | NO |
| 72282711 | 6.02 | NCG005-n.711.v0c | HNZ.01 | 36200 | 0.005 | 6231 | 31.155 | -0.7267 | 6156 | 0.001277 | -0.0037 | NO |
| 72282711 | 6.02 | NCG006-n.711.v0c | HNE.01 | 36200 | 0.005 | 6660 | 33.3 | 0.68662 | 4164 | 0.000434 | 0.0013 | NO |
| 72282711 | 6.02 | NCG006-n.711.v0c | HNN.01 | 36200 | 0.005 | 6705 | 33.525 | -1.05912 | 2118 | -0.001974 | 0.0017 | NO |
| 72282711 | 6.02 | NCG006-n.711.v0c | HNZ.01 | 36200 | 0.005 | 6651 | 33.255 | 0.40241 | 3458 | 0.000988 | 0.0012 | NO |
| 72282711 | 6.02 | NCGAXB-n.711.v0c | HNE.-- | 18100 | 0.01 | 3131 | 31.31 | 1.94177 | 3109 | -0.001714 | -0.015 | NO |
| 72282711 | 6.02 | NCGAXB-n.711.v0c | HNN.-- | 18100 | 0.01 | 3213 | 32.13 | 1.84514 | 3048 | 0.001821 | 0.0241 | NO |
| 72282711 | 6.02 | NCGAXB-n.711.v0c | HNZ.-- | 18100 | 0.01 | 3054 | 30.54 | 0.80275 | 2828 | -0.00311 | 0.0084 | NO |
| 72282711 | 6.02 | NCGCVB-n.711.v0c | HNE.-- | 18100 | 0.01 | 3188 | 31.88 | 2.01397 | 3181 | -0.001468 | -0.0048 | NO |
| 72282711 | 6.02 | NCGCVB-n.711.v0c | HNN.-- | 18100 | 0.01 | 3195 | 31.95 | 1.59148 | 3158 | 0.028221 | 0.0059 | NO |
| 72282711 | 6.02 | NCJ013-n.711.v0c | HNN.01 | 36200 | 0.005 | 6230 | 31.15 | 1.37152 | 6177 | 0.017827 | 0.0264 | NO |
| 72282711 | 6.02 | NCJ013-n.711.v0c | HNZ.01 | 36200 | 0.005 | 6131 | 30.655 | 0.80777 | 5051 | -0.003612 | -0.0185 | NO |
| 72282711 | 6.02 | NCJ015-n.711.v0c | HNE.01 | 36200 | 0.005 | 6277 | 31.385 | 0.90498 | 6267 | 0.002582 | -0.0057 | NO |
| 72282711 | 6.02 | NCJ015-n.711.v0c | HNN.01 | 36200 | 0.005 | 6418 | 32.09 | -0.7775 | 4547 | 0.003138 | -0.0074 | NO |
| 72282711 | 6.02 | NCJ015-n.711.v0c | HNZ.01 | 36200 | 0.005 | 6092 | 30.46 | 0.37635 | 4574 | 0.000914 | -0.002 | NO |
| 72282711 | 6.02 | NCJ016-n.711.v0c | HNE.01 | 36200 | 0.005 | 6386 | 31.93 | -0.80968 | 6326 | -0.000856 | 0.015 | NO |
| 72282711 | 6.02 | NCJ016-n.711.v0c | HNN.01 | 36200 | 0.005 | 6285 | 31.425 | -0.94549 | 3051 | -0.001179 | -0.0124 | NO |
| 72282711 | 6.02 | NCJ016-n.711.v0c | HNZ.01 | 36200 | 0.005 | 6089 | 30.445 | 0.45354 | 2846 | -0.003282 | -0.0056 | NO |
| 72282711 | 6.02 | NCJ017-n.711.v0c | HNE.01 | 36200 | 0.005 | 6271 | 31.355 | 1.11937 | 4364 | 0.009041 | 0.01 | NO |

Table 4-1. Example of ParameterLog comma-separated value (CSV) file for the 2014 moment magnitude 6.0 South Napa earthquake ground-motion processing—Continued.

[ABC, adaptive baseline correction; ACC, acceleration; CM, centimeters; CM/SEC, centimeters per second; DIS, displacement; G, gravitational acceleration; MAG, magnitude; PARM, parameter; POLY1, first polynomial; POLY2, second polynomial; SAMP, sampling; SEC, seconds; VEL, velocity; WIN, winning rank]

| EXIT STATUS | VEL INITIAL(CM/SEC) | VEL RESIDUAL(CM/SEC) | DIS RESIDUAL(CM) | BASELINE CORRECTION | POLY1 | ABC POLY2 | ABC 1ST BREAK | ABC 2ND BREAK | ABC PARM LENGTH | ABC WIN RANK |
|-------------|---------------------|----------------------|------------------|---------------------|-------|-----------|---------------|---------------|-----------------|--------------|
| GOOD | 0.000558 | 0.003523 | 0.001655 | ABC | 2 | 3 | 3274 | 4274 | 156 | 105 |
| NOEVENT | | | | | | | | | | |
| GOOD | 0.002265 | 0.002365 | 0.001341 | ABC | 2 | 3 | 6546 | 8746 | 309 | 208 |
| GOOD | 0.000458 | 0.00173 | 0.000922 | BESTFIT | 2 | | | | | |
| GOOD | 0.001114 | 0.000793 | 0.000421 | BESTFIT | 2 | | | | | |
| GOOD | 0.000138 | 0.00102 | 0.001137 | BESTFIT | 2 | | | | | |
| GOOD | 0.000167 | 0.00092 | 0.001539 | BESTFIT | 2 | | | | | |
| GOOD | 0.00025 | 0.000145 | 0.000463 | BESTFIT | 2 | | | | | |
| GOOD | 0.002054 | 0.000654 | 0.000578 | BESTFIT | 2 | | | | | |
| GOOD | 0.002194 | 0.001668 | 0.001263 | BESTFIT | 2 | | | | | |
| GOOD | 0.001477 | 0.001205 | 0.00077 | BESTFIT | 2 | | | | | |
| GOOD | 0.000868 | 0.003763 | 0.003217 | BESTFIT | 2 | | | | | |
| GOOD | 0.000664 | 0.00153 | 0.000951 | ABC | 2 | 3 | 3195 | 4195 | 156 | 105 |
| GOOD | 0.000042 | 0.000794 | 0.000666 | ABC | 2 | 1 | 6230 | 28430 | 312 | 102 |
| GOOD | 0.000642 | 0.000113 | 0.000406 | BESTFIT | 2 | | | | | |
| GOOD | 0.000035 | 0.005565 | 0.002257 | BESTFIT | 2 | | | | | |
| GOOD | 0.000069 | 0.002021 | 0.000447 | BESTFIT | 2 | | | | | |
| GOOD | 0.000068 | 0.00203 | 0.001668 | BESTFIT | 2 | | | | | |
| GOOD | 0.000142 | 0.000566 | 0.001094 | BESTFIT | 2 | | | | | |
| GOOD | 0.000087 | 0.000739 | 0.000715 | BESTFIT | 2 | | | | | |
| GOOD | 0.000264 | 0.001121 | 0.000655 | BESTFIT | 2 | | | | | |
| GOOD | 0.00022 | 0.000084 | 0.001361 | BESTFIT | 2 | | | | | |

Table 4–2. Example of an apktable comma-separated value (CSV) file for the 2014 moment magnitude 6.0 South Napa earthquake ground-motion processing

[Biol., Biological; CA, California; EPIC, closest distance to epicenter; FAULT, closest distance to fault; LAT, latitude; LON, longitude; PGAV1, peak ground acceleration after volume 1 [V1] processing; PGAV2, peak ground acceleration after volume 2 [V2] processing; PGD, peak ground displacement; PGV, peak ground velocity; SA0p3, spectral acceleration at 0.3 second; SA1P0, spectral acceleration at 1 second; SA3P0, spectral acceleration at 3 seconds; SCNL, station, component, network, and location code; USA, United States of America]

| SCNL | STATION_TYPE | STATION_NAME | LAT | LON | EPIC | FAULT | PGAV1 | PGAV2 | PGV | PGD | SA0P3 | SA1P0 | SA3P0 |
|----------------|--------------|--|----------|------------|-----------|-------|-----------|-----------|-----------|-----------|----------|----------|----------|
| BDM.HNE.BK.00 | 4 | Black Diamond Mines Park Antioch CA USA | 37.95397 | -121.86554 | 48.68528 | (--) | -0.008223 | -0.008126 | -0.957186 | -0.415597 | 0.016495 | 0.020884 | 0.003311 |
| BDM.HNN.BK.00 | 4 | Black Diamond Mines Park Antioch CA USA | 37.95397 | -121.86554 | 48.68528 | (--) | 0.005893 | 0.005918 | -1.054496 | -0.439677 | 0.020534 | 0.013529 | 0.003645 |
| BDM.HNZ.BK.00 | 4 | Black Diamond Mines Park Antioch CA USA | 37.95397 | -121.86554 | 48.68528 | (--) | -0.010281 | -0.010216 | 0.964186 | 0.249788 | 0.019627 | 0.015995 | 0.002895 |
| BKS.HNE.BK.00 | 4 | Byerly Seismographic Vault Berkeley CA USA | 37.87622 | -122.23558 | 38.31004 | (--) | -0.010038 | -0.009907 | 0.989405 | 0.443692 | 0.028059 | 0.014399 | 0.004137 |
| BKS.HNN.BK.00 | 4 | Byerly Seismographic Vault Berkeley CA USA | 37.87622 | -122.23558 | 38.31004 | (--) | -0.008042 | -0.008025 | -0.876773 | -0.632057 | 0.023366 | 0.013659 | 0.003751 |
| BKS.HNZ.BK.00 | 4 | Byerly Seismographic Vault Berkeley CA USA | 37.87622 | -122.23558 | 38.31004 | (--) | -0.006208 | -0.006128 | 0.554539 | -0.357247 | 0.0149 | 0.006917 | 0.001854 |
| BL67.HNE.BK.00 | 1 | LBL Building 67 Berkeley CA USA | 37.87492 | -122.24318 | 38.34269 | (--) | 0.013115 | 0.012555 | 1.089866 | 0.442891 | 0.036383 | 0.016917 | 0.00313 |
| BL67.HNN.BK.00 | 1 | LBL Building 67 Berkeley CA USA | 37.87492 | -122.24318 | 38.34269 | (--) | -0.018868 | -0.018667 | -1.144372 | -0.546976 | 0.040608 | 0.010443 | 0.00378 |
| BL67.HNZ.BK.00 | 1 | LBL Building 67 Berkeley CA USA | 37.87492 | -122.24318 | 38.34269 | (--) | 0.00895 | 0.007635 | 0.439829 | -0.356205 | 0.013358 | 0.009627 | 0.001516 |
| BL88.HNE.BK.00 | 1 | LBL Building 88 Berkeley CA USA | 37.87715 | -122.25429 | 37.9568 | (--) | 0.013302 | 0.013166 | -1.186477 | 0.438145 | 0.041416 | 0.019958 | 0.002373 |
| BL88.HNN.BK.00 | 1 | LBL Building 88 Berkeley CA USA | 37.87715 | -122.25429 | 37.9568 | (--) | 0.014377 | 0.014251 | -1.071321 | 0.502574 | 0.026938 | 0.019192 | 0.003058 |
| BL88.HNZ.BK.00 | 1 | LBL Building 88 Berkeley CA USA | 37.87715 | -122.25429 | 37.9568 | (--) | -0.006859 | -0.006733 | 0.508487 | -0.346283 | 0.017828 | 0.007762 | 0.000989 |
| BRIB.HNE.BK.00 | 3 | Briones Reserve Orinda CA USA | 37.91886 | -122.15179 | 35.8314 | (--) | 0.008158 | 0.00802 | 1.2791 | 0.635742 | 0.019829 | 0.032954 | 0.003382 |
| BRIB.HNN.BK.00 | 3 | Briones Reserve Orinda CA USA | 37.91886 | -122.15179 | 35.8314 | (--) | -0.010749 | -0.010551 | 1.048171 | 0.74415 | 0.017406 | 0.017076 | 0.003283 |
| BRIB.HNZ.BK.00 | 3 | Briones Reserve Orinda CA USA | 37.91886 | -122.15179 | 35.8314 | (--) | -0.005236 | -0.005153 | 0.758956 | 0.249344 | 0.01029 | 0.019938 | 0.002924 |
| BRK.HNE.BK.00 | 5 | Haviland Hall Berkeley CA USA | 37.87352 | -122.26099 | 38.28451 | (--) | 0.00518 | 0.005041 | 0.337486 | 0.192037 | 0.011534 | 0.004834 | 0.000761 |
| BRK.HNN.BK.00 | 5 | Haviland Hall Berkeley CA USA | 37.87352 | -122.26099 | 38.28451 | (--) | 0.005393 | 0.005279 | -0.3715 | -0.213665 | 0.013837 | 0.005308 | 0.001081 |
| BRK.HNZ.BK.00 | 5 | Haviland Hall Berkeley CA USA | 37.87352 | -122.26099 | 38.28451 | (--) | 0.001851 | 0.001781 | -0.194847 | -0.174753 | 0.004578 | 0.003182 | 0.000493 |
| FARB.HNE.BK.00 | 3 | Farallon Islands CA USA | 37.69782 | -123.0011 | 83.46995 | (--) | 0.005439 | 0.005309 | -0.596148 | 0.303266 | 0.013626 | 0.005234 | 0.001142 |
| FARB.HNN.BK.00 | 3 | Farallon Islands CA USA | 37.69782 | -123.0011 | 83.46995 | (--) | -0.004686 | -0.004552 | 0.427667 | -0.232807 | 0.013546 | 0.006467 | 0.000936 |
| FARB.HNZ.BK.00 | 3 | Farallon Islands CA USA | 37.69782 | -123.0011 | 83.46995 | (--) | -0.004338 | -0.004213 | 0.284141 | -0.130146 | 0.011436 | 0.002917 | 0.000967 |
| HOPS.HNE.BK.00 | 4 | Hopland Research and Extension Center Hopland CA | 38.99349 | -123.07234 | 108.87071 | (--) | 0.003534 | 0.003637 | 1.316314 | 0.795343 | 0.003874 | 0.005312 | 0.0068 |
| HOPS.HNN.BK.00 | 4 | Hopland Research and Extension Center Hopland CA | 38.99349 | -123.07234 | 108.87071 | (--) | 0.002361 | 0.002369 | 0.839468 | -0.505543 | 0.002447 | 0.005301 | 0.005544 |
| HOPS.HNZ.BK.00 | 4 | Hopland Research and Extension Center Hopland CA | 38.99349 | -123.07234 | 108.87071 | (--) | -0.001827 | -0.001868 | 0.684018 | 0.35384 | 0.002006 | 0.004893 | 0.005435 |
| JRSC.HNE.BK.00 | 4 | Jasper Ridge Biol. Preserve Stanford CA USA | 37.40373 | -122.23868 | 90.49214 | (--) | -0.004015 | -0.00397 | 0.482482 | -0.201448 | 0.015567 | 0.004775 | 0.001531 |
| JRSC.HNN.BK.00 | 4 | Jasper Ridge Biol. Preserve Stanford CA USA | 37.40373 | -122.23868 | 90.49214 | (--) | 0.003203 | 0.003164 | -0.330101 | -0.180643 | 0.007106 | 0.003235 | 0.001557 |
| JRSC.HNZ.BK.00 | 4 | Jasper Ridge Biol. Preserve Stanford CA USA | 37.40373 | -122.23868 | 90.49214 | (--) | -0.002169 | -0.002107 | 0.256643 | 0.219632 | 0.00617 | 0.002693 | 0.001154 |